Contribution of Biofilm Matrix Components to Physical Properties of *Bacillus subtilis* Biofilms at all Phases of Biofilm-Formation

Sara Kesel

München 2020

Contribution of Biofilm Matrix Components to Physical Properties of *Bacillus subtilis* Biofilms at all Phases of Biofilm-Formation

Sara Kesel

Dissertation
an der Fakultät für Physik
der Ludwig–Maximilians–Universität
München

vorgelegt von
Sara Kesel
aus München

München, den 3. 2. 2020

Erstgutachter: PD Dr. habil. Madeleine Opitz

Zweitgutachter: Prof. Dr. Erwin Frey

Tag der mündlichen Prüfung: 3.6.2020

Contents

Summary

The discovery of antibiotics was a big step in modern medicine. Infections that once were deadly and could only be treated symptomatically can now be cured. But not even 100 years later, resistant and even multiresistant bacteria are on the rise that are resistant against most common antibiotics. Non-treatable bacterial infections become a problem more and more often. Most of these infections are caused by bacteria forming a biofilm. Inside the self-secreted biofilm matrix, composed of proteins, carbohydrates and other polymers, the bacteria are protected from harmful environmental conditions such as the presence of antibiotics. This matrix is not only the reason the bacteria are resistant against antibiotics and other chemicals, it also protects them from mechanical stresses such as shear forces. These characteristics stem from physical properties. Some selected are discussed in this thesis.

The (bio-) physical properties of the matrix depend on the composition of the biofilm that varies from species to species. The biofilms used in this thesis were produced by different strains of the species *Bacillus subtilis* NCIB 3610 and *Bacillus subtilis* B-1 that differ in their biofilm matrix composition. The most important matrix components of NCIB 3610 biofilms are proteins BslA and TasA and a carbohydrate that is produced by the *epsA-O* operon. The matrix *B. subtilis* B-1 is mainly composed of γ-polyglutamate. Every one of those matrix components impacts specific physical properties. Consequently, selected knock-out mutants of *B. subtilis* NCIB 3610 were used to investigate the importance of single matrix components.

This thesis connects the highlighted components with specific (bio-) physical properties. The BslA protein that coats the surface of *B. subtilis* NCIB 3610 biofilms not only determines surface structure and surface roughness, it also facilitates 3D-growth by providing structural stability and surface stiffness. The filament forming protein TasA has no effect on surface stiffness and elasticity of the total biofilm, but provides structural integrity inside the *B. subtilis* NCIB 3610 biofilm by forming a scaffold. This scaffold restricts the maximal height of the biofilm construct, though. The carbohydrate that is produced by the *epsA-O* operon not only serves as a filling material to increase the volume of *B. subtilis* NCIB 3610 biofilms, it is also important for lateral biofilm growth.

This thesis also shows, that the production of biofilm matrix components not only affects the physical properties of mature, fully grown biofilms, it also affects the interaction with the environment, like attachment to a surface. While a surface coating with carbohydrates reduces binding of planctonic bacteria to gold surfaces, the carbohydrate produced by the *epsA-O* operon enables binding to carbohydrate-coated surfaces by unspecific carbohydrate-carbohydrate interactions.
These physical properties were also investigated for *B. subtilis* B-1. In this strain, the main biofilm matrix component γ-polyglutamate serves as filler and is responsible for surface stiffness and structure. Additionally, the γ-polyglutamate protects the biofilm matrix from ethanol induced stiffening and dehydration after ethanol treatment. This specific physical property was successfully transferred from one biofilm to another, by adding the γ-polyglutamate artificially to *B. subtilis* NCIB 3610 biofilms.
Every new insight on which component is responsible for certain (bio-) physical properties will help eventually altering them and, together with the knowledge of the bacteria involved and the exact biofilm composition, will lead to the development of optimal treatments of bacterial biofilm infections. Incomplete or wrong treatment of biofilm infections lead to the above mentioned multiresistant bacteria. These will become non-treatable and will set back modern medicine and health care in an era before the discovery of the penicillin.

Zusammenfassung

Die Entdeckung von Antibiotika hat die moderne Medizin revolutioniert. Bis dato nur symptomatisch behandelbare Infektionskrankheiten konnten fortan geheilt werden. Doch nicht einmal 100 Jahre später haben sich resistente und sogar multiresistente Keime gebildet, die gegen gängige Antibiotika immun sind. Nichtbehandelbare, bakterielle Infektionen werden immer mehr zu einem Problem und ein Großteil dieser Infektionen werden durch Bakterien verursacht, die bakterielle Biofilme bilden. In diesen Biofilmen haben sich die Bakterien in einer selbstproduzierten Matrix aus Proteinen, Zuckern und anderen langkettigen Bestandteilen eingekapselt, um sich vor schädlichen Umwelteinflüssen zu schützen, wie zum Beispiel die Gegenwart von Antibiotika. Diese Matrix macht Bakterien nicht nur resistent gegen die Antibiotika und andere Chemikalien, sie macht auch widerstandsfähiger gegen einwirkende Scherkräfte. Die Matrix verleiht dem Biofilm also bestimmte (bio-) physikalische Eigenschaften, von denen Ausgewählte in dieser Arbeit untersucht wurden.

Abhängig von der Spezies der Bakterien unterscheidet sich auch die sekrierte Matrix. In dieser Arbeit wurden Biofilme untersucht, die von verschiedenen Stämmen der Spezies *Bacillus subtilis*, *B. subtilis* NCIB 3610 und *B. subtilis* B-1, produziert werden, die sich im Aufbau ihrer Biofilm-Matrix unterscheiden. Die wichtigsten Bestandteile der Biofilme von *B. subtilis* NCIB 3610 sind die Proteine BslA und TasA, sowie der vom *epsA-O* Operon produzierte Zucker. In Biofilmen von *B. subtilis* B-1 befindet sich haupsächlich Gamma-Polyglutamat. Jede dieser Matrix-Komponenten beeinflusst andere (bio-) physikalische Eigenschaften. Daher wurden zusätzlich ausgewählte Deletionsmutanten von *B. subtilis* NCIB 3610 verwendet, um den Einfluss der einzelnen Komponenten zu bestimmen.

Die Zusammenhänge zwischen den oben genannten Komponenten und der von ihnen vermittelten (bio-) physikalische Eigenschaften wurden in dieser Arbeit untersucht. Das Protein BslA, das die Biofilm Matrix von *B. subtilis* NCIB 3610 Biofilmen einhüllt, bestimmt nicht nur die Oberflächenstruktur und -rauheit, sondern gibt der Matrix Stabilität und bestimmt die Steifigkeit der einhüllenden Schicht, beides Eigenschaften, die das Wachstum in die Höhe begünstigen. Die Filamente, die das Protein TasA formt, sorgen für Stabilität im Inneren des *B. subtilis* NCIB 3610 Biofilms, haben aber keinen Einfluss auf die

Elastiziät des Biofilms und die Steifigkeit an der Oberfläche. Allerdings wird durch die Verstrebungen die maximale Höhe des Biofilms eingeschränkt. Der vom *epsA-O* Operon produzierte Zucker dient dem *B. subtilis* NCIB 3610 Biofilm als Füllmaterial, um das Volumen zu erhöhen und hat damit Einfluss auf das laterale Wachstum der Biofilme.
Zudem konnte gezeigt werde, dass die Produktion der Komponenten für die Biofilm Matrix nicht nur deren physikalische Eigenschaften bestimmt, sondern auch die Interaktionen mit der Umwelt beeinflusst. So ermöglicht beispelsweise der vom *epsA-O* Operon produzierte Zucker durch Kohlenhydrat-Kohlenhydrat Wechselwirkungen ein Anlagern von einzelnen Bakterien an goldbeschichteten Oberflächen, auf die zusätzlich Zucker aufgetragen wurden. Normalerweise führt eine Beschichtung mit Zuckern zu einer Reduzierung des Bindevermögens einzelner Bakterien.
Die gleichen physikalischen Eigenschaften wurden für *B. subtilis* B-1 Biofilme untersucht, deren Matrix hauptsächlich aus Gamma-Polyglutamat besteht, was bei diesem Stamm als Füllmaterial dient und gleichzeitig zuständig ist für Oberflächenstruktur und -steifigkeit. Zudem schützt das Gamma-Polyglutamat den Biofilm vor Austrocknung und damit einhergehender Versteifung der Matrix, die durch eine Behandlung mit Ethanol ausgelöst wird. Diese physikalische Eigenschaft konnte erfolgreich auch auf einen anderen Biofilm übertragen werden, indem das Gamma-Polyglutamat künstlich der Matrix von *B. subtilis* NCIB 3610 Biofilmen zugesetzt wurde.
Je mehr über die einzelnen Komponenten der Biofilme und der von ihnen vermittelten (bio-) physikalischen Eigenschaften bekannt ist, desto eher wird man in der Lage sein, diese Eigenschaften auch zu verändern und zusammen mit dem Wissen um die genaue Zusammensetzung der Biofilm Matrix und der darin eingekapselten Bakterien kann eine effektive Behandlung einer durch bakteriellen Biofilm ausgelösten Infektion entwickelt werden. Werden Biofilme nicht vollständig entfernt, oder mit den falschen Mitteln behandelt, kann dies zu den eingangs erwähnten multiresistenten Bakterien führen. Diese können dann zukünftig nicht mehr behandelt werden und drohen die Weltgesundheit und medizinische Versorgung in eine Zeit vor der Entdeckung des Penicillins zu versetzen.

1 Introduction

The discovery of Penicillin was ground-breaking for modern medicine. Within a few years, several severe infections and diseases became treatable thanks to antibiotics. Once life threatening, they are now easily cured by a widely available drug. But already at its discovery, the possibility of resistances that would make those infections and diseases life threatening again was predicted by Alexander Fleming himself:

> ***It is not difficult to make microbes resistant to penicillin in the laboratory by exposing them to concentrations not sufficient to kill them, and the same thing has occasionally happened in the body. The time may come when penicillin can be bought by anyone in the shops. Then there is the danger that the ignorant man may easily underdose himself and by exposing his microbes to non-lethal quantities of the drug make them resistant. -Alexander Fleming [1]***

Not even a hundred years later, once defeated infections and diseases are on the brink of coming back and threaten society, as multiresistant bacteria have invaded hospitals and food industries. Of those infections 80% are due to biofilm forming microbes [2]. Biofilms form on medical devices such as contact lenses, catheters, implants, hart valves, and syringes [3, 4]. They can also form on tissue, for example on teeth, gum or lung tissue [5, 6]. In factories they can cause clogging of pipes or impairing with heat transport [7, 8]. Not only are planctonic, meaning single floating cells, becoming resistant to antibiotics, but being in the biofilm complex is making them up to 1000 fold more resistant [9]. While resistance mechanisms of single cells are understood to a certain degree, those mechanisms explain the resistance only at the single cell level. In a biofilm however, other mechanisms have to be considered.

Inside the biofilm matrix, the single cell resistance mechanisms, such as pumping out the antibiotic, destroying the antibiotic with enzymes or reconstructing the targeted area [10], are still in place, but cannot explain the drastic increase in the resistance factor. The matrix around the bacteria influences the way the antibiotic is working. There are several

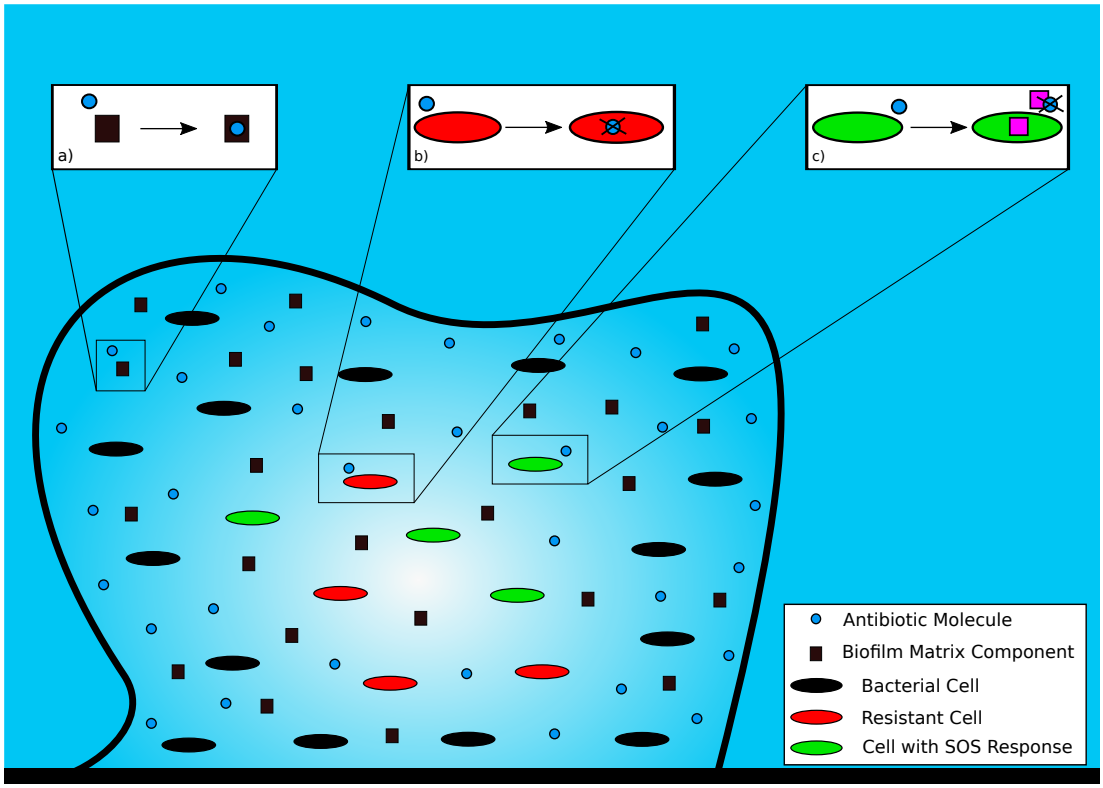

Figure 1.1: Schematic for Modes of Antibiotic Resistance in Bacterial Biofilms Biofilm matrix and enclosed bacteria are depicted in black. Antibiotics and other bacteriocides (represented by the blue dots as well as the color gradient) might not be able to penetrate the biofilm matrix completely, resulting in a gradient throughout the biofilm. This could be caused either by low permeability, or by a matrix component that is able to absorb the molecules (a). Due to this gradient, the killing concentration might not be reached in the depths of the biofilm, and therefore bacteria will survive. This can lead to resistant cells (red, b) that are able to deal with the antibiotic and will start growing anew, once the external stress from the antibiotic subsides. The same holds true for possible persister cells that develop due to low metabolism deep inside the biofilm. Other bacteria (green, c) might be able to produce metabolites as a SOS response that are able to neutralize the antibiotic and thus enable the survival of the colony. Neither biofilm matrix, nor bacteria and antibiotic molecules and their distribution are drawn to scale.

possible explanations what those influences are [2, 11, 12]. Figure 1.1 shows an overview on the different modes of antibiotic resistance in biofilms. They can occur all together or in random combinations. For one, the antibiotic might be unable to penetrate completely into the biofilm matrix, either because the antibiotic molecules are too big, or because a matrix component is binding to the molecule [13] and thus, creating a gradient of concentration inside the biofilm (Figure 1.1 in blue). That way, most bacteria will be killed, but some will survive, as long as the Minimal Inhibitory Concentration (MIC) is not reached. If that is the case, the remaining bacteria can not only start growing again once the antibiotic treatment stops, an environment with low concentration of antibiotics also promotes the development of new resistances of single cells by mutation (Figure 1.1 red cells). In other scenarios, those resistant cells could already be in place, for example in the form of persister cells that form in low metabolism conditions, as are given deep inside the biofilm matrix [14]. Other cells, just like in non biofilm colonies, might trigger an SOS response and thus neutralize the antibiotic (Figure 1.1 green cells) [15].

Antibiotics have to be carefully chosen, especially in the presence of a biofilm. Different types of antibiotics work by blocking different functionalities of a cell, for example: blocking cell division, inhibiting uptake or cell membrane development. Most antibiotics work on dividing cells and will not work on cells inside a biofilm, as they can be in an inactive, non-dividing state [16]. Additionally, most naturally grown biofilms consist of not only one single bacterial species, but multiple. Thus an antibiotic that can kill one species, might be harmless for the other one. Additionally, the interaction in multi-species biofilms add a whole new level to the resistance against antibacterial agents [17, 18].

All those different scenarios show how difficult it is to effectively eliminate a biofilm, if only the bacteria are accounted for during treatment and not the biofilm matrix as well. The biofilm matrix that consists of different proteins, polysaccharides and other self-secreted metabolites, needs to be treated as well. There are different possibilities to try and remove the matrix before antibacterial treatment. Physical treatment alone often is not sufficient, as the architectural structure of the biofilm also rends it resistant against e.g. shear flow [7]. There are possibilities, like protein removal with different salts and chemicals [19] or short pulses of ultrasound [20], to first weaken the biofilm matrix. All these approaches aim either at the adhesion (attachment of planctonic cells to a surface prior to biofilm-formation) or the cohesion (interactions inside the biofilm matrix) [21].
A complex and foremost individual treatment is therefore necessary to treat each biofilm infection in order to remove cells and matrix alike, as treatments that remove the matrix

may not affect the bacteria and vice versa [19]. Treatment that intended to kill bacteria was shown to lend the matrix the ability to better withstand other types of removal strategies. For example metal ions that are harmful for planctonic cells are integrated into the biofilm matrix, helping it withstand shear forces [22]. As not all mechanics of biofilm resistances are understood and there is more to a successful treatment than just treating the planctonic cells, it is important to not only look at the bacteria inside the biofilm, but also at the biofilm matrix itself. More specifically, the mechanical and physical properties of the biofilm matrix and the contributions of the single matrix components have to be thoroughly understood throughout all stages of biofilm-formation.
As biofilm matrices are composed of such a huge variety of components, diverging in different species, the physical properties and the specific interactions of biofilms and their environment as well as the specific interactions of matrix elements inside the biofilm are largely unknown and dependent on the exact composition. Generally, on a molecular level, there are a couple of interactions to be considered ([21], chapter 2), namely Van der Waals forces in form of London dispersion forces (a), hydrogen bonds (b) and electrostatic interactions (c).
These interactions give the biofilm matrix specific properties: While the proteins inside the biofilm matrix are also needed for the architectural structure of the 3-D colonies, they are needed for their enzymatic activities as well [21], in order to break down macromolecules to make them accessible as nutrients (a, b, c). Furthermore, the matrix components allow to the biofilm to interact with its environment in the form of surface-active compounds [23](a). An important feature of the biofilm matrix is its sorption capacity (b). Usually, biofilms are able to hold high concentrations of water, working like a sponge, but can also absorb chemical solutions [21]. The majority of the polysaccharides inside the biofilm matrix have anionic groups [24] letting them bind and absorb different cations from the surrounding medium (c). The same must hold true (at least for a small part) for anions, as amino groups provide positive charges, and for polar molecules, although this is without documentation [21].

At the same time it is especially important to not only look at the interactions processes themselves but to also understand their time resolutions and statistical variances. The aim of this thesis is shedding light onto some of the properties and dynamics of biofilm matrices from the early stages to fully formed matured 3-D biofilm colonies. This is done using physical methods such as (light- and atomic force-) microscopy, a cantilever array system, rheology, profilometry and statistical analysis as well as biological methods like gene analysis and cloning of specific knock-out mutants of the gram positive model organism *Bacillus subtilis*.

The parameters that are being investigated are the ability to attach to (un-) modified gold surfaces, growth dynamics both for lateral and vertical growth for various biofilm forming strains that express different matrix components and the properties of fully matured biofilm surfaces such as elasticity and roughness, the bulk viscoelasticity and the net produced biomass.
As surface attachment is the first step in biofilm-formation this is crucial to understand in order to being able to prevent biofilm growth in the first place. Modifications of the physico-chemical properties of a surface may make a difference in the ability of the planctonic cells (with or without basaly expressed biofilm matrix components) to bind and form biofilm colonies. Knowing how fast the different biofilm forming strains grow in dependence on the matrix components expressed during formation will help getting a head start at identification of the bacterial strain and consequently proper treatment. And lastly, the more is known about the properties of fully formed biofilms, the better individual treatment plans can be devised, as stated above. This is especially important, as the absorption of different molecules into the biofilm matrix can alter the properties of the biofilm surface or of the bulk of the biofilm matrix in such a way that it is more resistant against removal strategies.
In the first chapter, chapter 2, bacterial biofilms are introduced, as well as the important genes for biofilm-formation and biofilm matrix components for *B. subtilis* biofilms and in chapter 3, the experimental methods are summarized. Chapter 4 presents the contribution of biofilm matrix components to physical properties of *B. subtilis* biofilms, beginning with the sequencing of a strain that differs in its matrix components from the other strains used in this study in section 4.1. Section 4.2 presents a study on how basally expressed biofilm matrix elements influence the ability of planctonic cells to attach to gold surfaces. In section 4.3, the contribution of biofilm matrix components to different stages of biofilm-formation, especially vertical and lateral growth that is also quantified by theoretical modeling, is analyzed and section 4.4 presents how matrix composition affects selected physical properties of fully grown biofilms. Chapter 5 concludes this thesis, discusses the findings and gives an outlook.

2 Basic Concepts

In this thesis, the influence of the biofilm matrix components on the physical properties of bacterial biofilms is analyzed. In the following chapter, the term bacterial biofilm is introduced, as well as the key matrix components that form the biofilm. Further, removal strategies are discussed and a theoretical model for biofilm-formation is presented.

2.1 Bacterial Biofilms

Biofilms are a complex community of microbes that are encased in a self-secreted matrix of Extracellular Polymeric Substances (EPS) [25, 26], that contains a variety of different polysaccharides, proteins, lipids and nucleic acids [27–30]. Biofilms mostly form on solid surfaces [31], either completely submerged in liquids [32], only temporarily flooded [28] or even on the liquid air interface [33, 34]. The surfaces can be of organic nature, like plant or body tissue [5, 35, 36] or of inorganic nature, like metal or minerals [28], and do not only serve as structural base, but can also serve as nutrient [37]. Water channels within the biofilm structure make an effective exchange of nutrients and waste products possible [28, 38–40].
Many different organisms, gram-negative bacteria like *Escherichia coli* and *Pseudomonas aeruginosa* [25] and gram-positive bacteria like *Bacillus subtilis* [26, 34] can form bacterial biofilms and their matrices naturally differ from each other. Additionally, the exact matrix composition is dependent on environmental conditions, such as nutrient availability, temperature or hydrodynamic properties of the surrounding media [29, 41], which allows the biofilms to be perfectly adapted to its environment [25]. While different in its compositions, the biofilm matrix serves the same purpose in all organisms: protection. Not only is the ability to stick together necessary to be able to form complex 3-D structures [28], but also helps the distribution of public goods within the biofilm [42]. But most importantly, the biofilm matrix provides protection against a variety of external stresses, such as UV-light [43], metal toxicity [22, 44], dehydration [45], bacterial invasion [46], mechanical forces [47] and against different antimicrobial agents, such as antibiotics and chemical treatment [2, 9, 48–50].

The most studied model organism for biofilm-formation is the gram-negative pathogenic bacterium *Pseudomonas aeruginosa*, that forms submerged biofilms [51, 52]. In this work, bacterial biofilms were investigated that are formed by different *B. subtilis* strains, the non-pathogenic gram-positive model organism [34]. As they form the biofilm on solid surfaces at air, reproducible conditions can be achieved, which is necessary to investigate the relationship between the physical properties and the biofilm matrix composition. Its characteristics are presented in the following sections.

2.1.1 Phases of Biofilm-Formation

B. subtilis is found nearly everywhere [53] and can form biofilms on natural surfaces such as plant roots, where it lives symbiotically with the plant [34]. While in nature the bacteria form biofilms on the solid-air interface, in laboratory conditions, the biofilms can also form at the liquid-air interface (so called pellicles) or even at the solid-liquid interface, depending on the strain [34]. Despite the different environments where biofilms can form, the consecutive steps in biofilm-formation are basically the same. Figure 2.1 shows the life-cycle of a biofilm colony.
At first, single cells settle on a surface and attach. These cells start to divide and form microcolonies. Then, the production of biofilm matrix elements starts. With the matrix elements, the biofilm is able to form 3D-structures. Within the biofilm, there is a heterogeneous bacterial population. While some produce matrix components, others deep inside the biofilm structure might sporulate due to restricted nutrient availability . At the end of biofilm maturation, bacteria are released into the surrounding environment. This process is called dispersal [34].

2.1.2 *B. subtilis* NCIB 3610 Biofilms Matrix Components and their Role in Biofilm Matrix Development

As mentioned in section 2.1, the biofilm matrix is composed of polysaccharides, proteins, lipids and nucleic acids. The composition and nature of these constituents depends on the organisms involved. The genome of lab-strain *B. subtilis* WT168 is fully sequenced, well studied and the genes are mostly identified. The strain *B. subtilis* NCIB 3610 that is used in this study is basically identical to the widely used laboratory strain *B. subtilis* WT168 with the exception of point mutations in the four genes *epsC*, *degQ*, *sfp* and *swrA*. The main reason *B. subtilis* WT168 is incapable of producing a proper biofilm matrix is the lack of the plasmid present in NCIB 3610, which contains the regulatory gene *rapP* [54]. Apart from that, both strains have the genes for the important biofilm components, which

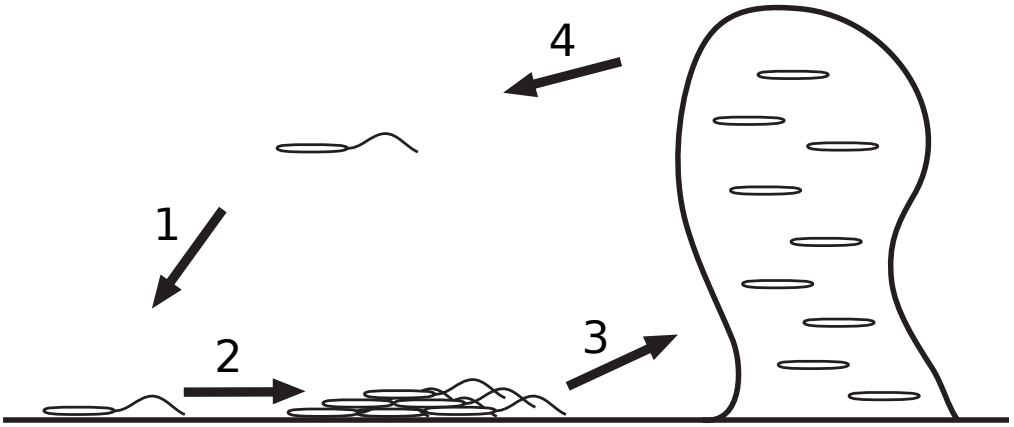

Figure 2.1: Schematic of the Cycle of Biofilm-Formation 1: Attachment of single cells. 2: Growth of microcolonies. 3: Growth of macrocolonies, biofilm maturation and formation of 3D structures. 4: Detachment of single cells. Figure adapted from [52]

are presented in table 2.1.

B. subtilis NCIB 3610 biofilms consist mainly of the protein TasA and the polysaccharide formed by the *epsA-O* operon. TasA is a fiber forming protein, encoded by the 3-gene-operon *tapA-sipW-tasA* [55]. It is important for the structural integrity, and therefore for the biofilm-formation [56]. Together with the polysaccharide produced by the *epsA-O* operon, TasA is the most important element of the *B. subtilis* NCIB 3610 biofilm [56]. During biofilm-formation, TasA is assumed to provide the scaffold for the 3D structure, while the polysaccharide serves as soft and flexible filling material [57]. At the same time, TasA also shows broad-spectrum antibacterial properties, presumably aiding the developmental process in fending off other bacteria and also plays a role in sporulation. Hence it was named translocation-dependent antimicrobial spore component, TasA. [58].

The *epsA-O* operon has its name from the exopolysaccharide product it produces [59], not to be confused with the broadly used abbreviation EPS for Extracellular Polymeric Substances, a general term for the substances found in a biofilm matrix. The product from the *epsA-O* operon consists of glucose, N-acetyl-galactose and galactose [59]. The carbohydrates ensure the agglomeration of cells into bundles within the biofilm [60]. While TasA provides the overall structure, the *epsA-O*-product is the glue that holds everything together. Both *tasA* and *epsA-O* knock-out mutants can be restored to again form healthy biofilms, by complementing the one with the other [56] and a *epsA-O-tasA* double

knock-out mutant can be successfully integrated into a wild-type strain, forming complete biofilms [61].

Another important biofilm matrix component is BslA, a protein that is -even if not relevant for biofilm mass- very important for its surface structure. It was shown that biofilms (those that grow on the air interface) are resistant to wetting and gas penetration [62]. This property even allows them to repel antimicrobial agents like ethanol, which is due to their surface topology [62]. This is achieved by the self-assembling hydrophobin BslA, the biofilm surface layer protein, formerly known as YuaB, which is not responsible for the wrinkles of the biofilm morphology, but rather for the micro-structure of those wrinkles [63, 64]. Production of the exopolysaccharides is necessary for *bslA* transcription [65] and a *tasA-tapA* deletion causes a delay in BslA production, thus the biofilm surface coating via BslA happens after the biofilm agglomeration via the exopolysaccharides and TasA [64].

Table 2.1: Genes involved in Biofilm-Formation This table lists the key components for NCIB 3610 biofilms, TasA, EpsA-O and BslA, as well as the primary gene for *B. subtilis* B-1 biofilms, *ywsC* that encodes for γ-polyglutamate. The list also includes genes responsible for general biofilm regulation.

Gene	Matrix Component	Reference
tasA	matrix fiber	[66]
epsA-O	polysaccharide	[59]
bslA	surface layer protein	[64]
tapA	lipoprotein (assembly of TasA)	[67]
sipW	type I signal peptidase (surface adhesion)	[68]
ywsC	γ-polyglutamate	[69]
abrB	transcription factor	[70]
sinR	master regulator for biofilm-formation	[71]

Those three components, TasA, the exopolysaccharide and BslA, are the most important biofilm matrix components for *B. subtilis* NCIB 3610 biofilms and in the focus of this study (see figure 2.2 right side). But the regulatory system needs mentioning too.

The fiber forming protein TasA is encoded by the 3-gene-operator *tapA-sipW-tasA* [55], where *tapA*, formerly known as *yqxM*, helps assemble the TasA fibers and serves as an anchor for those fibers in order to connect to the cells [67].

The other gene in this 3-gene-operator, *sipW*, encodes a type I signal peptidase that is

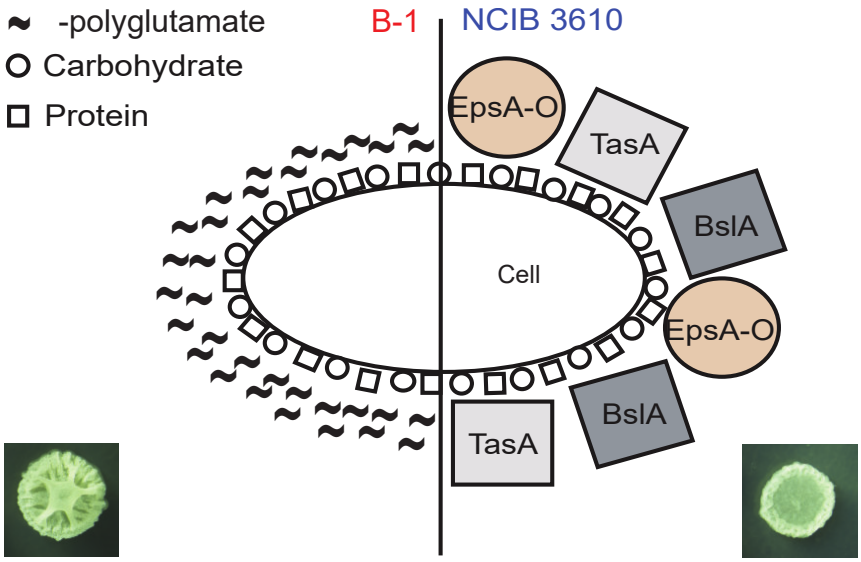

Figure 2.2: Schematic of the Biofilm Matrix Composition of *B. subtilis* NCIB 3610 and *B. subtilis* B-1 Left: Schematic depiction of the cell wall of *B. subtilis* B-1 and its main biofilm matrix component γ-polyglutamate. Right: Schematic depiction of the cell wall of *B. subtilis* B-1 and its main biofilm matrix components TasA, BslA and the exopolysaccharide produced by the *epsA-O* operon. Throughout the thesis *B. subtilis* B-1 will be depicted in red and *B. subtilis* NCIB 3610 in blue, for better recognition. Part of a figure originally published in [72], edited and complemented.

processing TasA. *sipW* is also necessary for upregulation of formation of the biofilm matrix components as well as for the adhesion of the biofilm to the surface [68].
The protein AbrB is a transcription factor for over 100 genes, biofilm-formation included [70]. The protein SinR on the other hand is an inhibitor for the operons *epsA-O* and *tapA-sipW-tasA* [71].

The last notable biofilm matrix component is the hydrophilic macromolecule γ-polyglutamate encoded by the *ywsC* gene. *ywsC* per se is not necessary for biofilm-formation in *B. subtilis* NCIB 3610 [73], but there are *B. subtilis* strains, where biofilm production is linked to the production of γ-polyglutamate [69], like the *B. subtilis* B-1 strain that was used in this study. Most γ-polyglutamate producing bacteria are gram-positive, but there is at least one gram-negative bacterium and even archae and euchariotes that also produce it [74]. It can serve multiple purposes, such as augmenting survivability in high salt concentrations and in the presence of toxic metal ions [75]. It may also serve as a glutamate source in times of starvation or can increase virulence [74]. In *B. subtilis* B-1 the production of γ-polyglutamate (see figure 2.2 left side) is regulated by the *ywsC* gene (also known as *pgsB*). Apart from its benefits for the bacteria that produce the γ-polyglutamate, it is also used for a variety of applications ranging from food supplement (Japanese dish natto), over

medicine (drug carrier, tissue engineering) to cosmetics and even biodegradable plastic production [74].

2.1.3 Composition of the Biofilm Matrix determined by the Growth Medium

Apart from the bacterial species and the genes involved in biofilm-formation, one of the most important factors that determine the biofilm matrix composition is the availability of nutrients, or - in laboratory conditions - the growth medium. Depending on the choice of the medium, the biofilm is growing differently. For some bacteria it can be necessary to restrict nutrient availability in order to promote biofilm-formation. For example one step in the biofilm life cycle, the sporulation that occurs as a survival strategy in low nutrient conditions, requires specific nutrient combinations [76]. In some cases nutrient regulation can also be necessary in order to promote EPS production [77], therefore it can often be found that *B. subtilis* biofilms are cultivated on the minimal Medium Msgg (a growth medium with exactly determined nutrients) [78], especially if the focus of the study lies on one specific stage of biofilm-formation.
Here, the focus is on general growth and the resulting physical properties of bacterial biofilms. As the *B. subtilis* B-1 strain was reported to grow on LB medium [69] (a nutritional rich medium for general cultivation of bacterial strains) and the other strains in this study did not have problems forming proper biofilms plated on LB medium, this medium was chosen in order to be able to compare the resulting biofilm matrices (for detailed cultivation see chapter 3.1). In general, *B. subtilis* strains need a carbon source in form of glucose or glycerol and various ions, such as Mn^{2+}, Fe^{2+}, Mg^{2+} and K^{+} [78, 79].
In order to be able to compare the resulting biofilm matrices, it is important to not only choose the right medium, but also to keep the conditions constant. Most of the existing studies use different growth conditions making it complicated to compare the results. As the aim of this study is to investigate the physical properties of different *B. subtilis* strains, it is especially crucial to always have the same experimental conditions.

3 Materials and Methods

3.1 Biofilm Strains and Growth Conditions

In this study, various strains of *Bacillus subtilis* were used. Table 3.1 shows an overview of those strains and the biofilm matrix component they produce. For a more detailed description of the biofilm matrix components see chapter 2.1.2. The table includes the antibiotic resistance and concentration of applied antibiotic for the knock-out mutants that replaced the respective biofilm gene for selection purposes.

Table 3.1: *B. subtilis* strains used in this study This table shows all *B. subtilis* strains used in this thesis. For the knock-out strains, the antibiotic resistance and the concentration of the applied antibiotic is included. Additionally, it lists the biofilm matrix components that this particular strain is able to form.

Strain	Knocked-out Gene	Antibiotic Resistance and Concentration [μg/ml]	Remaining Biofilm Matrix Components	Source
B. subtilis NCIB 3610	n/a	n/a	TasA, *epsA-O* product, BslA	[56]
B. subtilis ZK3660	*epsA-O*	Tetracycline 12,5	TasA, (BslA)	[59]
B. subtilis CA017	*tasA*	Kanamycin 50	*epsA-O* product, BslA	[66]
B. subtilis N24	*bslA*	Chloramphenicol 5	TasA, *epsA-O* product	[64]
bslA/tasA	*bslA*, *tasA*	Chloramphenicol 5, Kanamycin 50	*epsA-O* product	[80]
B. subtilis B-1	n/a	n/a	γ-polyglutamate	[69]
B. subtilis BD630	n/a	n/a	n/a	[81]

All strains were cultured with LB-medium (Luria-Miller, Carl Roth GmbH, Germany). As a first cultivation step, the strains that are stored frozen at $-80\,^{\circ}\mathrm{C}$ are plated on LB-Agar-plates and placed in an incubator at a temperature of (37 °C) and humidity con-

trolled incubator over night. The next morning, grown colonies were optically controlled for their biofilm growth and colony morphology and the plates were stored in a refrigerator at 8 °C. The control step is important in order to only use colonies for the experiments whose biofilm looks the same and healthy for every experiment. This is especially crucial for the wild-type strains that do not grow under the selective pressure of the antibiotic, hence natural mutations can occur.
As preparation for the experiments, overnight cultures were prepared by scraping a little piece of the colony with a pipet tip and placing it in 5 ml LB medium and put in the incubator at 37 °C and 300 rpm overnight (17 hours). The agitation helps with the oxygen supply of the culture in order to ensure aerobic growth. The growth medium contained the selection antibiotic, if applicable.
The next morning, the overnight cultures were diluted with LB medium from an optical density (OD 600 nm) of 1.8-2 to an optical density (600 nm) of 0.05. Depending on the following experiments and the stages of biofilm-formation that were investigated (see chapter 2.1.1), these day cultures were let grown for different lengths of time.

Preparations for the attachment experiments (chapter 4.2) are the following: the day cultures were let grown until the they have reached the stationary growth phase and then centrifuged at 1300 rpm for 5 min. The cells were re-suspended in a Tris buffer (100 mM NaCl, 10 mM Tris [pH 7], 0.005% Tween 20, 1 mM $CaCl_2$). This was repeated once more in order to ensure that no organic components of the LB medium are left in the bacterial suspension that would interfere with sensitivity of the cantilever array system. The bacteria were further diluted to an optical density (600 nm) of 0.1.

For the growth experiments (chapter 4.3), the culture grew until the density doubled just once, reaching the beginning of the exponential growth phase. The culture was then diluted again to 0.05 and 5 μl per spot were pipetted on an agar plate (see section 3.2.3, figure 3.2). The plate was warmed in the incubator in order to minimize the lag in growth that occurs due to the transfer from liquid to solid medium. Consequently, the observed growth will start almost directly at the beginning of the exponential growth phase.

For the experiments with the fully grown biofilms (chapter 4.4), the day cultures were let grown for 8-9 hours, deep into the stationary growth phase. The liquid culture was then confluently plated onto an agar plate and let grown for another night (18 hours), resulting in biofilm cultures that completely covered the agar plates.
Some biofilms were let grown in the presence of additional γ-polyglutamate that was kindly

provided by the AG Lieleg, extracted from B-1 biofilms following the protocol described in [82]. The γ-polyglutamate was added in a concentration of 4.75 mg/ml right before plating.

3.2 Experimental Methods

3.2.1 Sequencing and Gene Expression Analysis

In order to characterize the genome of the previously unsequenced wild-type strain *B. subtilis* B-1, its DNA was extracted using a precipitation protocol. The extracted genomic material was sequenced by Eurofins Genomics (Eurofins MWG GmbH,Germany) using a standard Illumina shotgun library and the Illumina MiSeq platform (Illumina, Inc., San Diego, CA). The resulting 120,000 paired-end reads, equivalent to 85 Mbp were then processed using the *de novo* assembly programs Velvet [83] and Newbler (454 sequencing; Roche, Branford, CT). The genome draft can be accessed at the GenBank/DDBJ/EMBL database under the accession number CP009684 [84]. Further analysis of the scaffold and the genes were done using the NCBI online tools LAST [85], BLASTx and BLASTn [86]. With those tools, the genes responsible for biofilm-formation could be identified and compared to other wild-type strains (chapter 4.1).
In order to analyze the biofilm matrix composition, the expression of the four key genes relevant for biofilm-formation (see chapter 2.1.2) was analyzed. For that, the RNA was extracted from biofilms covering agar plates using the Qiagen RNeasy extraction kit. The biofilm was grown as described in section 3.1 for fully grown biofilms. The plates were let grown for 10 and 18 hours, respectively. The gene expression analysis was performed by IMGM Laboratories, using quantitative real-time PCR with 40 cycles in custom TaqMan gene expression assays. Three experimental samples were analyzed with three technical replicas for each strain and time point and then averaged. The 16S ribosomal RNA (rRNA) housekeeping gene serves as positive control, as it is a highly conserved gene present in all bacterial species and encodes a subunit of the bacterial ribosome [87]. The parameter that is compared is the threshold cycle (C_T) value, representing the number of PCR cycles after which the signal first surpasses the background level [88]. This value is inverse proportional to the number of RNA copies present in the cell prior to amplification, meaning the stronger the gene expresses, the lower the C_T value.

3.2.2 Cantilever Array System

The first step of biofilm-formation, the attachment to a surface (chapter 2.1.1), was investigated using the Cantisens cantilever array system (Concentris GmbH, Switzerland). This system allows for a measurement of the attachment of single cells in solution with several cantilevers, representing different surface conditions, in parallel.
The cantilever array system detects a deflection of a laser beam that is reflected at the tip of the cantilever. The cantilever deforms due to a difference in surface stress that occurs as a reaction to physical or chemical changes on just one side of the surface. Stoney's equation [89,90] gives the surface stress σ of a one sided coating in relation to the deflection:

$$\frac{1}{r} = 6\frac{\sigma t}{Ed} \tag{3.1}$$

with r being the curvature of the bend, E the Young's elasticity module, t the thickness of the coating and d the thickness of the beam.
The cantilevers can be seen as a beam that is fixed at one end and is uniformly loaded. The deflection δ of the free end can be calculated by:

$$\delta = \frac{Fl^3}{3EI} \tag{3.2}$$

with F being the load, l the length of the beam and I the second moment of area equal to $wt/12$ (where w is the width and t the thickness of the beam). With the assumption of a plane strain [90–92] and with the geometric relation of $1/R = 2\Delta z/l^2$, the deflection at the end of the cantilever Δz can be written as:

$$\Delta z = 3\frac{(1-\nu)l^2}{Et^2}\Delta\sigma \tag{3.3}$$

with the Poisson's ratio ν and $\Delta\sigma$ the difference in surface stress on both sides of the cantilever.

The cantilever arrays (Concentris GmbH, Switzerland) comprise 8 parallel gold coated silicon cantilevers (500μm by 100μm by 1μm). They are first put under UV light (Novascan PSD - UV) for 1.5 hours. This prepares the gold surface of the cantilevers for the next step, the functionalization, and cleans the cantilevers by removing impurities and most importantly smooths the surface [93]. Irregularities in the gold layer will lead to surface stress, decreasing the sensitivity of the cantilever [94].
The cantilevers can be functionalyzed with different carbohydrates (see figure 3.1 A) in or-

der to study different surfaces (see chapter 4.2). The special carbohydrates, two monosaccharides galactose and mannose and the disaccharide lactose, were provided by AG Seeberger [95]. They have a thiol linker at one end which allows them to bind to the gold side of the cantilever leaving the other end of the carbohydrates free for the bacteria to bind (see figure 3.1 B). The carbohydrates were applied using micro-capillaries by inserting one end of the capillary into the carbohydrate solution (all diluted to 40 μM in 10 mM Tris buffer (see section 3.1)), which then rises to the other end by capillary force. The cantilever is inserted into that other end and left in there for 10 minutes, while the carbohydrates will self-assemble on the gold surface. For better consistency throughout the experiments, two cantilevers were left unfunctionalized and for each of the three different carbohydrates, two cantilevers were functionalized the same, providing internal references. In order to achieve a stable measurement, the setup is let running for three hours at a constant buffer flow, equilibrating cantilever and flow system [96]. As the vibrations of the motor for the pump could be detected by the sensitive cantilevers, an air bubble was sucked up into the pump piston for a dampening effect. Equally important is a constant temperature of 22 °C. Due to its bimetal nature (the silicon and the gold expand with heat at different rates) a change in temperature results in bending. This effect is used in order to test the cantilever for uniform bending before the experiments. For better comparability between the experiments, only cantilever arrays were used that showed the same bending behavior throughout the heat test with a change of temperature from 22 °C to 25 °C and back. For the measurements, a volume of 100 μl of bacteria solution with an optical density (OD_{600}) of 0.1 in Tris buffer (see section 3.1) is inserted into the sample loop using a syringe (see figure 3.1 C). The buffer is necessary to ensure stable pH and ion concentrations as the cantilever reacts sensitive to their changes. The buffer also prevents further growth.

With this sample volume and optical density, the signal was found to give the best results, as it gives a strong signal, but will not saturate the cantilever (with a bacteria count of approximately $2 \cdot 10^6$, determined in a previous Diploma thesis by Andreas Mader [97]). Once the bacteria start to bind to the carbohydrates on the functionalized side of the cantilever, the resulting surface stress leads to bending of the cantilever according to equation 3.3.

The bending of the individual cantilever is read out via laser array (an array of eight VCSEL - vertical cavity surface emitting lasers), the change of deflection detected with a PSD (Position Sensitive Device). Figure 3.1 D shows a typical measurement curve. During the time when the bacteria pass the cantilever, the cantilever continues bending as more and more bacteria bind to the carbohydrates, resulting in a continuously increasing

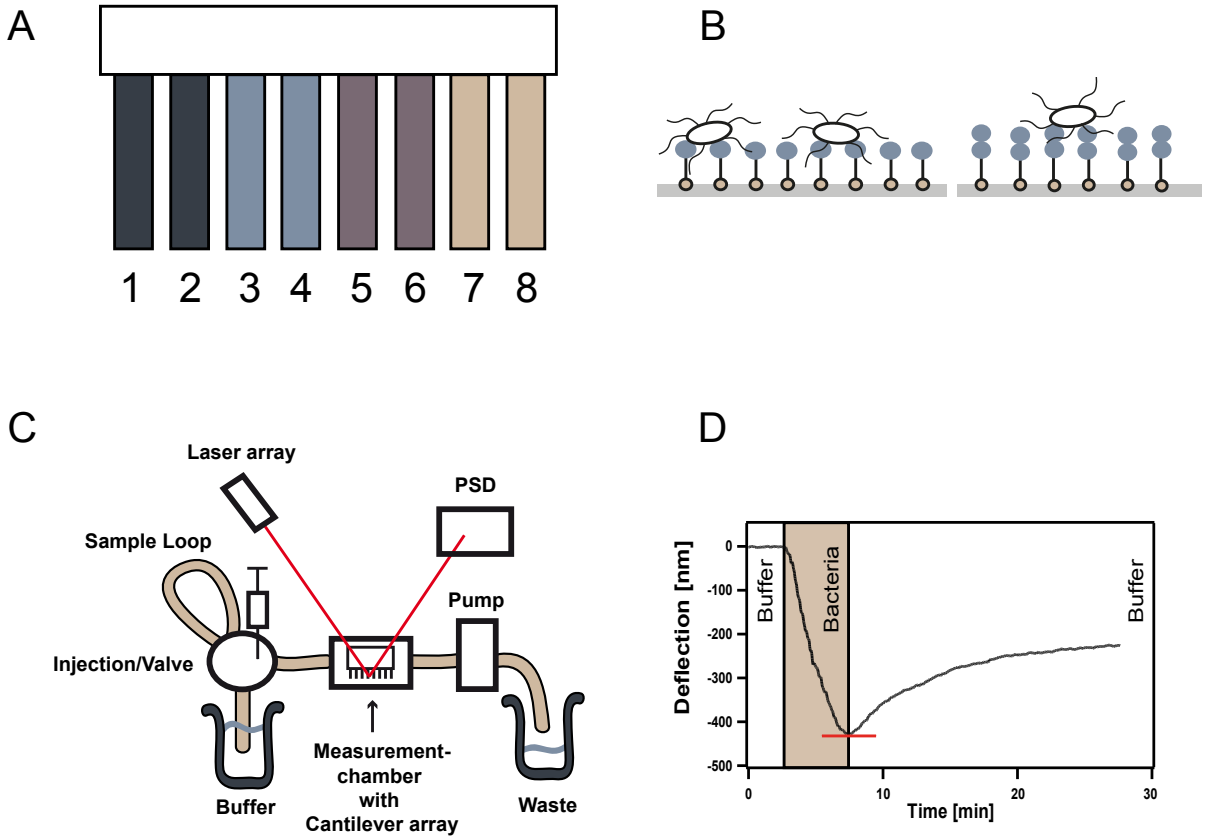

Figure 3.1: Setup for the Measurement of Bacterial Attachment A: The 8 cantilever of the cantilever array are coated with carbohydrates that are installed with thiol groups which enables them to bind to the gold surface of the cantilever. Always two cantilevers were coated with the same carbohydrate. B: The bacteria bind to the exposed end of the carbohydrates. C: The setup of the Cantisens cantilever array system has a flow system with adjustable buffer flow rates and a sample loop where the sample is injected which then is coupled into the buffer stream. The laser array has 8 laser, one for each individual cantilever. The binding of the bacteria on the functionalized canilever causes the cantilever to bend due to a change in surface tension. The change in deflection is detected by a PSD (position sensitive device). The measurement chamber, where the cantilever array is located, is temperature controlled. D: Immediately when the bacteria pass by the cantilever, it starts bending, resulting in a change of deflection that continues until all of the bacteria have passed. The maximal deflection is depicted by a bar. Bacteria that bound reversibly will detach again, leaving only irreversible bound bacteria on the cantilever, hence the deflection signal decreases. Originally published in [72].

deflection signal. Once all bacteria have passed by, the deflection signal decreases, due to the fact that reversibly bound bacteria detach again, until only irreversibly bound bacteria stay attached.
The deflection signal is then analyzed with the Concentris Data Viewer software. The natural occurring drift is corrected with a tilt in the opposite direction, for every new beginning of a sample signal, the signal curve was set to zero, the respective graph was captured and the difference of the deflection values was read out. The results of cantilevers that were functionalized with the same carbohydrates were averaged. These data sets were normalized to the gold coated cantilevers without functionalization.

3.2.3 Time-lapse Microscopy

For the analysis of 2D- and 3D-growth (see chapter 4.3), agar plates with a 18 spot matrix were prepared (see section 3.1). The matrix was designed to ensure that the growth on all 18 spots was identical (spacing and distance of the pipetted colonies, see figure 3.2). The spot distance was chosen so that the biofilms did not grow into each other and no growth inhibition could occur due to nutrient limitations. The small circles have a diameter of 0,5 cm, which correlates with the the maximal colony size for biofilm building strains in the conditions of the microscope after 18 h of growth (previous observations).

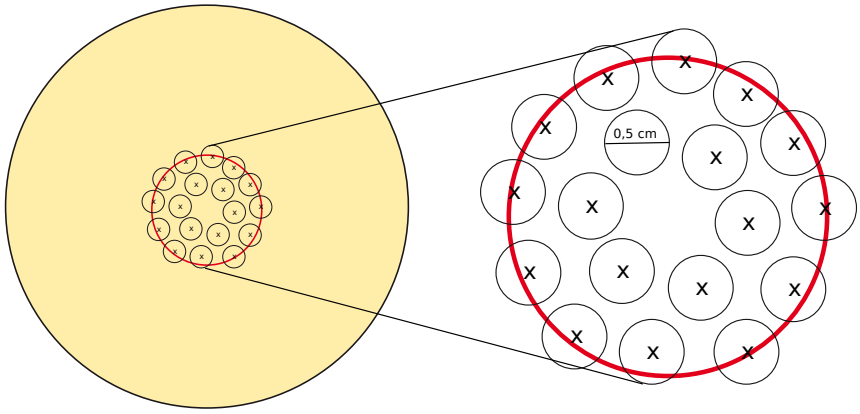

Figure 3.2: Matrix for Droplet Application for Analysis of Biofilm Growth Colonies were spaced as evenly as possible to ensure optimal growth for every spot. The matrix consists of 12 spots in the outer ring, along the maximal movement radius of the objective in the opening of the lid (red circle), and 6 spots in the inner ring. The center was deliberately left free, in order to not confine the spots from every side. The agar plate is represented in tan color.

The prepared plates were observed with a Nikon upright microscope (90i, Nikon, Düsseldorf, Germany). The microscope is equipped with a heat box to control the temperature (kept at 37 °C). In order to ensure stable and constant humidity, the stage was equipped

with an additional cover (Co2 cover from PeCon GmbH, Germany) that minimizes the volume around the plate and keeps the agar plates from drying out. As the opening of this lid is small, the field of work is restricted (red circle in figure 3.2 depicts the center of the objective of the microscope).

The first 90 minutes, an image was taken from every spot in the matrix every 15 min with the 50x magnification objective. The frame of the images (see figure 3.3 A, square a), while only showing a small section of each spot, was chosen in order to represent the average distribution of bacteria (see figure 3.3 B, arrow a) (not at the border of the droplet, as the surface tension of the droplets during application on the agar plate accumulates more bacteria than average).

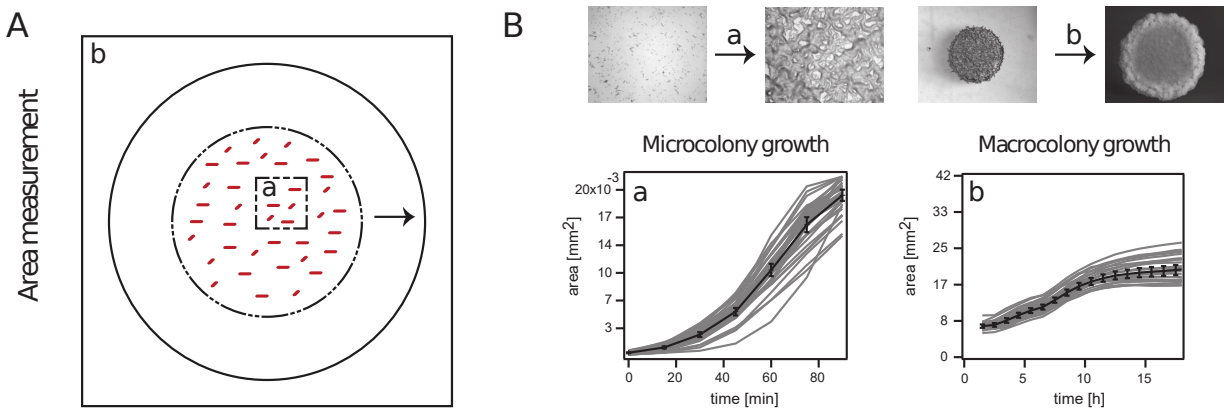

Figure 3.3: Biofilm Growth Analysis using Time Lapse Microscopy A: Schematic for the procedure of the area growth measurements (not in scale). Square a (dotted line) represents the image section of the 50x objective. As the microcolonies grew, the initial area (dotted line circle) was completely covered by bacteria. After 90 minutes, the objective was changed to a 1x objective, the image section is now represented by square b. For the rest of the measurements, the growth of the entire macro-colony (from the dotted line circle to the full line circle) is observed. B: Graph a shows the area for the single measurement curves of the microcolony growth for *B. subtilis* NCIB 3610 in gray. The black curve is the average of the single curves, the error bars are the 95% confidence intervals. Graph b shows the macrocolony growth using the same principle. Part of a figure originally published in [80].

After 90min, the area of the droplet (see figure 3.3 A, dotted line circle) started to fill in completely and subsequently colonies started to grow beyond the border of the initial droplet. With the onset of biofilm matrix production, the colony started to grow vertically as well and therefore it was necessary to now observe the whole spot (see figure 3.3 B, arrow b). The objective was changed to a 1x magnification and for the next 16 hours, images of the whole colonies were taken every hour (see figure 3.3 A, square b).

3.2.4 Image Analysis

Images obtained with the procedure in section 3.2.3 were analyzed using MATLAB R2014a. The images obtained with the 50x objective had to be evaluated by hand, using the free hand draw command to define the outline of single cells and microcolonies, as no automation could be found, that was able to recognize both to full satisfaction, but both structures are present in the images at the same time. The area was then plotted against time (see figure 3.3 B left). The structures in the images, the bacterial macro-colonies, obtained with the 1x objective allowed for automatic image analysis (the script was kindly provided by Benedikt von Bronk), where the area of the colony was calculated and displayed. This was again plotted against time (see figure 3.3 B right).

3.2.5 Profilometry

The profilometer experiments were used for the surface roughness determination as well as colony height analysis (see chapters 4.3 and 4.4). A Nano Focus μsurf profilometer (NanoFocus AG, Oberhausen, Germany) was used. Image analysis was done with the inhouse software μsoft (version 6.0, NanoFocus AG, Oberhausen, Germany) in order to determine the parameters Sq, the root mean square of the surface roughness, and Sz(10) for the height, which represents the mean value between the 5 highest peaks and the 5 lowest values. The Sq parameter (the most commonly used parameter for surface roughness) of a given area A indicates how much the roughness of a surface deviates from a mean [98] and is calculated as follows:

$$Sq = \sqrt{\frac{1}{A}\int_A \int z^2(x,y)dxdy} \tag{3.4}$$

For Sq measurements (for chapter 4.4), one-day old biofilms, plated on an agar plate, were scanned with a 50x objective in a 300 by 320 μ area. If ethanol was applied, the biofilm was covered by it, left for one hour and then discarded. The plates were left for 10 min to dry, in order to remove excess ethanol by evaporation.

For Sz(10) and Sq measurements of single colonies (for chapter 4.3), a 20x objective was used, scanning image sections of 800 x 772 μm. The image sections were chosen to always be on the edge of the biofilm, in order to have a small corner of agar as reference, see figure 3.4 A. This results in a methodical error, as the highest point in some biofilms was in the middle of the colonies and was often lost. But as the intention was to get a relative measure of the height growth, this method seemed more appropriate. The images were

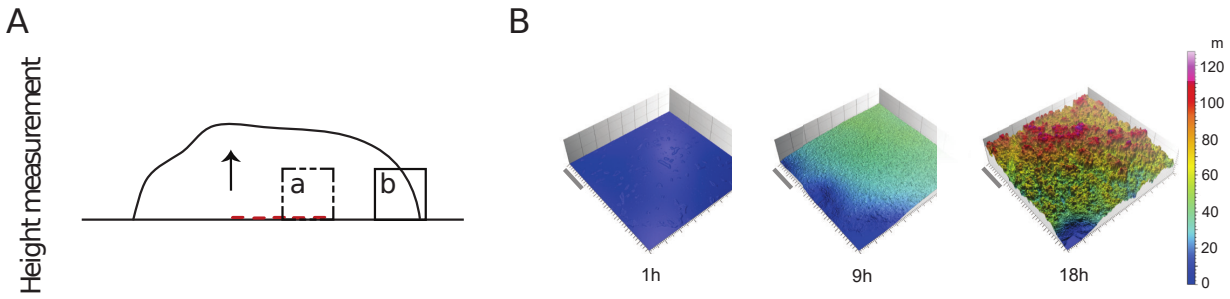

Figure 3.4: Analysis of Biofilm Height Development using Light Profilometry A: Schematic for the procedure of the height growth measurements (not in scale). The image section moves along with the area growth, capturing the edge of the colony on every image. B: Selected images showing the heatmap for the biofilm height, demonstrating the vertical growth of textitB. subtilis NCIB 3610 with single cells at 1h and fully formed biofilm at 18h. These images were the basis for the calculation of the parameters Sz(10) and Sq. Part of a figure originally published in [80], labeling of panels adjusted accordingly.

corrected for the natural tilt of the agar, at least for the first time points (it was not possible to correct the images for later time points without falsifying the results). The topological properties are analyzed and the Sz(10) and Sq values calculated.

3.2.6 Atomic Force Microscopy

The Nano-indentation measurements were performed using a JPK NanoWizard BioScience Atomic Force Microscope (AFM) with the CellHesion module. Soft cantilevers (sQube CP-PNPSSiO-C-5, NanoAndMore GmbH, USA) with silicon dioxide (SiO_2) beads (diameter, 6.62 μm) (recommended for soft, sticky materials) were used, with a resonance frequency of $\approx$ 17 kHz. The information provided by the company on the force constants of the cantilevers of 0,08 N/m was confirmed via thermal noise analysis, as recommended by JPK. This also determined the spring constants (in mN/m) for each cantilever. Additionally a baseline for the sensitivity (in nm/V) was determined for each individual cantilever by fitting the retraction part of a force curve measured on plastic under ethanol. These calibrations are necessary in order to determine the Young's Modulus later on (see chapter 4.4). The agar plates (for reasons of space in the confinements of the AFM, smaller plates with a diameter of 3.9 cm were used for this setup) were prepared as described in section 3.1. In order to reduce electrostatic attraction between the biofilm and the cantilever, the biofilm was covered in 100% ethanol (Sigma-Aldrich, St. Louis, MO, USA) (see figure 3.5 A). The measurement of the surface was done in 8x8 grid of spots, each spot 1,25 μm apart. Contact mode was used with a sample rate of 6000 Hz, a z-length of 20 μm, a set point of 5.0 nN and speed of 5.0 μm/s. This was repeated 10 times on 9 different days. As the ethanol impacts the biofilm, only measurements were taken into consideration for

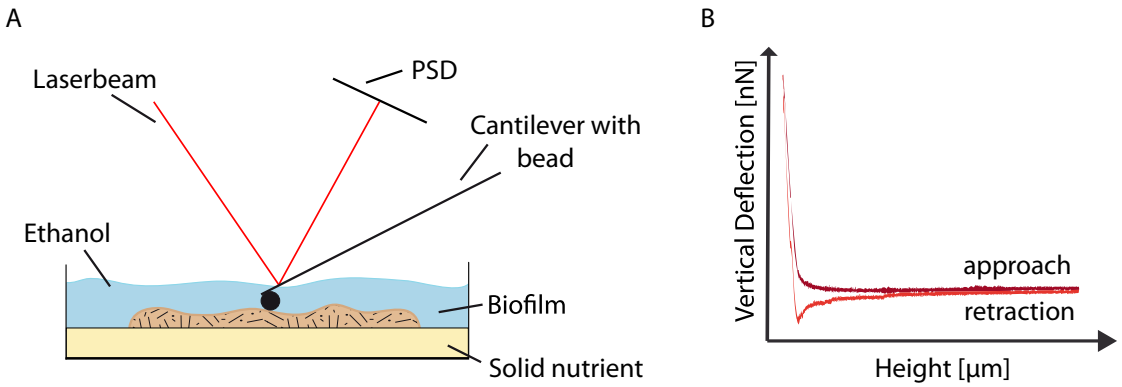

Figure 3.5: Analysis of Biofilm Surface Stiffness using AFM Nano-Indentation Measurement A: Using a cantilever with the SiO_2 beads, indentation measurements were performed. When the cantilever is pushed into the biofilm, the cantilever bends, resulting in a change of reflection of the laser beam, that is detected with the PSD. Prior to the measurement, the biofilm, that grew on the agar plates is covered with 100% Ethanol in order to reduce electrostatic interactions. B: Exemplary measurement curve with the approach of the cantilever to the biofilm surface in dark red, and the retraction in light red. The difference between those curves is the hysteresis resulting from the plastic deformation. Originally published in [99].

the calculation of the Young's Modulus, that were obtained between 10 and 25 minutes after the exposure to ethanol. Prior 10 min, no measurements could be taken for technical reasons. Due to the high roughness of some biofilm surfaces (e.g. of the wild-types), the day to day variances were quite high, as it could not be controlled if the spots were placed on folds or valleys on the biofilm surface. Biofilms with smoother surfaces had lower variances. Hence a minimum of three spots with an area of 10 μm x 10 μm were selected and 64 runs with a distance of 1.25 μm to each other were averaged, resulting in an average elasticity over the whole surface, not in an elasticity of local biofilm surface properties.

The obtained data were analyzed using the JPK Instruments data-processing software, version spm-5.1.7. The Hertz-model [100] for soft cantilevers and spherical tips (see equation 3.5, JPK application note) was applied to the data in order to get the Young's Modulus (exemplary measurement curve in figure 3.5 B). The force-indentation curves measured by the AFM are fitted with the Hertz-model for the respective tip geometry with the Young's Modulus E as the fitting parameter. The Young's Modulus describes the relation between stress and strain of a sample that is stretched or compressed in one direction.

$$F = \frac{E}{1-\nu^2}\left[\frac{a^2+R^2}{2} ln \frac{R+a}{R-a} - aR\right] \tag{3.5}$$

F is the force applied to the cantilever, E is the elasticity modulus, or Young's Modulus, ν the Poisson ratio (the parameter that represents the sample). The exact ratio is not known and was set to 0,5, as the biofilm was assumed to be a elastically deforming material that is perfectly incompressible (0.5 is usually used for soft biological samples (JPK application note)). This will only affect the absolute values and not the relative difference between the biofilm samples. The variable a is the contact radius between the tip and the surface and R the radius of the tip.

3.2.7 Rheology

The bulk viscoelasticity was measured using the shear rheometer MCR 302 (Anton Paar GmbH, Graz, Austria) with a 25-mm plate-plate geometry and 300μm plate separation (see figure 3.6 A).
The moving measurement plate deforms the biofilm (γ) by applying the shear stress σ. These can be used to calculate the storage modulus G [101]:

$$G = \frac{\sigma}{\gamma} \tag{3.6}$$

As the plate oscillates with a sinusoidal frequency f, which creates an oscillatory shear deformation. τ and γ now read as follows:

$$\sigma(t) = \sigma_0 sin(2\pi f t + \delta) \tag{3.7}$$

$$\gamma(t) = \gamma_0 cos(2\pi f t) \tag{3.8}$$

with δ the resulting phase shift. The shear modulus G has two components, the storage modulus G' that represents the energy stored in the material and is therefore the elastic part and the loss modulus G" that represents the energy that is lost, i.e. as heat, which is the viscous part. G can then be written as the complex modulus $G* = G' + iG''$, with:

$$G' = \frac{\sigma_0}{\gamma_0} cos(\delta) \tag{3.9}$$

$$G\text{"} = \frac{\sigma_0}{\gamma_0} sin(\delta) \tag{3.10}$$

In order to guarantee linear material response, experiments were performed with a low torque of 1 μNm, a frequency of 1 Hz and at 21 °C. The shift between the applied shear deformation via the oscillating plate and the measured stress (see figure 3.6 B) is then

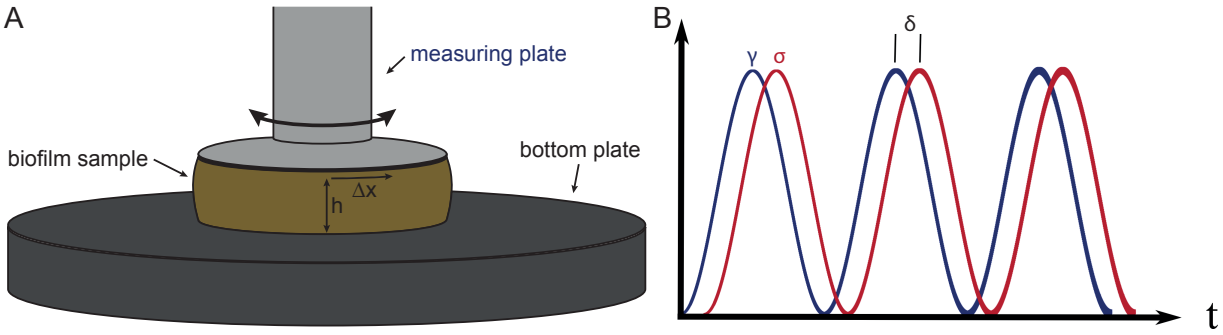

Figure 3.6: Analysis of Biofilm Bulk Stiffness using Macro Rheology A: The biofilm material gathered from fully grown biofilms was pooled and put between the two plates of the rheometer. The measuring plate is oscillating with one Hertz. B: The oscillating blue curve is the applied shear deformation, the red curve represents the resulting shear stress. Originally published in [99].

used to calculate the storage modulus G'.

3.2.8 Mass Determination

For the analysis of total and dried masses (see chapter 4.4), biofilms on agar plates were prepared as described in section 3.1. In order to analyze the influence of the biofilm matrix component γ-polyglutamate on the protection against ethanol induced dehydration, some biofilms have been treated with 99% ethanol before harvesting and some additionally with γ-polyglutamate during growth. The biomass of fully grown biofilms was scraped of of the agar plates and collected in Eppendorf tubes and weighted to determine the total mass. The tubes were then frozen with liquid nitrogen at $-169\,^{\circ}\mathrm{C}$ and left for 8 hours in an Alpha 1-2 lyophilizer (Martin Christ Gefriertrocknungsanlagen GmbH, Osterode am Harz, Germany) at $-55\,^{\circ}\mathrm{C}$ and 2.1 Pa. The tubes were then weighted again, in order to determine the dried mass.

3.2.9 Further Data Processing and Analysis

All data were further analyzed using Igor Pro version 4.06. All calculations like averaging of data and curves, as well as error calculation (standard deviation and Gauss error propagation if required) and plotting were done using this program. Fits were applied to the graphs using Igor Pro version 4.06 as well. In addition to the image analysis done in section 3.2.4, MATLAB R2014a was also used for significance analysis using two-sample t-tests [102] or Tukey's honestly significant difference procedure [103].

4 Contribution of Biofilm Matrix Components to Physical Properties of *Bacillus subtilis* Biofilms at all Phases of Biofilm-Formation

In this thesis, selected physical properties and growth dynamics of the biofilm matrices of *Bacillus subtilis* strains were examined. In all stages of biofilm-formation, the influence of the most important biofilm matrix components on the respective physical properties was investigated. As shown in chapter 2.1.1, biofilm-formation is divided into different stages: the attachment of single bacterial cells to a surface, the growth from microcolonies to macrocolonies with the production of biofilm matrix components and development of characteristic (bio-)physical properties and the eventual release of new single cells closing the circle. This chapter is divided in four sections. The first section 4.1 compares the genomes of the two biofilm producing wild-type strains of *B. subtilis* that were used in this study in order to reveal the presence of biofilm matrix genes in the newly sequenced strain *B. subtilis* B-1. The section also analyzes the gene expression of this strain. Both, comparison and analysis, will give information about which biofilm matrix components will be expected to be present in different steps of biofilm-formation and will ultimately have an influence on the physical properties that are discussed in the following sections. The second section 4.2 examines the first step of biofilm-formation, the attachment of single cells to surfaces. This was done using a cantilever array instrument, with which measurements of different surfaces can be done in parallel, to mention only one of its perks. In the third section 4.3, biofilm colony growth, from microcolony growth to macrocolony growth, was investigated. It was examined which biofilm matrix components have an influence on the lateral and the vertical growth. The fourth and last section 4.4 investigates selected physical properties of mature biofilms. Here, different biofilm matrix components impact

different properties.
For all these analyses, not only the wild-type strains that are able to form complete biofilms were investigated. For the matrix components of interest (see chapter 2.1.2), knock-out mutants were used that lack this specific matrix component in order the be able to determine its influence.

4.1 Prerequisite: Expression of Biofilm Matrix Components in *B. subtilis* NCIB 3610 and *B. subtilis* B-1

For one of the *B. subtilis* strains used in this study, the γ-polyglutamate producing strain *B. subtilis* B-1, no knock-out mutants existed. In order to be able to produce them and in order to classify the strain and analyze its similarities to other closely related strains, the sequence of the genome needs to be known. As this was not yet the case for *B. subtilis* B-1, a genome sequencing was necessary. This was done as described in chapter 3.2.1 and in this process, 90% of the B-1 genome could be assembled in a scaffold of 3.9 Mbp (Mega base pairs)(accessible at the genome data bank under the number CP009684, fist published in [84]) with a G-C content of 47%, which is slightly higher than other for *B. subtilis* strains with around 43% (see genome data bank CP010052). The scaffold was matched to the genome of laboratory strain *B. subtilis* WT168 and the most important biofilm genes involved in biofilm-formation were compared (the comparison was done in the scope of a bachelor thesis by Frederike Moormann [104]). The focus of the comparison was on the genes that produce the key components required for biofilm matrix production in *B. subtilis* NCIB 3610 and *B. subtilis* B-1 (see chapter 2.1.2). *B. subtilis* WT168, although not able to produce biofilm due to the lack of the regulation plasmid, does contain the genes necessary for biofilm production as it is mostly homologue to the biofilm producing wild-type strain *B. subtilis* NCIB 3610 [54]. As laboratory strain, its genome is mapped better. Hence, the genome of *B. subtilis* B-1 was compared to this *B. subtilis* WT168 rather than to *B. subtilis* NCIB 3610. The genomes were compared using the NCBI online tools LAST [85], BLASTx and BLAStn [86]. Table 4.1 (first published in [84] and [99]) shows a list of those important biofilm genes and their homology between *B. subtilis* B-1 and *B. subtilis* WT168 in percent.
The overall DNA homology of *B. subtilis* B-1 and *B. subtilis* WT168 was found to be about 50%. This number, however, does not include very small fragments of DNA that could not be matched with certainty. Together with the consideration of the missing

Table 4.1: Genome Comparison between the Non-Biofilm forming Strain *B. subtilis* WT168 and the newly Sequenced Strain *B. subtilis* B-1 A list of genes involved in biofilm-formation. The genes *tasA*, *epsA-O* and *bslA* are the key-regulators for *B. subtilis* NCIB 3610 biofilms, γ-polyglutamate, encoded by the *ywsC* gene, the major component for *B. subtilis* B-1 biofilms. The other genes are encoding for general biofilm-formation regulation. The NCBI tools LAST and BLASTx, that are available online were used to compare the genome. The position of the gene sequence is the beginning on the genome in the data base. The genome for *B. subtilis* B-1 can be accessed in the GenBank under the number CP009684 and the genome for *B. subtilis* WT168 under the number CP010052.

Gene	Gene Homology (%)	Matrix Component	Position of Gene Sequence (bp) *B. subtilis* B-1 / *B. subtilis* WT168	Source
ywsC	82	γ-polyglutamate	3360079 / 3700627	[69]
tasA	75	matrix fiber	3450573 / 2553866	[66]
epsA-O	78	polysaccharide	2140149 / 3529911	[59]
bslA	74	surface layer protein	2873830 / 3187503	[64]
tapA	72	lipoprotein (assembly of TasA)	3452069 / 2555247	[67]
sipW	72	type I signal peptidase (surface adhesion)	489452 / 2554502	[68]
degU	86	two-component response regulator	628676 / 3645296	[105]
abrB	91	transcription factor	50582 / 45138	[70]
sinR	97	master regulator for biofilm-formation	3450190 / 2552653	[71]

10% of the genome, a calculated maximal homology of 62% could be achieved. This lies within the expected homology between *B. subtilis* subspecies of 58 to 69% [106]. As explained in chapter 2.1.2, the main component of the *B. subtilis* B-1 biofilm matrix, the γ-polyglutamate, which is produced by the *ywsC* gene shows a quite high homology of 82%. Whereas *B. subtilis* WT168 (and the closely related strain *B. subtilis* BD630, which was used in this study when a non-biofilm forming strain was needed for reference) does not produce biofilm, strain *B. subtilis* NCIB 3610 does produce biofilm. The main reason for the lack of (proper) biofilm production in strain *B. subtilis* WT168 is the fact that as a laboratory strain it is highly domesticated for molecular and genetic studies as a representative for the gram-positive bacterium *B. subtilis* [53]. Four mutations on biofilm relevant genes and the loss of the regulation plasmid [54] have impaired the colony morphology compared to the wild-type strain *B. subtilis* NCIB 3610. Although all of those strains possess the *ywsC* gene, only the *B. subtilis* B-1 biofilm was described to produce a matrix mainly consisting of γ-polyglutamate. Therefore, it is surprising that the genes for the key components for the *B. subtilis* NCIB 3610 biofilm, the fiber forming TasA, the exopolysaccharide EpsH, encoded by the *epsA-O* operon and the surface layer protein BslA are present in *B. subtilis* B-1 and show homologies between 74 and 78%.
The comparison of the genes also showed that the order of the genes within the whole genome are not the same in *B. subtilis* B-1 and *B. subtilis* WT168 (see table 4.1). *B. subtilis* WT168 is part of the subspecies *Bacillus subtilis subtilis*, other well known subspecies of *B. subtilis* are *natto*, *vallismortis* and *spizizenii* [107]. *B. subtilis* B-1 shows an overall homology of around 58% to the *B. subtilis spizinenii* strains found in the genome data bank (namely *B. subtilis* TU-B-10 and *B. subtilis* W23). This leads to the conclusion that *B. subtilis* B-1 is not part of the same subspecies *Bacillus subtilis subtilis* as the other strain that is in the main focus of this study, *B. subtilis* NCIB 3610, but is closer related to the subspecies *B. subtilis spizinenii*. With its biofilm matrix that mainly consists of γ-polyglutamate, *B. subtilis* B-1 is an other interesting strain to investigate in order to examine the influence of different biofilm matrix components to the physical properties that are studied in this thesis.

Given the wide diversity in *B. subtilis* strains, with some of them being able to form biofilm, it would be interesting to have an analysis of the exact composition of their biofilm matrix. But as the biofilm matrix consists of proteins, carbohydrates and DNA it is difficult to determine the actual amounts of produced biofilm matrix components. In order to analyze if the genes encoding key biofilm matrix elements and genes whose gene products are involved in biofilm-formation are expressed, a gene expression analysis was

Table 4.2: p-Values for Gene-Expression Data shown in Figure 4.1 The mean values for mRNA production have been tested pairwise with a student t-test in order to compare the amount for the *ywsC* gene, the main component of *B. subtilis* B-1 with the corresponding matrix component producing genes expressed in *B. subtilis* B-1 representing the main biofilm matrix components for *B. subtilis* NCIB 3610 biofilms. Pairs are significantly different for p-values lower than 0.05.

Gene	p-Values for Fig.4.1A	p-Values for Fig.4.1B
ywsC	n/a	n/a
tasA	3.659e-05	4.2949e-15
bslA	0.00048	8.282e-15
epsH	0.7039	0.0035

performed as described in chapter 3.2.1. The amount of mRNA present at the time point of harvesting the biofilm and the bacteria inside was measured. The amount of mRNA present in the cells is no true measure for the actual amount of produced biofilm matrix elements, but will show which elements can be expected to be present inside the biofilm matrix. As in chapter 4.4 the samples of mature biofilm are taken after 18 hours of growth, that was also the time point at which the gene expression analysis was performed. A second time point, 10 hours of growth, was chosen as reference at the beginning of biofilm maturation.

The gene expression analysis (first published in [99]), shown in figure 4.1, where all the key biofilm forming genes express at low levels in *B. subtilis* B-1, significantly lower than the housekeeping gene 16S rRNA, a conserved gene that serves as positive control, lets to the conclusion that the *B. subtilis* B-1 biofilms matrix may also contain low amounts of the proteins BslA, TasA and the exopolysaccharide EpsH at both time points. The expression of *ywsC* in *B. subtilis* B-1 for 10 and 18 hours, represented by the threshold cycle (C_T) values, differs significantly with a p-value of 0.0033, which was expected as 10 hours is just at the beginning of biofilm maturation. The C_T values for 10 hours for the *B. subtilis* NCIB 3610 biofilm genes, *tasA* and *bslA*, expressed in *B. subtilis* B-1 differ significantly from the C_T value for *ywsC*, the main gene in the *B. subtilis* B-1 biofilm-formation. Whereas all C_T values of the *B. subtilis* NCIB 3610 genes expressed in *B. subtilis* B-1 are significantly different than for *ywsC* for 18 hours (see table 4.2).

As *B. subtilis* B-1 was described to produce a biofilm matrix that mainly consists of γ-polyglutamate [69], it was interesting to find that not only were the three genes of *B. subtilis* NCIB 3610 for its biofilm matrix key components present in the *B. subtilis* B-1 genome and homologue, but also that those genes are indeed expressed. The *ywsC* gene

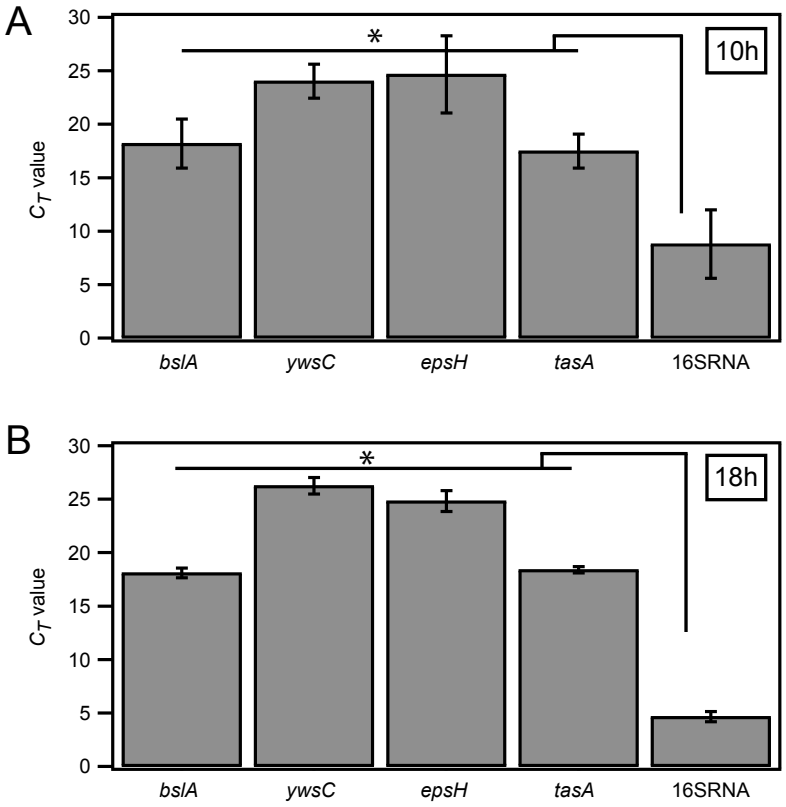

Figure 4.1: Expression of the Genes encoding Key Biofilm Matrix in *B. subtilis* B-1 A: Amount of mRNA produced during gene expression in *B. subtilis* B-1 for the key components of the two wild-type biofilms, *B. subtilis* NCIB 3610 and *B. subtilis* B-1, for 10 hours after plating. B: For 18 hours after plating.
The bars are the mean values of three experimental and three analytical replicates. The error bars are the standard deviations. The star indicates that the comparison between the C_T values for the genes and the conserved 16S rRNA housekeeping gene with one way ANOVA and Tukey's honestly significant difference test found the ensemble of genes significantly different than the control. Additionally, pairwise significant t-test were performed, the results are given in table 4.2.

for γ-polyglutamate production is present in *B. subtilis* NCIB 3610 as well, but is not expressed.

This study showed that although the genome of the two wild-type strains is similar, even homologue in the genes involved in biofilm production, and while *B. subtilis* B-1 does indeed express the genes for the key component of the biofilm matrix produced by*B. subtilis* NCIB 3610, the biofilm matrices of both strains vary in their key components. The biofilm matrix of *B. subtilis* B-1 consists mainly of γ-polyglutamate [69], while the biofilm matrix of *B. subtilis* NCIB 3610 has three key components, the proteins TasA and BslA and the polysaccharide produced by the *epsA-O* operon [56, 62]. While there are other genes involved in biofilm matrix production (see table 2.1), these four biofilm matrix components are in the focus of this thesis, which is analyzing the physical properties of both biofilm matrices and highlighting similarities and differences.
Unfortunately, even with the genome sequence of *B. subtilis* B-1, it was not yet possible to construct knock-out mutants for those four interesting biofilm genes. The knock-out mutants for *B. subtilis* NCIB 3610 were obtained from other labs (see table 3.1).

4.2 Biofilm Matrix interferes with Attachment of Planctonic Cells to Surfaces

As described in chapter 2.1.1, the first step of biofilm-formation is the attachment of planctonic cells to a given surface of organic or inorganic nature (see chapter 2.1). Once bacteria are bound to a surface, they will begin growing and developing the biofilm matrix, leading to infections, clogging or other harmful consequences (see chapter 1). When the biofilm is matured, a (complete) removal is much harder to accomplish. In order to be able to prevent biofilm growth, one possibility is to prevent attachment in the first place. Therefore, it is necessary to understand the underlying interactions facilitating or hindering binding of single bacteria to surfaces with distinct properties. In the following section, the binding of single cells to different surfaces and the interactions affecting this process are studied using a cantilever array instrument as described in chapter 3.2.2 (results and figures of this section first published in [72]). This method is highly sensitive and has no need of a modification of the cells. It is used to detect various molecules [108, 109] and bacteria [108,110,111]. It is even sensitive enough to identify chemicals and gases [108,112]. Here, the main advantage is that this system allows for a measurement of the attachment of single cells in solution with several cantilevers, representing different surface conditions, in parallel.

Not only do the surface properties have an influence on the binding quality of the bacteria [94], the matrix components that make up the biofilm play their role in the interaction as well. Although the binding of single cells takes place way before the actual formation of the biofilm, an ongoing basal expression of the different proteins and carbohydrates might also benefit the binding to a new surface. For this study, gold was chosen as an exemplary metal surface, as in industry and medicine [113–117] binding of bacteria on metal surfaces are crucial to prohibit. Another advantage of gold is the strong interaction between the bacteria and the surface leading to a strong deflection signal [118, 119].

As a first step to characterize the binding of *B. subtilis* NCIB 3610 on various surfaces, the binding to gold was analyzed (see figure 4.2). The wild-type shows an average deflection of 270 ± 30 nm, a strong signal for the used optical density (OD_{600}) of 0.1. In order to determine if one of the up to this point only basaly expressed biofilm matrix components influences the binding to a gold surface with molecular interactions, knock-out mutants were used. For *B. subtilis* NCIB 3610, there are three biofilm matrix elements of interest (see chapter 2.1.2). Two proteins, BslA and TasA, and a carbohydrate encoded by the *epsA-O* operon. For the knock-out strains unable to produce one particular biofilm matrix component, the maximal average deflection is 370 ± 30 nm for *B. subtilis* NCIB 3610

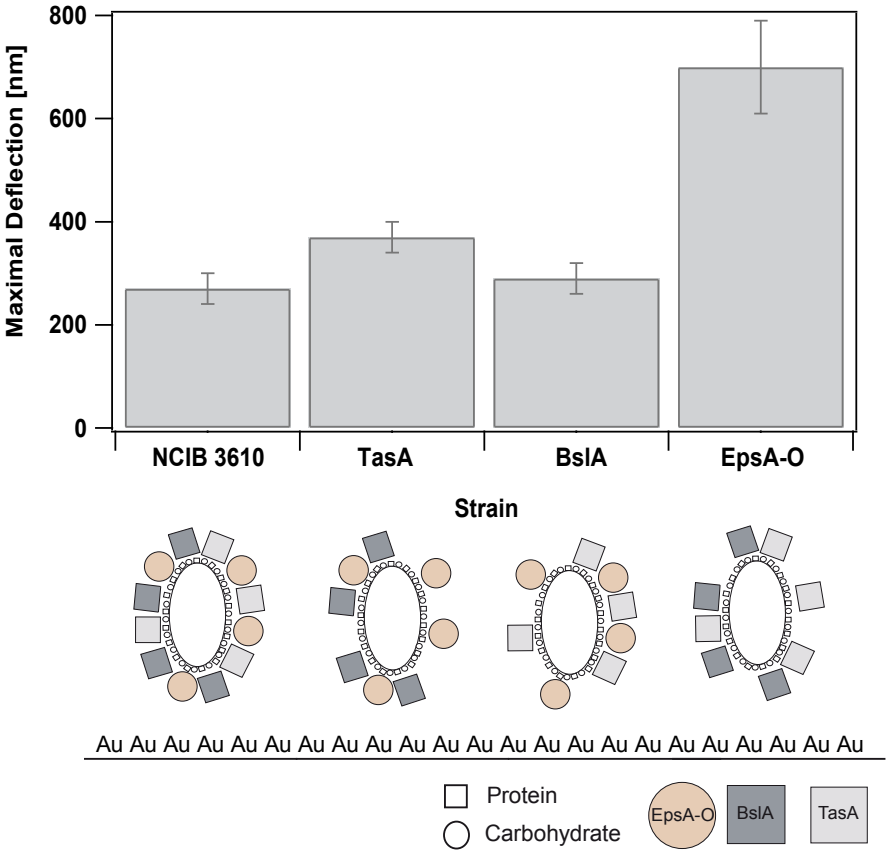

Figure 4.2: Influence of Biofilm Matrix Components on Binding to Gold Surface for *B. subtilis* NCIB 3610 and Strains Unable to Produce a Particular Biofilm Matrix Component The cell membrane (small symbols) and the components of the respective biofilm matrix (large symbols) are depicted schematically (not to scale), with proteins as squares and carbohydrates as circles. For each knock-out strain of *B. subtilis* NCIB 3610, the possible remaining biofilm matrix is shown. The graph shows the maximal averaged deflection of the gold coated cantilevers for each strain. Error bars represent the standard deviation. Exact values are shown in table 4.3.

lacking TasA and 290 ± 30 nm for *B. subtilis* NCIB 3610 lacking BslA respectively (see table 4.3). The *B. subtilis* NCIB 3610 knock-out mutant that is lacking the polysaccharide encoded by the *epsA-O* operon on the other hand, shows a huge increase for the deflection with 700 ± 90 nm, which is about doubled. (As was stated in chapter 2.1.2, the expression of the *epsA-O* operon is necessary for the production of BslA. Therefore, the schematic depiction of the biofilm matrix for this knock-out mutant in figure 4.2 is not correct. The figure was not changed as it was published like this and the results of the study are not affected.)

Table 4.3: Values for the Maximal Averaged Deflection shown in Figure 4.2 Errors are the standard deviation.

Strain	Maximal Deflection [nm]
B. subtilis NCIB 3610	270 ± 30
B. subtilis NCIB 3610 lacking TasA	370 ± 30
B. subtilis NCIB 3610 lacking BslA	290 ± 30
B. subtilis NCIB 3610 lacking *epsA-O*	700 ± 90

For the wild-type strain, as seen in the schematic in figure 4.2, the binding can occur with either the carbohydrates or the proteins in the cell membrane, or, as assumed, with the carbohydrates or proteins that are already basally expressed for the biofilm matrix by the planctonic cells. A lack of one of the matrix proteins does not significantly change the binding to the gold surface. For the *B. subtilis* NCIB 3610 strain lacking *epsA-O*, only the biofilm matrix proteins (mainly TasA) additionally to the proteins and carbohydrates in the cell membrane are present, leading to a strong binding signal. This translates to a strong binding via gold-protein interaction, attributed to the thiol groups in the proteins [118].

Those findings lead to the conclusion that proteins are most important for binding of the bacteria to the gold surfaces or from another point of view, present carbohydrates reduce the binding to gold by 38%.

In order to further investigate the influence of carbohydrates to the attachment to gold surfaces, the gold coated cantilevers were functionalized with different carbohydrates (see chapter 3.2.2). For this test, two monocarbohydrates were chosen, galactose and mannose, as those can serve as nutrient source for many bacteria. Additionally, the disaccharide lactose was chosen, as biofilm-formation is a huge problem in the food industry where this

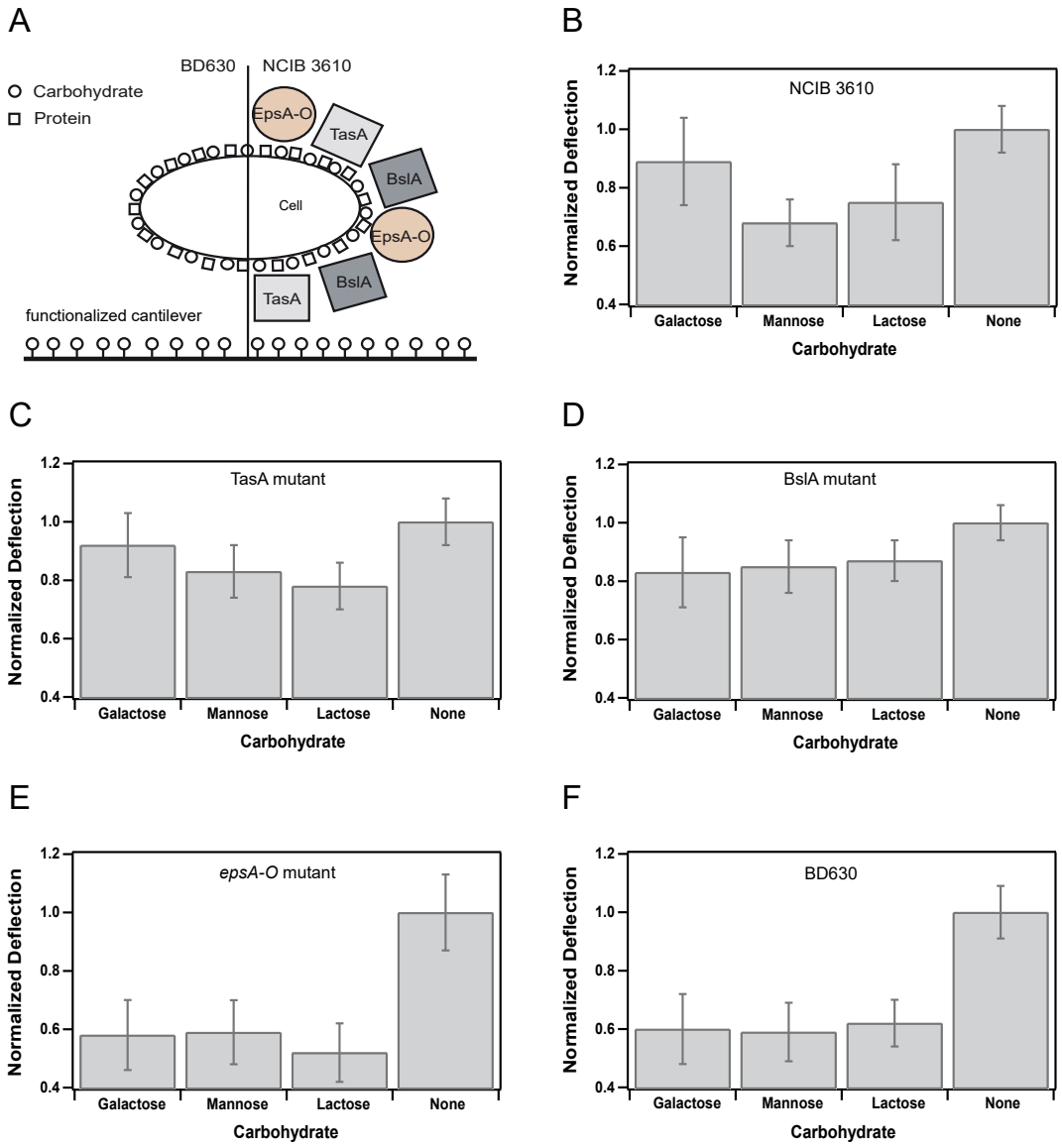

Figure 4.3: Carbohydrate Coating reduces Attachment of *B. subtilis* NCIB 3610 Strains to Gold Surfaces A) Schematic of the cell membrane of *B. subtilis* BD630, the non biofilm producing strain and of the biofilm producing strain *B. subtilis* NCIB 3610 with its matrix components binding to a carbohydrate coated cantilever. B-F) Average deflection of various *B. subtilis* strains, normalized to the values obtained for the uncoated gold cantilevers. Error bars represent the standard deviation following Gaussian error propagation. B) shows the attachment strength for *B. subtilis* NCIB 3610, C) for the *B. subtilis* NCIB 3610 lacking TasA mutant, D) for the *B. subtilis* NCIB 3610 lacking BslA mutant, E) for the *B. subtilis* NCIB 3610 lacking *epsA-O* mutant and F) for *B. subtilis* BD630. Exact values are shown in table 4.4. Figure complemented with strain names compared to the originally published one in [99].

sugar is often found. As a control, the non biofilm-forming strain *B. subtilis* BD630 was included as well. All maximal averaged deflections for each carbohydrate were subsequently normalized to the maximal averaged deflection of the unfunctionalized cantilever for each bacterial strain respectively. For the wild-type *B. subtilis* NCIB 3610 (figure 4.3 B) the deflection for the binding on the various carbohydrates, galactose, mannose and lactose, is reduced compared to the binding to gold by about 23% (for exact data see table 4.4), further punctuating the finding that carbohydrates are able to reduce binding to metal surfaces. A difference between the carbohydrates, especially between the monosaccharides mannose and galactose and the disaccharide lactose, could not be found. It was not surprising to find this outcome for galactose and lactose, as *B. subtilis* NCIB 3610 does not possess an uptake system for those sugars [120,121]. There was also no difference between those two carbohydrates and mannose, although there is an uptake system for mannose in *B. subtilis* NCIB 3610 [122]. Therefore, there probably is no specific interaction happening between the bacteria and the sugar in this form.

Table 4.4: Maximal Normalized Deflection as shown in Figure 4.3 Errors are the standard deviation following Gaussian error propagation.

Carbohydrate	*B. subtilis* NCIB 3610	*B. subtilis* NCIB 3610 lacking TasA	*B. subtilis* NCIB 3610 lacking BslA	*B. subtilis* NCIB 3610 lacking *epsA-O*	*B. subtilis* BD630
Galactose	0.89 ± 0.15	0.92 ± 0.11	0.83 ± 0.12	0.58 ± 0.12	0.60 ± 0.12
Mannose	0.68 ± 0.08	0.83 ± 0.09	0.85 ± 0.09	0.59 ± 0.11	0.59 ± 0.10
Lactose	0.75 ± 0.13	0.78 ± 0.08	0.87 ± 0.07	0.52 ± 0.10	0.62 ± 0.08
Gold	1.00 ± 0.08	1.00 ± 0.08	1.00 ± 0.06	1.00 ± 0.13	1.00 ± 0.09

This was also found for both protein knock-out mutant strains, which reduce the binding by 16% for *B. subtilis* NCIB 3610 lacking TasA and 15% for *B. subtilis* NCIB 3610 lacking BslA respectively (figure 4.3 C & D) on any of the carbohydrates.

These findings lead to the conclusion that carbohydrates seem to interfere with the interaction of the thiol-groups present in either the proteins of the (basally) expressed biofilm matrix or the proteins in the cell membrane and the gold surface.

In order to further prove this theory, the *B. subtilis* NCIB 3610 mutant lacking *epsA-O* was analyzed for its ability to bind to the carbohydrates. With the carbohydrate EpsH

missing, the binding was expected to be not as reduced as for the other mutants, as the protein-gold interaction analogue to the experiments described above should be facilitated. But surprisingly, the binding of the *B. subtilis* NCIB 3610 strain lacking *epsA-O* was even more reduced, the mean decrease is 44%. An explanation could be, that the bacteria use the carbohydrates provided by the biofilm to bind to the carbohydrates on the surface of the cantilever via carbohydrate-carbohydrate interactions. These are already described for eucaryotic cell adhesion [123–125]. In order to strengthen that hypothesis, the non biofilm-forming strain *B. subtilis* BD630 was analyzed that does not produce biofilm matrix components, including the carbohydrate. Here, a similar reduction of 40% could be observed. For this strain, binding in general is probably supported by unspecific carbohydrate-carbohydrate or protein-carbohydrate interactions between elements in the cell wall and the cantilever surface.

In summary, this study showed how basal expression of biofilm-matrix components, especially the exopolysaccharides, affect the initial attachment of planctonic cells to metal and carbohydrate coated surfaces.

4.3 Biofilm Growth determined by Biofilm Matrix Components

As described in chapter 2.1.1, the next step in the life cycle of biofilms after the attachment of single cells is the growth of the bacteria and the expression of the biofilm matrix. Of course for biofilm colonies, like for every bacterial culture, the environmental conditions like temperature or nutrient availability are the determining factors contributing to growth. Before biofilm matrix expression, biofilm cultures grow lateral by bacterial cell division into microcolonies. With increasing density and the onset of biofilm matrix production the colony will start to grow vertically as well and is then referred to as macrocolony. If biofilm growth can be observed and quantified and characteristics attributed to biofilm matrix components, biofilms (and eventually the biofilm forming bacteria themselves) can be identified, which will consequently help preventing biofilm-formation and removing harmful bacteria as soon as possible.
In order to analyze if and how the biofilm matrix components affect the two growth phases, three characteristic traits were observed. First, the lateral growth is investigated, measuring the area that is covered by the colony as described in chapter 3.2.3 with time-lapse microscopy both for micro- and macrocolonies. For the second parameter, the vertical growth, the height and surface roughness of macrocolonies are determined as described in chapter 3.2.5 using light profilometry. The light profilometer, while mainly used for surface roughness measurements, can also provide a contactless and fast method to analyze the topography and thereby a height profile of the surface in question. The profilometer measurements were done in collaboration with and image analysis was performed by Carolina Falcón García (results and figures of this section first published in [80]).

The two wild-type strains *B. subtilis* NCIB 3610 and *B. subtilis* B-1 that differ in their biofilm matrix composition are compared to the non-biofilm forming strain *B. subtilis* BD630.
As the biofilm colony grows, starting from single cells in a predetermined area, microcolonies form and start closing the initial area. Once only some small patches are left open, the biofilm starts growing in height as well and it starts expanding outward. Biofilm colonies that are 18 hours old have a size of 2-3 mm (see figure 4.4 A). This growing process is of course biased due to the geometry that is used to spot the biofilm on the plates, as in natural environments, the spots were bacterial biofilms form, will not be perfectly circular, as the pipetted spots are. But the observed effects hold true, as also randomly streaked out single cells on agar form circular colonies. Figure 4.4 B shows the growth of those microcolony patches as they cover the image section (image section is a little over

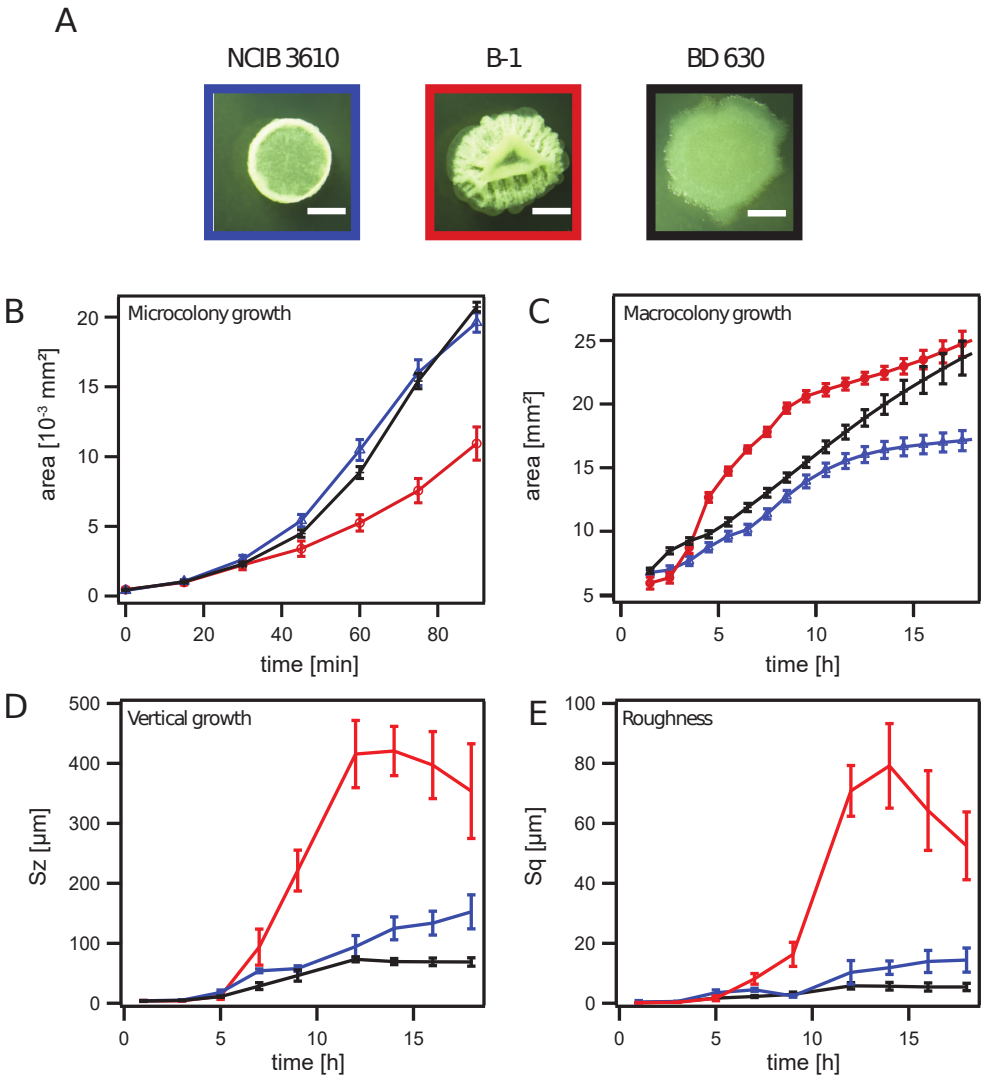

Figure 4.4: Biofilm Colony Growth for the Wild-type Strains *B. subtilis* NCIB 3610, *B. subtilis* B-1 and *B. subtilis* BD630 A: Images of fully grown biofilm colonies. The scale bar represents 1mm. B: Microcolony area growth for the wild-type strains, *B. subtilis* NCIB 3610 (blue), *B. subtilis* B-1 (red) and *B. subtilis* BD630 (black) between 0 minutes and 90 minutes after plating. C: Macrocolony area growth starting 90 minutes after plating until 18 hours. D: Height growth of biofilm colonies represented by the Sz(10) value. E: Surface roughness of biofilm colonies represented by the Sq value. Error bars are the 95% confidence interval.

20x10-3 mm2 in size, after 90 min some strains have filled this area completely).

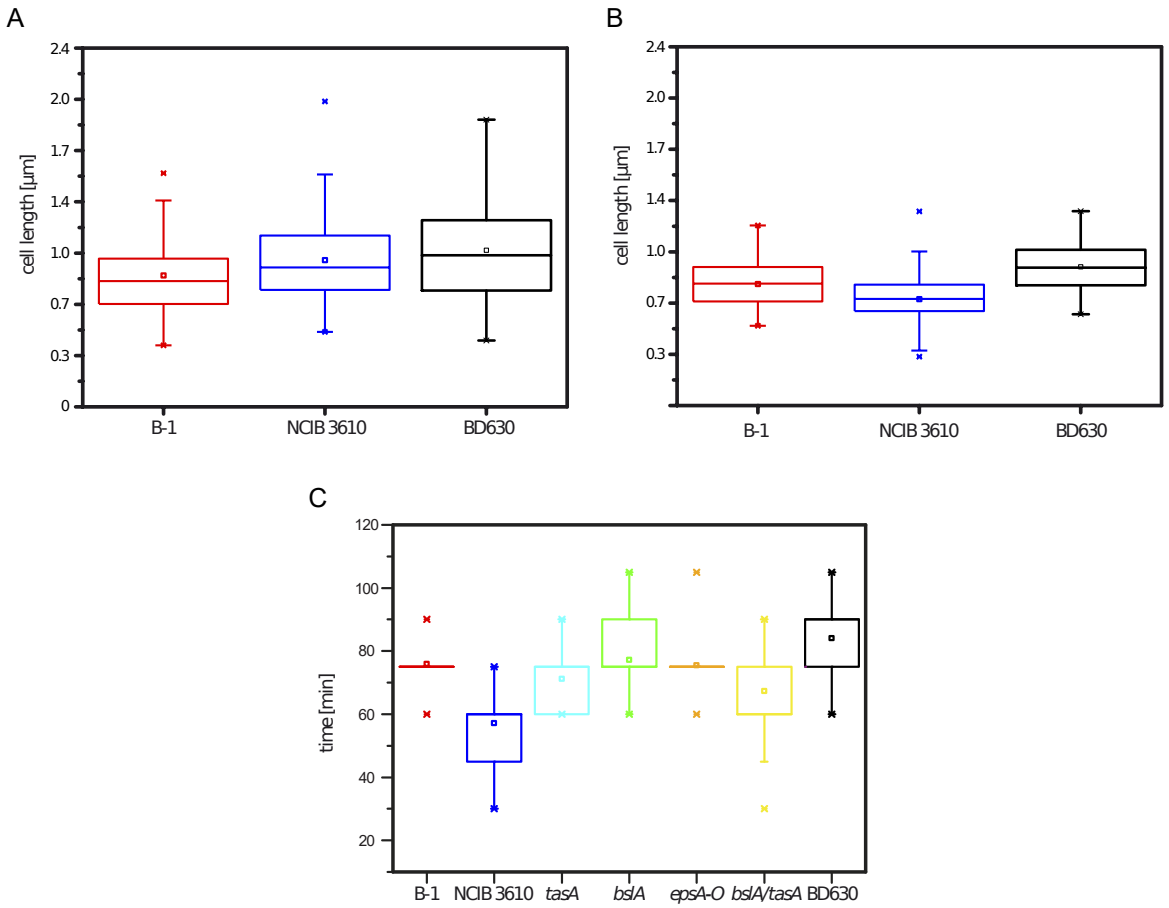

Figure 4.5: Cell Length Comparison for the *B. subtilis* Strains A: Cell length distribution at 0 min presented in a box plot for the three wild-type strains *B. subtilis* B-1 (red), *B. subtilis* NCIB 3610 (blue) and *B. subtilis* BD630 (black). The box plot shows the maximal and minimal values (stars), the 25, 50 (also called median) and 75 percentiles (lower, middle and upper bar of the box) and the 95 percentiles, represented by the bars. B: Cell length distribution at 60 min. C: Distribution of the time points of the beginning of 3D-growth for all strains. *B. subtilis* B-1 is displayed in red, *B. subtilis* NCIB 3610 in blue, *B. subtilis* BD630 in black, *B. subtilis* NCIB 3610 lacking TasA in turquoise, *B. subtilis* NCIB 3610 lacking BslA in green, *B. subtilis* NCIB 3610 lacking *epsA-O* in orange and *B. subtilis* NCIB 3610 lacking BslA/TasA in yellow. Panels rearranged compared to figure originally published in [80].

B. subtilis B-1 biofilms, although large as a colony, start out growing slower than the other wild-type strains. A possible reason for this effect could be the cell size, as starting number of cells and the division time is the same for all the *B. subtilis* strains used in this study. But figure 4.5 A and B shows, that the initial cell lengths and the cell length after at least one division does not differ from that of the other wild-types. Another explanation could be an earlier beginning of the vertical growth, but as figure 4.5 C shows, this is also not

the case. One last possibility could be, that *B. subtilis* B-1 cells are held closer together by the γ-polyglutamate, but that, unfortunately, was not measurable within this study.

After reaching the macrocolony growth phase, *B. subtilis* B-1 catches up and reaches larger area coverage than *B. subtilis* NCIB 3610 in shorter times. This is probably due to a higher biomass production (also see chapter 4.4). The non-biofilm producing strain *B. subtilis* BD630 reaches a comparable, if not larger, area size. A possible explanation could be that this is due to a lack of notable vertical growth. In a biofilm, during matrix production and biofilm maturation, the vertical growth could be more distinct than in non-producing strains.

In order to further quantify the biofilm growth, the height was analyzed using light profilometry (see chapter 3.2.5) by determining the surface parameter Sz(10). This was done for the macrocolony growth only, as vertical growth is only occurring this phase. Although first signs of the vertical growth start to become visible at around 60 to 75 minutes after spotting the single cells onto the plate, when the first layers of bacteria on the agar plate start to build. This is not yet the actual vertical biofilm growth, as every bacterial colony will build up a couple of layers of bacteria as cells divide and push against each other due to spatial restriction. The vertical biofilm growth starts approximately 5-6 hours after spotting, depending on the strain (see figure 4.4 D). As the images in figure 4.4 A already suggests, *B. subtilis* B-1 colonies grow much higher than *B. subtilis* NCIB 3610 biofilm colonies, which is, despite being a biofilm former, not growing that much higher than the non biofilm producer *B. subtilis* BD630. Both the *B. subtilis* B-1 and the *B. subtilis* BD630 start to saturate towards the end.
For all analyses, a sigmoidal growth was assumed as this holds true for all bacterial growth, first growing with an exponential rate and then saturating, which fits for this data within the error margins (except the *B. subtilis* BD630 colony, which does not saturate within the time frame of the experiments). Parallel to the height parameter, the surface roughness Sq was analyzed, as this is the first visible distinction between the morphology of the biofilm producing strains and the non biofilm producing strain. The images give a first clue about which of the colonies will be the roughest. Whereas *B. subtilis* BD630 colonies stay almost smooth, *B. subtilis* NCIB 3610 biofilms show a rougher surface, especially at the edges. *B. subtilis* B-1 biofilms with their pronounced winkles are even 5 times rougher (see figure 4.4). Due to the measurement method and the strongly pronounced wrinkles in *B. subtilis* B-1 biofilms, the errors increase towards the end of the experiment.
As stated above, the number of starting cells and the cell size and division time are very

similar in all the three *B. subtilis* wild-type strains. Therefore it leads to the conclusion that the presence (or absence in the case of *B. subtilis* BD630) of a biofilm matrix is responsible for the differences in those growth parameters.The biofilm matrix elements could serve as a "glue" that will hold bacteria together restricting fast area coverage in the case of *B. subtilis* B-1 but later on serve as "filler" due to the biomass produced, which results in a large biofilm colony with high prominent wrinkles. Whereas the absence of a biofilm matrix is favoring lateral growth for *B. subtilis* BD630 compared to *B. subtilis* NCIB 3610, which in turn is able to grow higher with its biofilm matrix elements giving the necessary strength.

In order to determine the matrix component responsible for the differences in growth, the same analyses were done for the knock-out mutants of *B. subtilis* NCIB 3610 as well. While the by *B. subtilis* NCIB 3610 lacking TasA produced biofilm still has the same morphology as the *B. subtilis* NCIB 3610 biofilm, the *B. subtilis* NCIB 3610 lacking BslA and *B. subtilis* NCIB 3610 lacking *epsA-O* biofilms are smooth and glossy (see figure 4.6 A). The microcolony growth is quite similar for all strains, which was to be expected, as all strains are derivatives from the same *B. subtilis* strain NCIB 3610, and in the early growth phase, the differences between the strains, namely the biofilm matrix components, are not dominant yet. For the macrocolony growth, *B. subtilis* NCIB3610 and *B. subtilis* NCIB 3610 lacking TasA also do reach similar area coverage. As *B. subtilis* NCIB 3610 lacking TasA visibly looks like its wild-type strain (top view), this finding is not surprising. The biofilm colony of *B. subtilis* NCIB 3610 lacking BslA on the other hand, while initially being delayed in the lateral growth, surpasses the area covered of *B. subtilis* NCIB3610 at around 10 hours, and is then significantly larger (one way ANOVA and Tukey's honestly significant difference tests were performed). This finding suggests that the surface protein BslA constrains the area growth, probably by holding the biofilm matrix more tightly together.
For the mutant strains *B. subtilis* NCIB 3610 lacking *epsA-O* and *B. subtilis* NCIB 3610 lacking BslA, the maximal height of the biofilm colonies is decreased as compared to the *B. subtilis* NCIB 3610 wild-type biofilm. As mentioned previously in chapter 2.1.2, the production of BslA is dependent on the carbohydrate from the *epsA-O* operon. Therefore, the reduction of biofilm height in those two mutant strains can probably be attributed to the missing carbohydrate, which serves as biomass to fill out the biofilm. For the *B. subtilis* NCIB 3610 lacking TasA biofilm colonies, an increase in biofilm height was observed. As the TasA protein is a fiber forming protein that is described as being the scaffold for the structural integrity (see chapter 2.1.2) in *B. subtilis* NCIB 3610 biofilms, the fact that it is giving a "rigid" framework, while enabling lateral and vertical growth, is probably

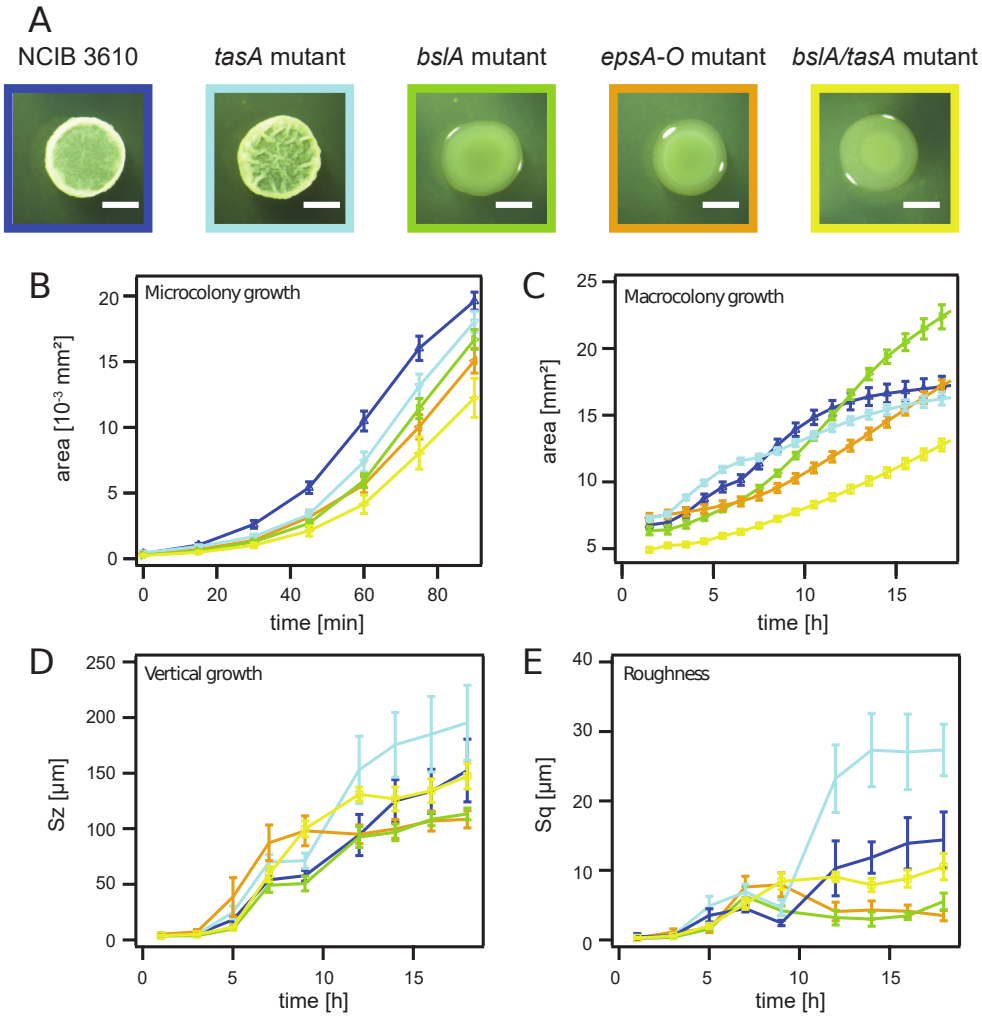

Figure 4.6: Biofilm Matrix Components influence Biofilm Growth A: Images of fully grown biofilm colonies. The scale bar represents 1 mm. B: Microcolony area growth for the wild-type strain *B. subtilis* NCIB 3610 (blue) and *B. subtilis* NCIB 3610 lacking TasA (turquoise), *B. subtilis* NCIB 3610 lacking BslA (green), *B. subtilis* NCIB 3610 lacking *epsA-O* (orange) and *B. subtilis* NCIB 3610 lacking BslA/TasA (yellow) between 0 minutes and 90 minutes after plating. C: Macrocolony area growth starting 90 minutes after plating until 18 hours. D: Height growth of biofilm colonies represented by the Sz(10) value. E: Surface roughness of biofilm colonies represented by the Sq value. Error bars are the 95% confidence interval.

constricting the maximal dimensions at the same time. Similar findings were observed for the surface roughness. The biofilm formed by *B. subtilis* NCIB 3610 lacking TasA is rougher than the biofilm formed by the wild-type *B. subtilis* NCIB 3610. As was already seen on the images for the colonies in figure 4.6, the biofilms for the *B. subtilis* NCIB 3610 lacking *epsA-O* and *B. subtilis* NCIB 3610 lacking BslA mutant on the other hand have smoother surfaces, leading to the conclusion, that those two strains are inhibited in their ability to form proper biofilms. The main reason being the lack of BslA in both strains, as the exopolysaccharide produced by the *epsA-O* is required for the transcription of *bslA* (see chapter 2.1.2).

In order to quantify the contributions of the biofilm matrix elements to the lateral and vertical macrocolony growth, the measured data points for those two parameters were then fitted with a mathematical model (mathematical modeling by Benedikt von Bronk). It was assumed that all curves would be sigmoidal, as all measurements showed saturation towards late time points, except for the *B. subtilis* BD630 wild-type, where the saturation will be reached outside of the time frame of the experiments. A standard procedure for modeling population dynamics is the logistic differential equation (equation 4.1) [126].

$$\frac{d}{dt}P = rP - \frac{rP^2}{k} \tag{4.1}$$

The solution to this equation is a sigmoidal for a population number of P that will reach saturation in form of the carrying capacity k when growing with the rate r (equation 4.2).

$$P(t) = \frac{kP_0e^{rt}}{k + P_0(e^{rt} - 1)} \tag{4.2}$$

During biofilm matrix formation, the biofilm matrix elements are either promoting one of the growth parameters (lateral or vertical macrocolony growth) or inhibiting it, by influencing either the rate or the maximally achieved area or height respectively. This leads to the fits (equation 4.3) that are applied to the recently acquired data for lateral and vertical macrocolony growth in figure 4.7 A-D.

$$P_i(t) = \frac{k_iP_{0,i}e^{r_it}}{k_i +_{P0,i} (e^{r_it} - 1)} + \overline{P_0} \tag{4.3}$$

with $P_i(t)$ the respective growth over time (lateral or vertical) for a given strain i. k, P_0 and r are the fitting parameters , where r is the growth rate, P_0 the initial value of the area or growth at t_0 and k the carrying capacity. $\overline{P_0}$ represents the initial average value per bacterial strain.

One of the characteristic points in a sigmoidal curve is the inflection point. As seen in

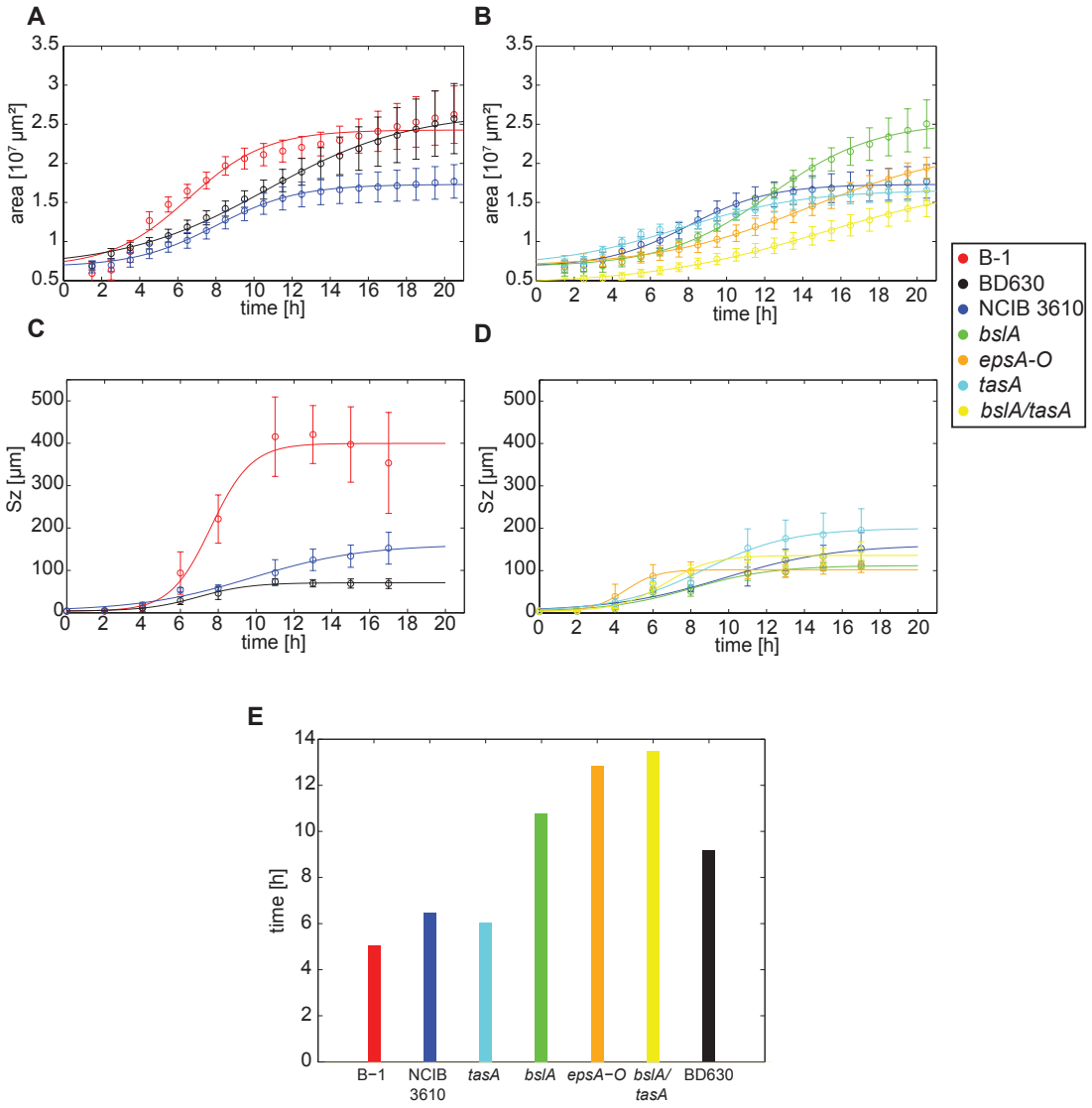

Figure 4.7: Fit of the Model to the Growth Curves A: Macrocolony area growth for the wild-types *B. subtilis* NCIB 3610 (blue), *B. subtilis* B-1 (red) and *B. subtilis* BD630 (black). Circles are the averaged values from the experiments, error bars the 95% confidence interval. The line is the fit. B: Macrocolony growth for *B. subtilis* NCIB 3610 (blue) and its knock-out mutants *B. subtilis* NCIB 3610 lacking TasA (turquoise), *B. subtilis* NCIB 3610 lacking BslA (green), *B. subtilis* NCIB 3610 lacking *epsA-O* (orange) and *B. subtilis* NCIB 3610 lacking BslA/TasA (yellow). C: Height growth for the wild types *B. subtilis* NCIB 3610 (blue), *B. subtilis* B-1 (red) and *B. subtilis* BD630 (black) represented by Sz(10). D: Height growth for *B. subtilis* NCIB 3610 (blue) and its knock-out mutants *B. subtilis* NCIB 3610 lacking TasA (turquoise), *B. subtilis* NCIB 3610 lacking BslA (green), *B. subtilis* NCIB 3610 lacking *epsA-O* (orange) and *B. subtilis* NCIB 3610 lacking BslA/TasA (yellow). E: Comparison of time points for the inflection points for the area growth fits.

figure 4.7 E, the biofilm forming strains (here both wild-types and the *B. subtilis* NCIB 3610 lacking TasA mutant) have the inflection point three hours, and even significantly more, earlier than non producing strains. This leads to the conclusion, that a sigmoidal fit to the area coverage and the form of the growth curve can give a hint at a strains ability to form proper biofilm primarily in lateral but consecutively in vertical dimensions as well. The model for the growth dynamics can also give conclusions about the quantitative influence of the individual matrix elements on the respective growths. For this, the carrying capacity k was analyzed for each strain. The assumption is, as mentioned above, that not only the growth of single bacteria determines the dimensions of the biofilm, but also the biofilm matrix components play a huge role, either enhancing or limiting lateral or vertical growth. With a multiplicative ansatz, the carrying capacity k_i for strain i read as:

$$k_{NCIB3610} = \beta_0 \cdot \beta_{TasA} \cdot \beta_{BslA} \cdot \beta_{epsA\text{-}O} \tag{4.4}$$

$$k_{TasA} = \beta_0 \cdot 1 \cdot \beta_{BslA} \cdot \beta_{epsA\text{-}O} \tag{4.5}$$

$$k_{BslA} = \beta_0 \cdot \beta_{TasA} \cdot 1 \cdot \beta_{epsA\text{-}O} \tag{4.6}$$

$$k_{epsA\text{-}O} = \beta_0 \cdot \beta_{TasA} \cdot 1 \cdot 1 \tag{4.7}$$

with β_0 the basal growth rate and β_i the multiplication factor for biofilm matrix component i. The β_i is 1 if the respective component is missing in the knock-out mutant, the β_i for the respective component can be greater than 1 or smaller, depending on its influence. Greater than 1 indicates a promotion of growth in the given dimension, lower than 1 an inhibition respectively. β_0 is the same for every strain, as it indicates the growth rate through bacterial division, which is similar for all strains, as the mutants derivate all from *B. subtilis* NCIB 3610. The co-dependency of *bslA* and *epsA-O* was respected in the way that while both components are present, the β_i are independent, but in the *B. subtilis* NCIB 3610 mutant lacking *epsA-O*, where both components are not expressed, both β_i are 1.

These four equations with four variables can be solved for the lateral, as well as the vertical growth. Figure 4.8 A shows the contributions of the biofilm matrix components to the respective growth (lateral or vertical), the results support the previous experimental findings. While TasA has an enhancing influence on the lateral growth, its influence on the vertical growth is limiting. The interconnecting fibers formed by TasA seem to give the biofilm complex structural stability, so that it can grow in height, but restricting its area expansion at the same time (see schematic in figure 4.8 B). The surface layer protein BslA on the other hand seems to enhance the ability of the biofilm colony to grow in height, by giving the biofilm the necessary stability but, with its encasing properties, presumably hindering the lateral expansion.

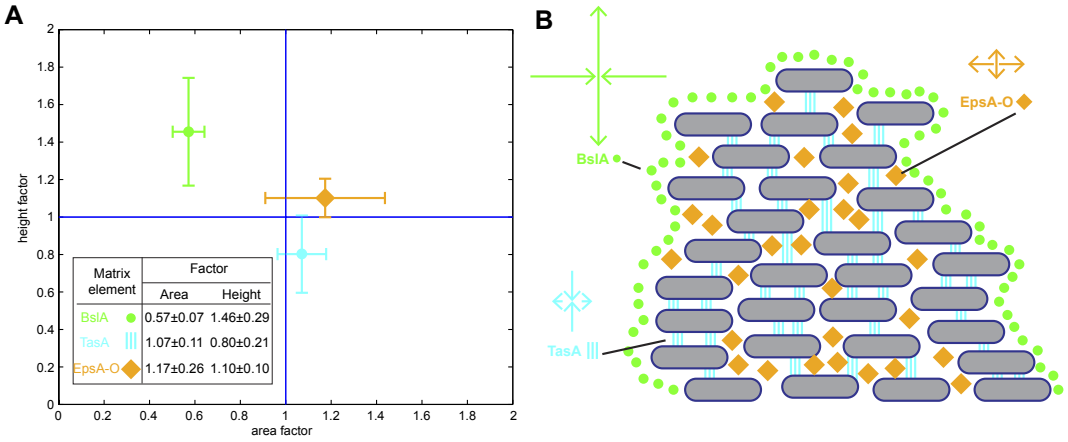

Figure 4.8: Quantitative Influence of Biofilm Matrix Components to Biofilm Growth A: Biofilm matrix Components with factors above 1 promote biofilm growth, factors below 1 inhibit biofilm growth. The errors are the standard deviation. B: Schematic depiction of a *B. subtilis* NCIB 3610 biofilm and its components. Surface layer protein BslA in green, the polysaccharide expressed by the *epsA-O* operon in orange and the fiber forming protein TasA in turquoise.

Therefore, these two components, TasA and BslA, seem to counteract each other. This hypothesis was put to the test by constructing a double mutant that is lacking both BslA and TasA (mutant construction by Alexandra Götz for this study). Analogue to the equations above (equations 4.4 - 4.7), the carrying capacity reads as follows:

$$k_{BslA/TasA} = \beta_0 \cdot 1 \cdot \beta_{epsA\text{-}O} \cdot 1 \tag{4.8}$$

The model predicts a lateral growth of 17.72 mm^2 and a vertical growth of 134.60 μm^2, based on the contribution of the components (see table 4.5). While the actually achieved height of 131.88 μm^2 matches the prediction (see figure 4.6), the model failed to predict the lateral growth (fitted experimental data is 13.85 mm^2). The reason the prediction is

not accurate, might be a coupling effect between the two components, that is present in the biofilm but missing in the model.

Table 4.5: Quantification of Growth Parameters as shown in Figure 4.8 Resulting β_0 and β_i from the model calculated by equations 4.4 - 4.7. The errors are the standard deviation.

Trait	β_0	β_{BslA}	β_{TasA}	$\beta_{epsA\text{-}O}$
Area [mm^2]	15.10 ± 3.41	0.57 ± 0.07	1.07 ± 0.11	1.17 ± 0.26
Height [μm^2]	122.21 ± 32.54	1.46 ± 0.29	0.80 ± 0.21	1.10 ± 0.10
Roughness Sq	0.08 ± 2.01	28.57 ± 62.38	2.91 ± 2.55	2.39 ± 59.22

Lastly, the exopolysaccharide that is encoded by the *epsA-O* operon has a small positive influence on both the lateral and vertical growth, leading to the conclusion that it serves as filler material. Therefore, by increasing the biomass with the production of the exopolysaccharide, the *B. subtilis* NCIB 3610 biofilm can expand laterally and vertically.

In conclusion, this study showed how specific biofilm matrix components determine both vertical and lateral biofilm growth. Furthermore, a mathematical model was used in order to quantify these dependencies.

4.4 Physical Properties of Mature Biofilms

Once a biofilm is fully matured it is, due to its high resistance to antibiotics and chemicals, very hard to remove. Therefore it is important to know the physical properties of those biofilms and which matrix component contributes to a certain attribute. With the following experiments, some physical characteristics of one-day old biofilms were analyzed (results and figures of this section first published in [99]).
As a first step, some surface properties were investigated, as the biofilm surface has an important part in its interaction with the environment. For the analysis of the surface stiffness of fully grown biofilms the AFM (Atomic Force Microscope) nano-indentation method was used (as described in chapter 3.2.6).

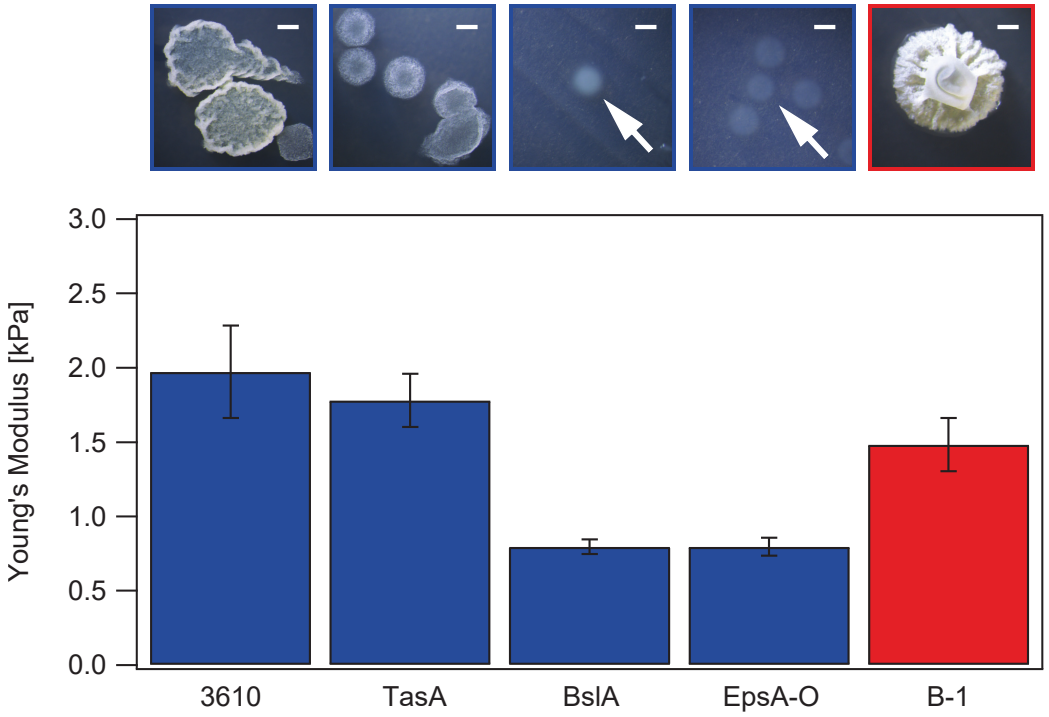

Figure 4.9: Influence of Biofilm Matrix Composition on Surface Elasticity The bar diagram shows the Young's Modulus of 1-day old biofilms formed by the two *B. subtilis* wild type strains that differ in their biofilm matrix composition, *B. subtilis* NCIB 3610 (blue) and *B. subtilis* B-1 (red), as well as several knock-out strains for *B. subtilis* NCIB 3610, that lack specific matrix components. The error bars are the errors that result from the method and from the Gaussian error propagation respectively. On top of the graph, the phenotype for single colonies for all strains is depicted. The white scale bar represents one mm, the arrows point to colonies that are only faintly visible.

The Young's Modulus of a material characterizes its stiffness, the compressibility or stretchability along one axis. Here, the surface elasticity of different biofilms was analyzed

(AFM measurements were performed by Ina Gümperlein within the scope of a master thesis [127]), e.g. biofilms produced by *B. subtilis* NCIB 3610 as well as biofilm produced by *B. subtilis* B-1, as the biofilm matrices of those two strains as described earlier differ distinctly in their composition. For these measurements, *B. subtilis* BD630 could not be taken as a reference, as it does not form a biofilm. Instead, in order to have a reference, the solid agar was measured on which the biofilms are grown.
The Young's Modulus of the agar was 37.82 ± 5.87 kPa. The biofilm formed by *B. subtilis* NCIB 3610 shows a Young's Modulus of 1.97 ± 0.31 kPa and is therefore much softer than the agar. *B. subtilis* B-1 biofilms are slightly but not significantly (see table 4.6) softer with a Young's Modulus of 1.48 ± 0.18 kPa (see figure 4.9). As the electrostatic interactions between the biofilm surface and the cantilever are too strong on air, the biofilm was covered with 99% ethanol. The values for the Young's Modulus were taken between 10 and 25 minutes after the application of the ethanol, as described in chapter 3.2.6. Although ethanol serves as a disinfectant, figure 4.10 does not show a change in the surface stiffness over the time course of the experiments of 25 minutes. Rather, the variances between the single sets of measurements are attributed to the high surface roughness (as already described in section 4.3), as it was impossible to perform the nano-indentation measurements on the same morphology every time.

Table 4.6: p-Values for Young's Modulus Data shown in Figure 4.9 A pairwise significance test (student t-test) was performed in order to compare the Young's Modulus data for *B. subtilis* NCIB 3610 with that of its mutant strains and the other wild-type, *B. subtilis* B-1. Pairs are significantly different for p-values lower than 0.05.

Strain	p-Value for Data shown in Fig.4.9
B. subtilis NCIB 3610	n/a
B. subtilis NCIB 3610 lacking TasA	0.7075
B. subtilis NCIB 3610 lacking BslA	0.0048
B. subtilis NCIB 3610 lacking *epsA-O*	0.0016
B. subtilis B-1	0.2699

After finding no significant difference between the two wild-type strains, the next important question is, which biofilm matrix component is responsible for this biofilm property. The focus, again, lies on the *B. subtilis* NCIB 3610 wild-type strain, because here all key biofilm matrix components are known and the respective knock-out mutants are available. The one mutant that still forms a proper, rough biofilm, *B. subtilis* NCIB 3610 lacking

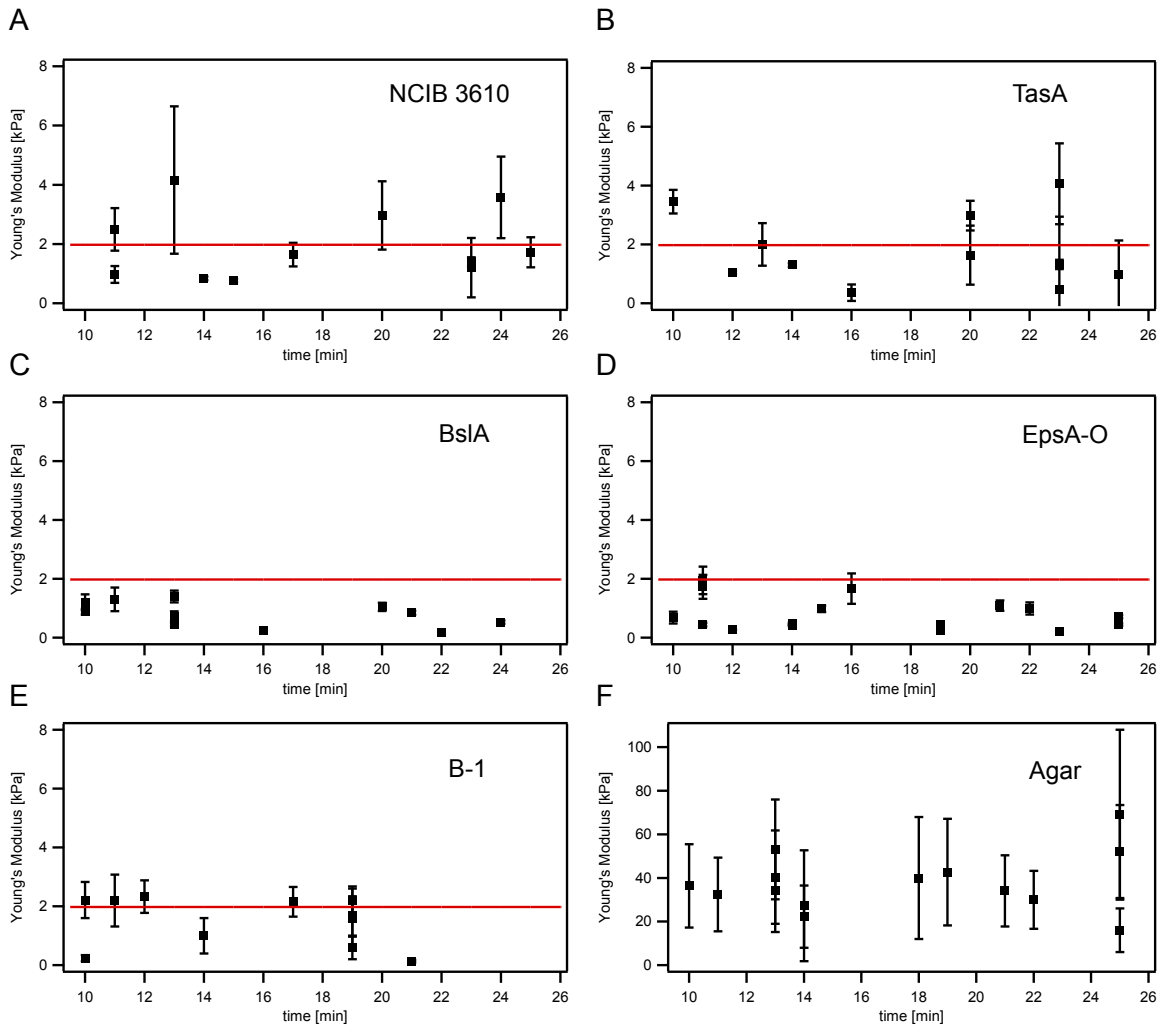

Figure 4.10: Young's Modulus does not Change over Time under the Influence of Ethanol Due to technical reasons, the measurements were taken between 10 and 25 minutes. Subsequently, the data points were then averaged, giving the Young's Modulus for this time-window. A: Data point distribution for *B. subtilis* NCIB 3610. B: *B. subtilis* NCIB 3610 lacking TasA. C: *B. subtilis* NCIB 3610 lacking BslA. D: *B. subtilis* NCIB 3610 lacking *epsA-O*. E: *B. subtilis* B-1. F: Pure agar surface. The error bars are the standard deviation of the average over 64 measurement runs. The red line represents the average Young's Modulus for *B. subtilis* NCIB 3610.

TasA (see images in figure 4.9), also does not differ significantly in its surface stiffness from that of *B. subtilis* NCIB3610 with a Young's Modulus of 1.78 ± 0.18 kPa. *B. subtilis* NCIB 3610 lacking BslA and *B. subtilis* NCIB 3610 lacking *epsA-O* biofilms on the other hand show significantly smaller values for the Young's Modulus with 0.08 ± 0.06 kPa for *B. subtilis* NCIB 3610 lacking BslA and 0.08 ± 0.05 kPa for *B. subtilis* NCIB 3610 lacking *epsA-O* respectively. As the knock-out of *tasA* did not change the surface stiffness, the fiber forming proteins (see chapter 2.1.2 and previous findings) do not contribute to this surface property. As the expression of the *epsA-O* operon is necessary for the production of BslA (see chapter 2.1.2), *B. subtilis* NCIB 3610 lacking *epsA-O* is missing both components and it is therefore probably the surface protein BslA contributing to the decrease in surface stiffness.

The next interesting characteristic is the surface roughness (that was already shown to be an interesting parameter for biofilm growth), measured as described in chapter 3.2.5. As the wild-type biofilms differ in their matrix composition, it was not surprising to find that the surfaces of these biofilms also differ in their surface roughness (see section 4.3). The surface of *B. subtilis* NCIB 3610 biofilms show high peaks on the heatmap (see figure 4.11 A, left)(data part of a shared first author paper, experiments done by Stefan Grumbein, first published in [99]), the *B. subtilis* B-1 biofilms even higher peaks, representing a rougher surface (see figure 4.11 A, right). This again matches their colony morphology. Biofilms produced by *B. subtilis* NCIB 3610 strain lacking TasA still shows a rough surface (not shown), whereas the strain *B. subtilis* NCIB 3610 lacking *epsA-O* (also not shown, for an image of colony morphology see figure 4.6 in section 4.3) and *B. subtilis* NCIB 3610 lacking BslA (see figure 4.11 A, middle) have much smoother colony surfaces. This suggests that the surface layer protein BslA is responsible for the roughness of the surface of *B. subtilis* NCIB 3610 biofilms. These findings are in line with those of section 4.3. This can be quantified by the Sq values, the root mean square surface roughness, shown in graph B, figure 4.11. The Sq value for *B. subtilis* B-1, 5.5 ± 3.85, is approximately ten times higher than that for *B. subtilis* NCIB 3610 with 0.53 ± 0.63.

While the 99% ethanol used during the AFM experiments (see 3.2.6) had no effect on the biofilm surface stiffness during a treatment of 10-25 minutes, it is still a widely used surface disinfectant. As the biofilm surface is important for its interaction with the environment, experiments with a longer exposure were performed, in order to observe if biofilm surface properties can be changed. Treated with 99% ethanol for 60 minutes, the surface roughness of *B. subtilis* NCIB 3610 biofilms, along with the surface roughness of biofilms of *B. subtilis* NCIB 3610 lacking TasA, decreases about 60%. The surface roughness of

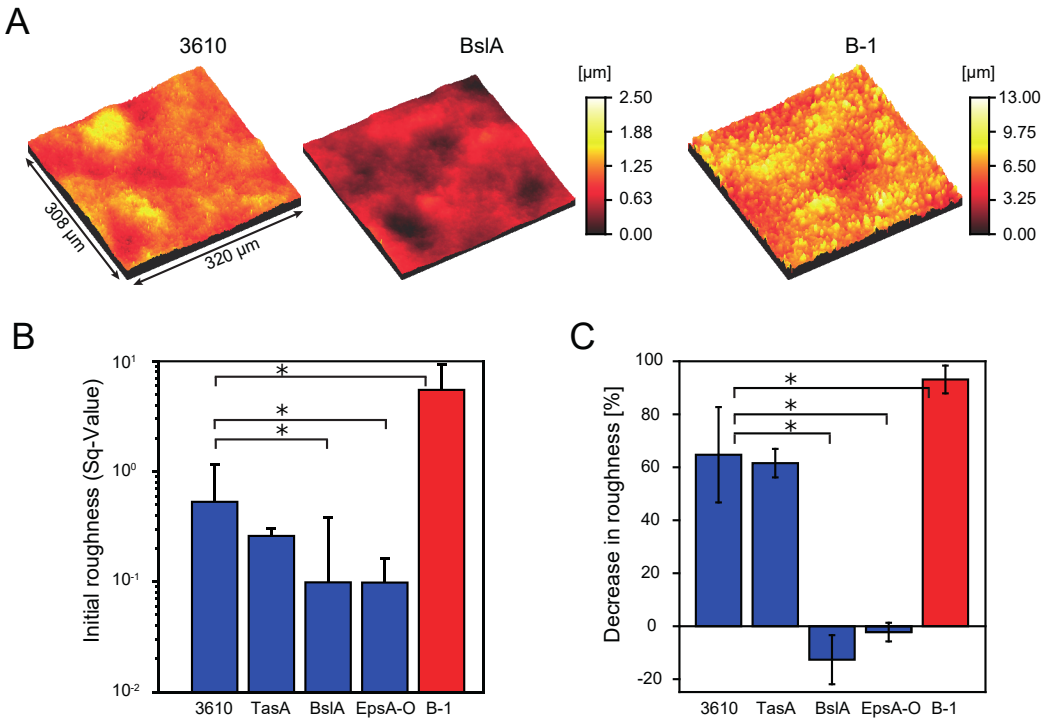

Figure 4.11: Surface Roughness of *B. subtilis* Biofilms under the Influence of Ethanol Treatment A: Biofilm surfaces of *B. subtilis* NCIB 3610 wild-type and the knock-out mutant *B. subtilis* NCIB 3610 lacking BslA. The biofilm height is color coded in μm. On the right side is a *B. subtilis* B-1 biofilm surface for comparison. The image sections show 308x320 μm of plated biofilms. B: Sq values for untreated biofilms. C: Decrease of biofilm surface roughness after 60 minutes of treatment with ethanol. The error bars for B and C are the standard deviations. The star above the brackets indicates that a comparison with *B. subtilis* NCIB 3610 with a two-sample t-test was found to be significant.

biofilms of *B. subtilis* NCIB 3610 lacking BslA and *B. subtilis* NCIB 3610 lacking *epsA-O* barely show a decrease of surface roughness, as they were already smooth in the beginning because they probably do not form proper biofilm in the first place. Whereas *B. subtilis* B-1 biofilms surfaces have not only shown the highest Sq values, but the decrease in surface roughness is even over 90%. Here, the ethanol treatment has the greatest effect, which shows that the biofilm surface of *B. subtilis* NCIB 3610 biofilms as well as *B. subtilis* B-1 biofilms can be altered with chemical treatment.

So far, the results show an influence of ethanol on the surface roughness. Another interesting property of mature biofilms is the bulk viscoelasticity, represented by the storage modulus measured via macro-rheology, as described in chapter 3.2.7.
The biofilm of wild-type strain *B. subtilis* NCIB 3610 has a storage modulus of 584 ± 132 Pa (see figure 4.12 A)(Rheometry experiments performed in collaboration with Stefan Grumbein), its mutants lying in the same range. *B. subtilis* B-1 biofilm on the other hand is much softer, with a 10-fold reduced storage modulus. The differences in biofilm matrix components between *B. subtilis* NCIB 3610 and *B. subtilis* B-1 biofilms therefore lead to a drastic difference in this particular physical property, while no biofilm matrix component of *B. subtilis* NCIB 3610 could be attributed to the creation of a stiffer biofilm matrix.

Table 4.7: p-Values for Rheology Data shown in Figure 4.12A The first column shows the p-values for the pairwise significance t-test for the untreated biofilms, compared to *B. subtilis* NCIB 3610. The other columns compare the data obtained for the ethanol treated biofilms with the respective data for their untreated counterparts. For fields with - no data was obtained. The pairs are significantly different for p-values lower than 0.05.

Strain	p-Values for untreated Biofilm Data in Fig.4.12A	p-Values for 10 min Ethanol Treatment in Fig.4.12A	p-Values for 60 min Ethanol Treatment in Fig.4.12A
B. subtilis NCIB 3610	n/a	2.49E-12	8.08E-19
B. subtilis NCIB 3610 + γ-polyglutamate	-	-	-
B. subtilis NCIB 3610 lacking TasA	2.63E-06	5.17E-10	1.22E-16
B. subtilis NCIB 3610 lacking BslA	0.1120	1.80E-10	4.85E-16
B. subtilis NCIB 3610 lacking *epsA-O*	0.0003	7.86E-15	1.38E-20
B. subtilis B-1	2.51E-12	0.2727	0.0032

In order to determine if a treatment with ethanol also has an influence on the bulk elasticity, the biofilms were treated with 99% ethanol for 10 minutes and 60 minutes respectively. Already 10 minutes of treatment with ethanol result in a significant (p-values see tables 4.7 and 4.8) increase in bulk elasticity for *B. subtilis* NCIB 3610 biofilms and and that of its mutants, whereas it is unchanged for *B. subtilis* B-1 biofilms. A longer treatment

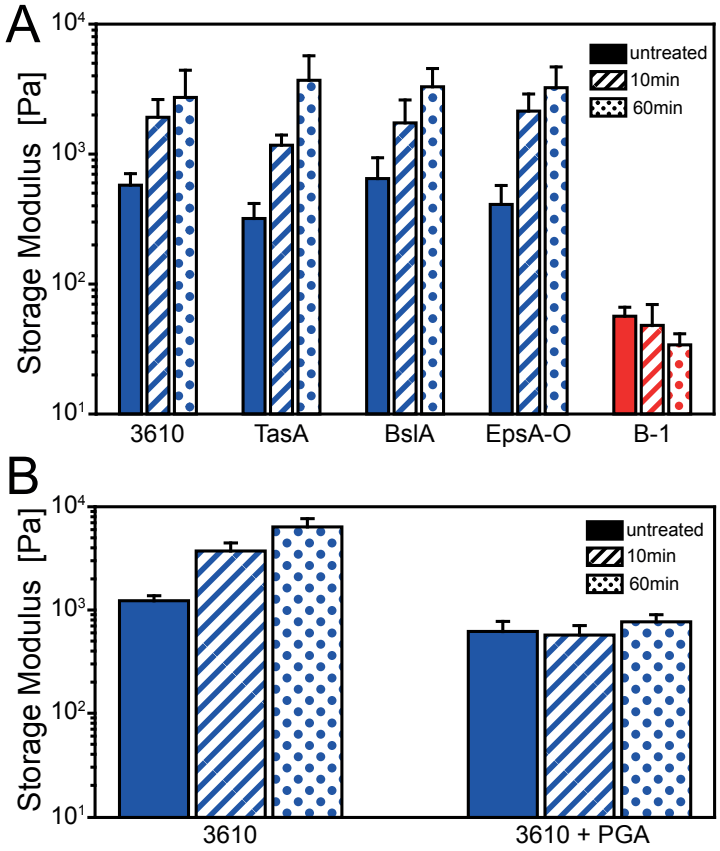

Figure 4.12: Storage Modulus for differently treated *B. subtilis* Biofilms A: The bar plot shows the storage modulus for *B. subtilis* NCIB 3610 (blue), its mutants and *B. subtilis* B-1 (red). The filled bars represent the untreated biofilm, striped bars the biofilm after treatment with 99% ethanol for 10 min and the dotted bars represent the biofilm after treatment with ethanol for 60 min. The error bars are the standard deviation. B: This graph shows the storage modulus for *B. subtilis* NCIB 3610, on the left without treatment with additional γ-polyglutamate, on the right biofilm that grew in the presence of additional γ-polyglutamate. The filled bars represent the untreated biofilm, striped bars the biofilm after treatment with 99% ethanol for 10 min and the dotted bars represent the biofilm after treatment with ethanol for 60 min. The error bars are the standard deviation.

amplified the increase in bulk stiffness of bacterial biofilms even more, for all strains but *B. subtilis* B-1.

These results lead to the conclusion that the hydrophilic γ-polyglutamate mainly present in the *B. subtilis* B-1 biofilm matrix protects it from ethanol induced stiffening, by binding water and thus preventing dehydration.

Table 4.8: p-Values for Rheology Data shown in Figure 4.12B The first column shows the p-values for the pairwise significance t-test for the untreated biofilms, compared to *B. subtilis* NCIB 3610. The other columns compare the data obtained for the ethanol treated biofilms with the respective data for their untreated counterparts. The pairs are significantly different for p-values lower than 0.05.

Strain	p-Values for 10 min Ethanol Treatment in Fig.4.12B	p-Values for 60 min Ethanol Treatment in Fig.4.12B
B. subtilis NCIB 3610	8.72E-11	2.95E-12
B. subtilis NCIB 3610 + γ-polyglutamate	0.4638	0.0149

Before this effect is further addressed, another fact needs mentioning. So far, 99% ethanol has been used, as it was used for the AFM measurements and its effects on the biofilms have been analyzed. For disinfection purposes although, much lower concentrations of 70 - 80% ethanol are used. Such low concentrations do not affect the decrease in surface roughness of *B. subtilis* NCIB 3610 biofilms (see figure 4.13 A), but the reduction for *B. subtilis* B-1 is about 50% less. Thus a lower concentration of ethanol does not affect the surface *B. subtilis* B-1 biofilms as much as the higher concentration of 99% For the storage modulus of *B. subtilis* NCIB 3610, both ethanol concentrations had a similar effect in increasing the bulk elasticity.

These auxiliary experiments help to underline the finding that chemical treatment of bacterial biofilms can alter their physical properties. A fact that is important to understand in order to develop the correct removal strategies.

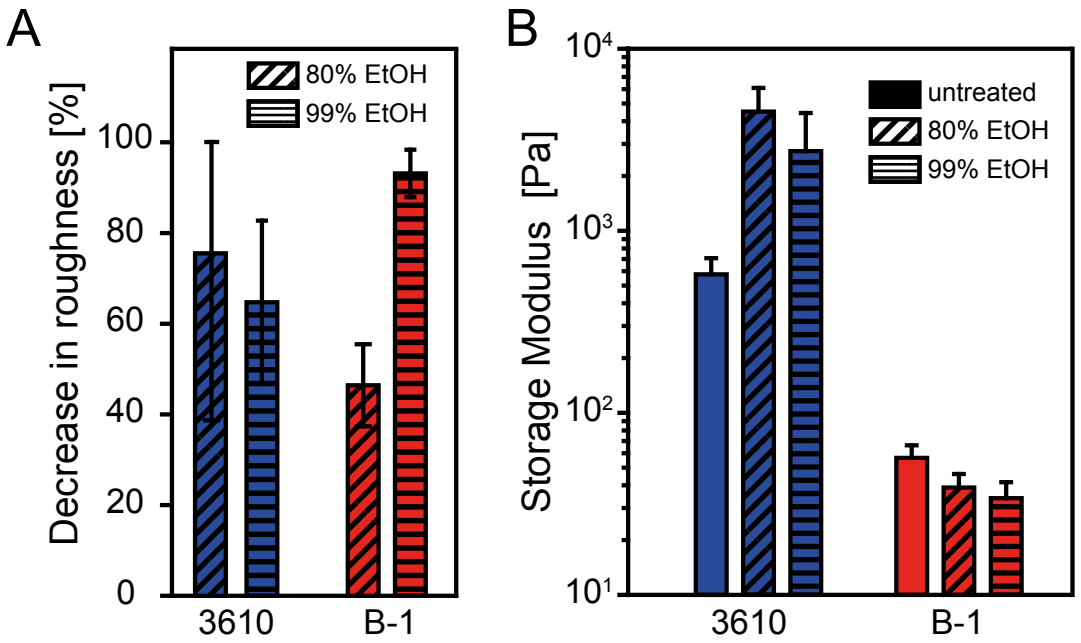

Figure 4.13: Comparison of the Influence of 80% and 99% Ethanol on Properties of Biofilms of *B. subtilis* A: Decrease in biofilm surface roughness is dependent on the concentration of ethanol applied to biofilms of wild-type strains *B. subtilis* NCIB 3610 (blue) and *B. subtilis* B-1 (red). B: Dependence of the storage modulus on treatment with different concentrations of ethanol. For both graphs error bars are the standard deviation. The filled bars represent the untreated biofilm, diagonally striped bars the biofilm after treatment with 80% ethanol and the horizontally striped bars represent the biofilm after treatment with 99% ethanol.

In order to further investigate the contribution of γ-polyglutamate to biofilms, a closer look on what is happening during ethanol treatment is necessary. Figure 4.14 shows images of *B. subtilis* biofilms covered with ethanol. Immediately after ethanol application, bubbles form on the surface of the *B. subtilis* B-1 biofilm. On *B. subtilis* NCIB 3610 biofilms no bubble formation was observed.

One explanation for this phenomenon is that the ethanol replaces air and possibly even water inside of the biofilm. As described in chapter 2 (section 2.1.2), γ-polyglutamate is a highly hydrophilic macromolecule, and as such may be able to prevent the dehydration of the *B. subtilis* B-1 biofilms, and therefore protect *B. subtilis* B-1 from ethanol induced stiffening.

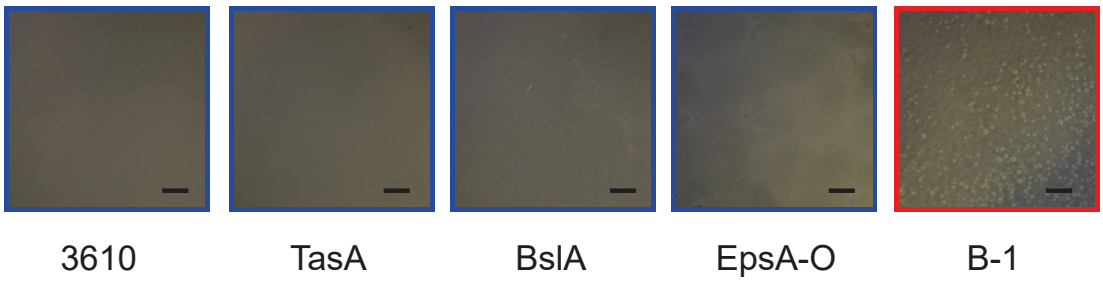

Figure 4.14: Air Bubble Formation on the Surface of *B. subtilis* B-1 Biofilms after Ethanol Application The images show the surface of different biofilms directly after application of ethanol. Biofilms of *B. subtilis* NCIB 3610 and its mutants in blue and *B. subtilis* B-1 in red. The scale bar represents 1 mm.

In addition to test the influence of γ-polyglutamate further, purified γ-polyglutamate was added to growing *B. subtilis* NCIB 3610 biofilms (as described in chapter 3.1) that normally do not produce this biofilm matrix component. Figure 4.12 B shows no increase in bulk elasticity for *B. subtilis* NCIB 3610 biofilms grown in the presence of γ-polyglutamate after 10 or 60 minutes of ethanol treatment. This supports the theory that γ-polyglutamate can protect *B. subtilis* NCIB 3610 biofilms from ethanol induced stiffening.

During these experiments, it became apparent that one of the biofilm matrix components, γ-polyglutamate, has an influence on how the ethanol treatment affected the properties of the mature biofilms. To analyze the dehydration effect further, the bio-masses of the wild-type strain biofilms was analyzed. Biofilms of *B. subtilis* NCIB 3610 and *B. subtilis* B-1 were let grown plated on agar plates. The samples were prepared as described in chapter 3.2.8. First, the total mass was determined, with *B. subtilis* B-1 biofilms yielding four times more biomass than *B. subtilis* NCIB 3610 biofilms, 1,170 mg/plate and 303 mg/plate, respectively (for significance analysis see table 4.9). Drying the collected biofilms with a lyophill (see chapter 3.2.8), shows that *B. subtilis* B-1 biofilms lose more mass during drying, therefore contain more water. This indicates that γ-polyglutamate binds water inside the *B. subtilis* B-1 biofilms.

Then, the samples were treated with ethanol before harvesting the biofilm. The ethanol treatment reduces the total masses of both strains down to about 55 and 40% (see figure 4.15). That is, within error bars, approximately the same loss for both strains (no significant difference, see table 4.10).

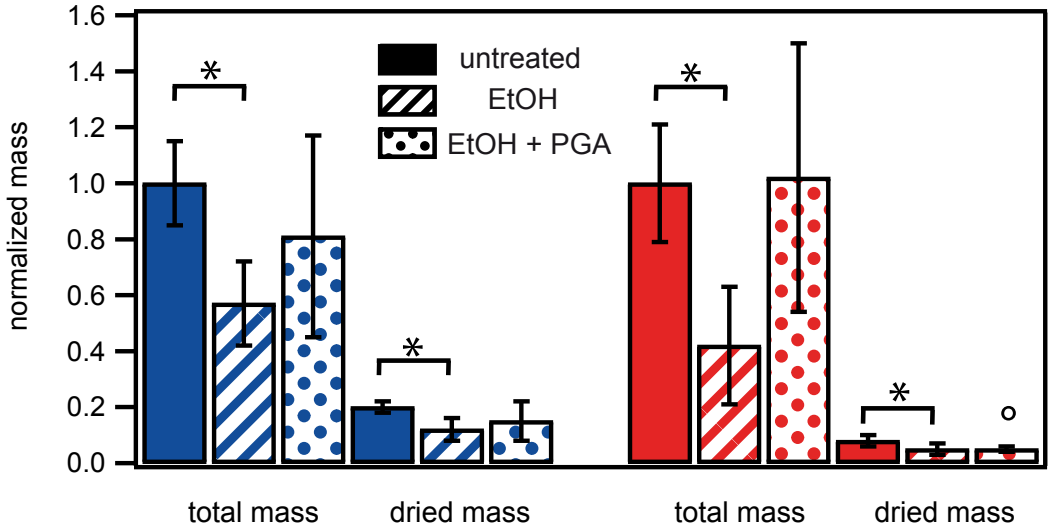

Figure 4.15: Effect of γ-polyglutamate on Dehydration of *B. subtilis* Biofilms This bar plot shows the normalized mass of untreated and ethanol treated biofilm of both the wild-types *B. subtilis* NCIB 3610 (blue) and *B. subtilis* B-1 (red). The full bars represent untreated biofilms. The lined bars represent biofilm treated with ethanol for one hour. And the dotted bars represent biofilm that grew in the presence of additional γ-polyglutamate and was then treated with ethanol for one hour. Error bars are the standard deviation as follows of Gaussian error propagation and the stars above the bars mean that those have been compared with a two-sample t-test and found to be significantly different. The circle indicates that for the biofilm treated with ethanol and γ-polyglutamate, not all samples could be lyophillized sufficiently, leaving some that were still moist.

Adding γ-polyglutamate to both biofilms during growth, increases the total mass after ethanol application back to the level of untreated biofilm. The dried masses show no difference to the untreated dried masses, with the sole exception that for *B. subtilis* B-1 biofilms that were treated with γ-polyglutamate as well as with ethanol, some samples could not be completely dried.

These effects lead to the conclusion, that both wild-type biofilms are dehydrated to the same degree and this effect can be dampened by the addition of γ-polyglutamate, but the previously observed prevention of ethanol induced stiffening is not necessarily due to a prevention of dehydration by the γ-polyglutamate.

Table 4.9: p-Values for Total Mass Data shown in Figure 4.15 The data for the total mass of the treated biofilms was tested pairwise with a student t-test against the untreated biofilm mass for each strain. Pairs are significantly different for p-values below 0.05.

Strain ± Ethanol	p-Value for total Mass Data shown in Fig.4.15
B. subtilis NCIB 3610	n/a
B. subtilis NCIB 3610 + Ethanol	0.0011
B. subtilis NCIB 3610 + Ethanol + γ-polyglutamate	0.3386
B. subtilis B-1	n/a
B. subtilis B-1 + Ethanol	0.0037
B. subtilis B-1 + Ethanol + γ-polyglutamate	0.9484

Table 4.10: p-Values for Dried Mass Data shown in Figure 4.15 The data for the dried mass of the treated biofilms was tested pairwise with a student t-test against the untreated biofilm mass for each strain. Pairs are significantly different for p-values below 0.05.

Strain ± Ethanol	p-Value for dried Mass Data shown in Fig.4.15
B. subtilis NCIB 3610	n/a
B. subtilis NCIB 3610 + Ethanol	0.0043
B. subtilis NCIB 3610 + Ethanol + γ-polyglutamate	0.2464
B. subtilis B-1	n/a
B. subtilis B-1 + Ethanol	0.0175
B. subtilis B-1 + Ethanol + γ-polyglutamate	0.1352

This study showed how specific biofilm matrix components affect physical properties that can be changed by chemical treatment. Additionally, some of the properties can be properly transferred from one biofilm to the other.

5 Discussion and Outlook

In this thesis, the contribution of biofilm matrix components to physical properties of *Bacillus subtilis* biofilms was analyzed.

The comparison of *B. subtilis* NCIB 3610 and *B. subtilis* B-1 has shown that, while similar in their genome, the phenotype of their respective biofilms differs quite significantly, mainly due to the product of the *ywsC* gene, the biofilm matrix component γ-polyglutamate, that makes the *B. subtilis* B-1 biofilm much thicker and more prominently wrinkled. These differences in biofilm structure and topography lead to the different physical properties of those two wild-type strains, and some of their knock-out mutants, that were investigated in this thesis.

With the attachment of single bacteria, the differences between strains producing a biofilm of different matrix composition start to appear. Using the cantilever array technique, with gold coated surfaces, it was shown that proteins, either in the cell membrane or in the biofilm matrix, play a role in attachment at the early biofilm-formation phase. The thiol groups in the proteins provide a strong attachment to the gold surface for *B. subtilis* strain NCIB 3610 and its knock-out mutants. This was most prominent in the NCIB 3610 strain lacking *epsA-O*, the exopolysaccharide. The stronger attachment in the absence of the carbohydrate suggests a reduction of attachment in the presence of carbohydrates. In order to test that finding, the cantilevers were coated with various carbohydrates, the monosaccharides mannose and galactose and the disaccharide lactose. The result was a clear reduction in surface attachment for *B. subtilis* strain NCIB 3610 for all carbohydrates. This reduction is in line with a previously described finding [128], where the complex glycoprotein mucin was found to suppress bacterial adhesion. This is opposite of what one would expect, as the assumption was that the attachment would be even stronger, due to various known carbohydrate uptake systems within the bacterial cell wall [129]. But as the attachment is similar for all different carbohydrates and *B. subtilis* only has uptake proteins for mannose [122], the overall present attachment is due to unspecific carbohydrate-protein interactions.

Two of the tested knock-out mutants, NCIB 3610 lacking TasA and NCIB 3610 lacking BslA, that lack one of the matrix proteins respectively, show a similar attachment profile as the wild-type. Interestingly enough, the knock-out mutant that is missing its carbohydrate component, strain NCIB 3610 lacking *epsA-O*, shows the most prominent reduction of attachment. This finding leads to the conclusion that carbohydrate-carbohydrate interactions are important for bacterial binding to carbohydrate coated surfaces. Carbohydrate-carbohydrate interactions are described for eucaryotic cells [123–125] as first steps in cell recognition and adhesion, but so far specific interactions have not yet been described for *B. subtilis*. As this might be one of the important properties for bacterial attachment, more research is necessary to understand the mechanisms in order to prevent bacterial adhesion and therefore infections before they even occur. Nonetheless it is not new that a coating with carbohydrates reduce bacterial binding [128, 130], it could recently be shown that carbohydrates on a surface can even have antimicrobial properties [131, 132].

The next stage of biofilm-formation is growth, from single cells over microcolonies to macrocolonies and mature biofilms. By observing the area covered by the growing bacteria and the height, those characteristics can be used to quantitatively describe bacterial biofilm growth. Additionally, using knock-out mutants, it can be determined which matrix components contribute to the dimensions of the biofilm. This was further investigated and confirmed by a mathematical model that describes biofilm growth dynamics dependent on the growth parameters that were set experimentally.
The exopolysaccharide produced by the *epsA-O* operon was described earlier as the glue that holds single cells within biofilm matrix together. The growth experiments and modeling confirmed this by showing that it is responsible for a small part of lateral growth. As it was shown earlier and also described in other studies [133], exopolysaccharides play a role in cell attachment which could explain that finding.
The fiber forming protein TasA was described as the scaffold for the vertical growth. This is reflected in the findings, as TasA restricts the vertical growth, presumably by interconnecting layers of bacteria in order to give strength to the 3D construct and therefore reducing the final height. This effect is more prominent than the contribution of the exopolysaccharide.
The biggest impact on biofilm growth is achieved by the BslA protein. As surface layer protein, it encases the entire biofilm, therefore giving strength and structure. The structural stability it provides decreases lateral growth in the presence of BslA, while increasing the vertical growth.

So far, biofilm development was analyzed. The following observations consider the physical properties of fully grown biofilms, especially selected surface properties among others. Again, the impact of the different matrix components on the physical properties of the biofilm formed by *B. subtilis* NCIB 3610 was analyzed by using single knock-out mutants that are unable to produce the main biofilm matrix components. Additionally, the biofilm formed by *B. subtilis* NCIB 3610 was compared to the biofilm formed by a related strain, *B. subtilis* B-1, whose biofilm matrix mainly consists of γ-polyglutamate.

The first property to investigate was the surface stiffness, represented by the Young's Modulus. Between the Young's Modulus of *B. subtilis* NCIB 3610 and *B. subtilis* B-1, although consisting of different matrix components, there is only a small, not significant difference, with *B. subtilis* B-1 being slightly softer with a Young' Modulus of 1.48 $\pm$ 0.18 kPa compared to one of 1.97 $\pm$ 0.31 kPa. The Young's Modulus of the biofilm formed by *B. subtilis* NCIB 3610 lacking TasA is also in the same range as the corresponding wild-type strain, showing that this matrix component does not contribute to the biofilms surface stiffness. The biofilms formed by *B. subtilis* NCIB 3610 lacking *epsA-O* and *B. subtilis* NCIB 3610 lacking BslA on the other hand show smaller values and are therefore softer. As the BslA production is dependent on the *epsA-O* operon as well [64], it is the BslA surface protein that has an influence on the surface stiffness of bacterial biofilms and, not surprisingly, on the surface roughness of the *B. subtilis* NCIB 3610 biofilm. The *B. subtilis* B-1 biofilm has an even rougher surface, although not dependent on BslA.
While the surface stiffness of *B. subtilis* B-1 biofilms and *B. subtilis* NCIB 3610 biofilms is approximately the same, their bulk elasticity differs by a factor of 10, with the *B. subtilis* B-1 biofilms being the lower one. The mutant strains of *B. subtilis* NCIB 3610 do not show any difference, therefore the biofilm matrix components do not have any influence, but rather the bacteria themselves determine the bulk elasticity. Whereas for *B. subtilis* B-1 biofilms the γ-polyglutamate seems to be the main contributing factor, resulting in the difference between the wild-type strains.
The measurements for the Young's Modulus could only be done with the biofilms submerged in ethanol. While the influence the ethanol had over time was only minor concerning the surface elasticity, its impact on the surface roughness was immense. The biofilms that showed rough surfaces, namely those formed by *B. subtilis* NCIB 3610, its TasA knock-out-mutant (this mutant forms the most intact biofilm compared to the wild-type strain) and *B. subtilis* B-1, had their surface drastically smoothened out by the ethanol, by 60% for *B. subtilis* NCIB 3610 and its mutant and by even over 90% for *B. subtilis* B-1. This change in surface roughness and with it a change of surface properties might

impact the uptake ability for an antimicrobial treatment, be it for better or worse.
While ethanol has a big influence on the surface roughness of biofilms produced by *B. subtilis* B-1, its bulk elasticity is unchanged by the treatment. For the biofilms produced by *B. subtilis* NCIB 3610 and by its mutants on the other hand, a treatment with ethanol increased bulk elasticity, which suggests that γ-polyglutamate is protecting *B. subtilis* B-1 biofilms from stiffening. As ethanol is one of the most commonly used surface disinfectants, this phenomenon is important to understand, as a stiffening of the biofilm matrix could just as well make it more difficult to remove. Especially knowledge about the surface properties such as surface stiffness, surface roughness, but also sorption properties is important, as the surface is the first "point" of contact with the environment. For example, *B. subtilis* biofilms are among the few bacterial species that are hydrophobic [134], which in turn could prevent proper wetting with a treatment solution. Hydrophilic rendered biofilms are less resistant against mechanical and chemical stressors [135].

All those findings show that the matrix of *B. subtilis* biofilms, more precisely the components of which the matrix consists of and their composition influences a variety of physical properties. These properties together can rend the biofilm irremovable. Every component gives the biofilm a specific property, each at its own time during biofilm development. Therefore, for optimal treatment, not only the influence of the biofilm matrix components has to be known in order to find the optimal window of opportunity and method of treatment, but also how exactly the biofilm is built and the time line of the development of the respective structures.
Given this knowledge, a treatment should be adjusted to each individual biofilm, as some antimicrobial agents have proven to further strengthen the biofilm matrix instead of killing the bacteria, as it would do to single cells. For example, metal ions like Cu^{2+}, Zn^{2+} and Fe^{2+} that would normally kill planctonic bacteria (bacteria that are suspended in a liquid) can be absorbed by the matrix into the biofilm. Inside the matrix, the ions will not kill the bacteria, but are incorporated into the biofilm matrix structure, making it more resilient, e.g. against shear forces [22]. A similar effect was observed for certain antibiotics [136].

Therefore, as stated in the introduction, it is important to know the exact composition of the biofilm matrix and the bacteria that produce it, the developmental stage the biofilm is in and the interactions that can occur between the matrix and the chemicals that are used for treatment or cleaning. Together with an understanding of the dynamics and statistical variances, a wholesome picture can be drawn in order to customize the treatment.

This work has contributed to gain more insights into the steps of biofilm-formation, beginning with the attachment. It has proven the concept, that with specific physico-chemical modifications, the attachment of bacterial cells can be reduced. This work further shed light onto the growth dynamics of biofilm micro- and macro-colonies as well as the respective contribution of the main biofilm matrix components to the lateral and vertical growth. And last but not least, this work has extended the knowledge about the physical properties of biofilm matrix surfaces and the biofilm matrix itself.

Nonetheless, future research has to be done. The better the relation between the biofilm matrix compositions and their physical properties is understood, the better infections with biofilm forming bacteria can be treated. But there are also applications that benefit from the properties of biofilms. For example, the elastic properties of bacterial biofilms, modified with genetical engineering, are used for synthetic 3D-printed gels [137] or can be used "living" glues [138]. Other researchers work on altering the properties like completing biofilm matrices via co-culture [139]. When the biofilm matrix components and their physical properties are understood, this knowledge can help prevent and treat bacterial biofilm infections, but also contribute to new and innovative ways these properties can be used.

Bibliography

[1] A. Fleming. Penicillin. Nobel Lecture, 11.12. 1945.

[2] D. Davies. Understanding biofilm resistance to antibacterial agents. *Nature Reviews Drug Discovery*, 2(2):114–122, 2003.

[3] R. M. Donlan. Biofilms and device-associated infections. *Emerging Infectious Diseases*, 7(2):277, 2001.

[4] K Vickery, A Pajkos, and Y Cossart. Cross infection: evaluation of the effectiveness of decontamination of dental syringes. *British dental journal*, 189(11):620, 2000.

[5] Vincent Zijnge, M Barbara M. van Leeuwen, John E. Degener, Frank Abbas, Thomas Thurnheer, Rudolf Gmür, and Hermie J M. Harmsen. Oral biofilm architecture on natural teeth. *PLoS One*, 5(2):e9321, 2010.

[6] J. W. Costerton, P. S. Stewart, and E. P. Greenberg. Bacterial biofilms: a common cause of persistent infections. *Science*, 284(5418):1318–1322, 1999.

[7] B. F. Picologlou, N. Zelver, and W. G. Characklis. Biofilm growth and hydraulic performance. *Journal of the Hydraulics Division ASCE*, 106(HY5):733–746, 1980.

[8] W. G. Characklis. Bioengineering report: Fouling biofilm development: A process analysis. *Biotechnology and Bioengineering*, 23(9):1923–1960, 1981.

[9] T. F. Mah and G. A. O'Toole. Mechanisms of biofilm resistance to antimicrobial agents. *Trends in Microbiology*, 9(1):34–39, 2001.

[10] Christopher Walsh. Molecular mechanisms that confer antibacterial drug resistance. *Nature*, 406:775–781, 2000.

[11] P. S. Stewart. Mechanisms of antibiotic resistance in bacterial biofilms. *International Journal of Medical Microbiology*, 292(2):107–113, 2002.

[12] N. Høiby, T. Bjarnsholt, M. Givskov, S. Molin, and O. Ciofu. Antibiotic resistance of bacterial biofilms. *International journal of antimicrobial agents*, 35(4):322–332, 2010.

[13] C. A. Gordon, N. A. Hodges, and C. Marriott. Antibiotic interaction and diffusion through alginate and exopolysaccharide of cystic fibrosisderived *Pseudomonas aeruginosa*. *Journal of Antimicrobial Chemotherapy*, 22(5):667–674, 1988.

[14] K. Lewis. Persister cells and the riddle of biofilm survival. *Biochemistry (Moscow)*, 70(2):267–274, 2005.

[15] Karen D Xu, Michael J Franklin, Chul-Ho Park, Gordon A McFeters, and Philip S Stewart. Gene expression and protein levels of the stationary phase sigma factor, RpoS, in continuously-fed *Pseudomonas aeruginosa* biofilms. *FEMS microbiology letters*, 199(1):67–71, 2001.

[16] S. Molin, A. T. Nielsen, B. B. Christensen, J. B. Andersen, T. R. Licht, T. Tolker-Nielsen, C. Sternberg, M. C. Hansen, C. Ramos, and M. C. Givskov. Molecular ecology of biofilms. In *Biofilms*, pages 89–120. John Wiley & Sons Ltd, 2000.

[17] S. Elias and E. Banin. Multi-species biofilms: living with friendly neighbors. *FEMS Microbiology Reviews*, 36(5):990–1004, 2012.

[18] Liang Yang, Yang Liu, Hong Wu, Niels Høiby, Søren Molin, and Zhi-jun Song. Current understanding of multi-species biofilms. *International journal of oral science*, 3(2):74, 2011.

[19] X. Chen and P. S. Stewart. Biofilm removal caused by chemical treatments. *Water Research*, 34(17):4229–4233, 2000.

[20] I. E. C. Mott, D. J. Stickler, W. T. Coakley, and T. R. Bott. The removal of bacterial biofilm from water-filled tubes using axially propagated ultrasound. *Journal of Applied Microbiology*, 84(4):509–514, 1998.

[21] H.-C. Flemming, J. Wingender, T. Griegbe, and C. Mayer. *Biofilms: Recent Advances in their Study and Control*. Amsterdam: Harwood Academic Publishers, 2000.

[22] S. Grumbein, M. Opitz, and O. Lieleg. Selected metal ions protect *Bacillus subtilis* biofilms from erosion. *Metallomics*, 6(8):1441–1450, 2014.

[23] T. R. Neu. Significance of bacterial surface-active compounds in interaction of bacteria with interfaces. *Microbiological reviews*, 60(1):151, 1996.

[24] I. W. Sutherland. Structure-function relationships in microbial exopolysaccharides. *Biotechnology Advances*, 12(2):393 – 448, 1994.

[25] L. Hall-Stoodley, J. W. Costerton, and P. Stoodley. Bacterial biofilms: from the natural environment to infectious diseases. *Nature Reviews Microbiology*, 2(2):95–108, 2004.

[26] C. Hobley, L.and Harkins, C. E. MacPhee, and N. R. Stanley-Wall. Giving structure to the biofilm matrix: an overview of individual strategies and emerging common themes. *FEMS Microbiology Reviews*, 39(5):649–669, 2015.

[27] I. W. Sutherland. Biofilm exopolysaccharides: a strong and sticky framework. *Microbiology*, 147(1):3–9, 2001.

[28] K. Sauer, A. Rickard, and D. Davies. Biofilms and Biocomplexity. *Microbe Magazine*, 2:247–353, 2007.

[29] H.-C. Flemming and J. Wingender. The biofilm matrix. *Nature Reviews Microbiology*, 8(9):623–633, 2010.

[30] M. Marvasi, P. T. Visscher, and L. Casillas Martinez. Exopolymeric substances (EPS) from *Bacillus subtilis* : polymers and genes encoding their synthesis. *FEMS Microbiology Letters*, 313(1):1–9, 2010.

[31] C. E. Zobell. The Effect of Solid Surfaces upon Bacterial Activity. *J Bacteriol*, 46(1):39–56, 1943.

[32] K. Drescher, Y. Shen, B. L. Bassler, and H. A. Stone. Biofilm streamers cause catastrophic disruption of flow with consequences for environmental and medical systems. *Proceedings of the National Academy of Sciences of the United States of America*, 110(11):4345–4350, 2013.

[33] L. S. Cairns, L. Hobley, and N. R. Stanley-Wall. Biofilm formation by *Bacillus subtilis*: new insights into regulatory strategies and assembly mechanisms. *Molecular Microbiology*, 93(4):587–598, 2014.

[34] Hera Vlamakis, Yunrong Chai, Pascale Beauregard, Richard Losick, and Roberto Kolter. Sticking together: building a biofilm the *Bacillus subtilis* way. *Nat Rev Microbiol*, 11(3):157–168, 2013.

[35] B. E. Ramey, M. Koutsoudis, S. B. von Bodman, and C. Fuqua. Biofilm formation in plant-microbe associations. *Current Opinion in Microbiology*, 7(6):602–609, 2004.

[36] T. Danhorn and C. Fuqua. Biofilm formation by plant-associated bacteria. *Annual Review of Microbiology*, 61:401–422, 2007.

[37] A. M. Baty, 3rd, C. C. Eastburn, S. Techkarnjanaruk, A. E. Goodman, and G. G. Geesey. Spatial and temporal variations in chitinolytic gene expression and bacterial biomass production during chitin degradation. *Applied Environmental Microbiology*, 66(8):3574–3585, 2000.

[38] J. R. Lawrence, D. R. Korber, B. D. Hoyle, J. W. Costerton, and D. E. Caldwell. Optical sectioning of microbial biofilms. *Journal of Bacteriology*, 173(20):6558–6567, 1991.

[39] D. de Beer, P. Stoodley, F. Roe, and Z. Lewandowski. Effects of biofilm structures on oxygen distribution and mass transport. *Biotechnology and Bioengineering*, 43(11):1131–1138, 1994.

[40] P. Stoodley, D. Debeer, and Z. Lewandowski. Liquid flow in biofilm systems. *Applied and Environmental Microbiology*, 60(8):2711–2716, 1994.

[41] P. Stoodley, I. Dodds, J. D. Boyle, and H. M. Lappin-Scott. Influence of hydrodynamics and nutrients on biofilm structure. *Journal of Applied Microbiology*, 85 Suppl 1:19S–28S, 1998.

[42] K. Drescher, C. D. Nadell, H. A. Stone, N. S. Wingreen, and B. L. Bassler. Solutions to the public goods dilemma in bacterial biofilms. *Current Biology*, 24(1):50–55, 2014.

[43] E. M. Espeland and R. G. Wetzel. Complexation, Stabilization, and UV Photolysis of Extracellular and Surface-Bound Glucosidase and Alkaline Phosphatase: Implications for Biofilm Microbiota. *Microbial Ecology*, 42(4):572–585, 2001.

[44] Gail M. Teitzel and Matthew R. Parsek. Heavy metal resistance of biofilm and planktonic *Pseudomonas aeruginosa*. *Appl Environ Microbiol*, 69(4):2313–2320, 2003.

[45] E. Le Magrex-Debar, J. Lemoine, M. P. Gellé, L. F. Jacquelin, and C. Choisy. Evaluation of biohazards in dehydrated biofilms on foodstuff packaging. *International Journal of Food Microbiology*, 55(1-3):239–243, 2000.

[46] Carey D. Nadell, Knut Drescher, Ned S. Wingreen, and Bonnie L. Bassler. Extracellular matrix structure governs invasion resistance in bacterial biofilms. *ISME Journal*, 9(8):1700–1709, 2015.

[47] O. Lieleg, M. Caldara, R. Baumgärtel, and K. Ribbeck. Mechanical robustness of *Pseudomonas aeruginosa* biofilms. *Soft Matter*, 7(7):3307–3314, 2011.

[48] P. S. Stewart and J. W. Costerton. Antibiotic resistance of bacteria in biofilms. *Lancet*, 358(9276):135–138, 2001.

[49] W. L. Jones, M. P. Sutton, L. McKittrick, and P. S. Stewart. Chemical and antimicrobial treatments change the viscoelastic properties of bacterial biofilms. *Biofouling*, 27(2):207–215, 2011.

[50] K Zrelli, O Galy, P Latour-Lambert, L Kirwan, J M Ghigo, C Beloin, and N Henry. Bacterial biofilm mechanical properties persist upon antibiotic treatment and survive cell death. *New Journal of Physics*, 15(12):125026, 2013.

[51] L. Hall-Stoodley and P. Stoodley. Evolving concepts in biofilm infections. *Cellular Microbiology*, 11(7):1034–1043, 2009.

[52] R. D. Monds and G. A. O'Toole. The developmental model of microbial biofilms: ten years of a paradigm up for review. *Trends in Microbiology*, 17(2):73–87, 2009.

[53] A. M. Earl, R. Losick, and R. Kolter. Ecology and genomics of *Bacillus subtilis*. *Trends in Microbiology*, 16(6):269–275, 2008.

[54] A. L. McLoon, S. B. Guttenplan, D. B. Kearns, R. Kolter, and R. Losick. Tracing the domestication of a biofilm-forming bacterium. *Journal of Bacteriology*, 193(8):2027–2034, 2011.

[55] S. S. Branda, J. E. González-Pastor, E. Dervyn, S. D. Ehrlich, R. Losick, and R. Kolter. Genes involved in formation of structured multicellular communities by *Bacillus subtilis*. *Journal of Bacteriology*, 186(12):3970–3979, 2004.

[56] S. S. Branda, F. Chu, D. B. Kearns, R. Losick, and R. Kolter. A major protein component of the *Bacillus subtilis* biofilm matrix. *Molecular Microbiology*, 59(4):1229–1238, 2006.

[57] D. Romero, C. Aguilar, R. Losick, and R. Kolter. Amyloid fibers provide structural integrity to *Bacillus subtilis* biofilms. *Proceedings of the National Academy of Sciences of the United States of America*, 107(5):2230–2234, 2010.

[58] A. G. Stöver and A. Driks. Secretion, localization, and antibacterial activity of TasA, a *Bacillus subtilis* spore-associated protein. *Journal of bacteriology*, 181(5):1664–1672, 1999.

[59] Y. Chai, P. B. Beauregard, H. Vlamakis, R. Losick, and R. Kolter. Galactose metabolism plays a crucial role in biofilm formation by *Bacillus subtilis*. *mBio*, 3(4):e00184–e00112, 2012.

[60] D. B. Kearns, F. Chu, S. S. Branda, R. Kolter, and R. Losick. A master regulator for biofilm formation by *Bacillus subtilis*. *Molecular Microbiology*, 55(3):739–749, 2005.

[61] M. Martin, A. Dragos, T. Hölscher, G. Maróti, B. Bálint, M. Westermann, and Á. T. Kovács. De novo evolved interference competition promotes the spread of biofilm defectors. *Nature Communications*, 8:15127, 2017.

[62] A. K. Epstein, B. Pokroy, A. Seminara, and J. Aizenberg. Bacterial biofilm shows persistent resistance to liquid wetting and gas penetration. *Proceedings of the National Academy of Sciences of the United States of America*, 108(3):995–1000, 2011.

[63] L. Hobley, A. Ostrowski, F. V. Rao, K. M. Bromley, M. Porter, A. R. Prescott, C. E. MacPhee, D. M F. van Aalten, and N. R. Stanley-Wall. BslA is a self-assembling bacterial hydrophobin that coats the *Bacillus subtilis* biofilm. *Proceedings of the National Academy of Sciences of the United States of America*, 110(33):13600–13605, 2013.

[64] K. Kobayashi and M. Iwano. BslA(YuaB) forms a hydrophobic layer on the surface of *Bacillus subtilis* biofilms. *Molecular Microbiology*, 85(1):51–66, 2012.

[65] A. T. Kovacs and O. P. Kuipers. Rok Regulates *yuaB* Expression during Architecturally Complex Colony Development of *Bacillus subtilis* 168. *Journal of Bacteriology*, 193:998–1002, 2011.

[66] Hera Vlamakis, Claudio Aguilar, Richard Losick, and Roberto Kolter. Control of cell fate by the formation of an architecturally complex bacterial community. *Genes Dev*, 22(7):945–953, 2008.

[67] A. Driks. Tapping into the biofilm: insights into assembly and disassembly of a novel amyloid fibre in *Bacillus subtilis*. *Molecular Microbiology*, 80(5):1133–1136, 2011.

[68] Rebecca Terra, Nicola R. Stanley-Wall, Guoqiang Cao, and Beth A. Lazazzera. Identification of *Bacillus subtilis* SipW as a bifunctional signal peptidase that controls surface-adhered biofilm formation. *J Bacteriol*, 194(11):2781–2790, 2012.

[69] M. Morikawa, S. Kagihiro, M. Haruki, K. Takano, S. Branda, R. Kolter, and S. Kanaya. Biofilm formation by a *Bacillus subtilis* strain that produces gamma-polyglutamate. *Microbiology*, 152(Pt 9):2801–2807, 2006.

[70] O. Chumsakul, H. Takahashi, T. Oshima, T. Hishimoto, S. Kanaya, N. Ogasawara, and S. Ishikawa. Genome-wide binding profiles of the *Bacillus subtilis* transition state regulator AbrB and its homolog Abh reveals their interactive role in transcriptional regulation. *Nucleic Acids Research*, 39(2):414–428, 2011.

[71] V. L. Colledge, M. J. Fogg, V. M. Levdikov, A. Leech, E. J. Dodson, and A. J. Wilkinson. Structure and organisation of SinR, the master regulator of biofilm formation in *Bacillus subtilis*. *Journal of Molecular Biology*, 411(3):597–613, 2011.

[72] S. Kesel, A. Mader, P. H. Seeberger, O. Lieleg, and M. Opitz. Carbohydrate coating reduces adhesion of biofilm-forming *Bacillus subtilis* to gold surfaces. *Applied Environmental Microbiology*, 80(19):5911–5917, 2014.

[73] N. R. Stanley and B. A. Lazazzera. Defining the genetic differences between wild and domestic strains of *Bacillus subtilis* that affect poly-γ-DL-glutamic acid production and biofilm formation. *Molecular microbiology*, 57(4):1143–1158, 2005.

[74] A. Ogunleye, A. Bhat, V. U. Irorere, D. Hill, C. Williams, and I. Radecka. Poly-γ-glutamic acid: production, properties and applications. *Microbiology*, 161(1):1–17, 2015.

[75] T. Candela and A. Fouet. Poly-gamma-glutamate in bacteria. *Molecular microbiology*, 60(5):1091–1098, 2006.

[76] E. Freese, J. E. Heinze, and E. M. Galliers. Partial purine deprivation causes sporulation of *Bacillus subtilis* in the presence of excess ammonia, glucose and phosphate. *Microbiology*, 115(1):193–205, 1979.

[77] J. Dervaux, J. Carmelo Magniez, and A. Libchaber. On growth and form of *Bacillus subtilis* biofilms. *Interface Focus*, 4(6):20130051, 2014.

[78] S. S. Branda, J. E. González-Pastor, S. Ben-Yehuda, R. Losick, and R. Kolter. Fruiting body formation by *Bacillus subtilis*. *Proceedings of the National Academy of Sciences of the United States of America*, 98(20):11621–11626, 2001.

[79] K. Kobayashi. Gradual activation of the response regulator DegU controls serial expression of genes for flagellum formation and biofilm formation in *Bacillus subtilis*. *Molecular microbiology*, 66:395–409, 2007.

[80] S. Kesel, B. von Bronk, C. Falcón García, A. Götz, O. Lieleg, and M. Opitz. Matrix composition determines the dimensions of *Bacillus subtilis* NCIB 3610 biofilm colonies grown on LB agar. *RSC Advances*, 7:31886–31898, 2017.

[81] M. Albano, J. Hahn, and D. Dubnau. Expression of competence genes in bacillus subtilis. *Journal of Bacteriology*, 169(7):3110–3117, 1987.

[82] A. Steinbüchel, F. B. Oppermann-Sanio, C. Ewering, and M. Pötter. *Mikrobiologisches Praktikum Versuch und Theorie, vol 2.* Springer Spektrum Verlag, Berlin, Germany, 2013.

[83] Daniel R. Zerbino and Ewan Birney. Velvet: Algorithms for de novo short read assembly using de Bruijn graphs. *Genome Research*, 18(5):821–829, 2008.

[84] S. Kesel, F. Moormann, I. Gümperlein, A. Mader, M. Morikawa, O. Lieleg, and M. Opitz. Draft Genome Sequence of the Biofilm-Producing *Bacillus subtilis* Strain B-1, Isolated from an Oil Field. *Genome Announcements*, 2(6), 2014.

[85] S. M. Kielbasa, R. Wan, K. Sato, P. Horton, and M. C. Frith. Adaptive seeds tame genomic sequence comparison. *Genome Research*, 21(3):487–493, 2011.

[86] S. F. Altschul, T. L. Madden, A. A. Schäffer, J. Zhang, Z. Zhang, W. Miller, and D. J. Lipman. Gapped BLAST and PSI-BLAST: a new generation of protein database search programs. *Nucleic Acids Research*, 25(17):3389–3402, 1997.

[87] Xin Wang, I. King Jordan, and Leonard W. Mayer. Chapter 29 - A Phylogenetic Perspective on Molecular Epidemiology. In Yi-Wei Tang, Max Sussman, Dongyou Liu, Ian Poxton, and Joseph Schwartzman, editors, *Molecular Medical Microbiology (Second Edition)*, pages 517 – 536. Academic Press, Boston, second edition edition, 2015.

[88] Ulrich Kück. *Praktikum der Molekulargenetik*, chapter 4-PCR-Analytik, pages 221–245. Springer Berlin Heidelberg, Berlin, Heidelberg, 2005.

[89] G. G. Stoney. The tension of metallic films deposited by electrolysis. *Proceedings of the Royal Society of London. Series A, Containing Papers of a Mathematical and Physical Character*, 82(553):172–175, 1909.

[90] K. M. Goeders, J. S. Colton, and L. A. Bottomley. Microcantilevers: sensing chemical interactions via mechanical motion. *Chemical reviews*, 108:522–542, 2008.

[91] A. W. McFarland and J. S. Colton. Role of material microstructure in plate stiffness with relevance to microcantilever sensors. *Journal of Micromechanics and Microengineering*, 15(5):1060–1067, 2005.

[92] A. W. McFarland, M. A. Poggi, M. J. Doyle, L. A. Bottomley, and J. S. Colton. Influence of surface stress on the resonance behavior of microcantilevers. *Applied Physics Letters*, 87(5):053505, 2005.

[93] U. Nowicka, A. M.and Hasse, G. Sievers, M. Donten, Z. Stojek, S. Fletcher, and F. Scholz. Selective knockout of gold active sites. *Angewandte Chemie International Edition*, 49(17):3006–3009, 2010.

[94] Jörg Weissmüller and Huiling Duan. Cantilever bending with rough surfaces. *Phys Rev Lett*, 101(14):146102, 2008.

[95] D. M. Ratner, O. J. Plante, and P. H. Seeberger. A Linear Synthesis of Branched High-Mannose Oligosaccharides from the HIV-1 Viral Surface Envelope Glycoprotein gp120. *European Journal of Organic Chemistry*, 2002(5):826–833, 2002.

[96] R. McKendry, J. Zhang, Y. Arntz, T. Strunz, M. Hegner, H. P. Lang, M. K. Baller, U. Certa, E. Meyer, H.-J. Güntherodt, and C. Gerber. Multiple label-free biodetection and quantitative DNA-binding assays on a nanomechanical cantilever array. *Proceedings of the National Academy of Sciences of the United States of America*, 99(15):9783–9788, 2002.

[97] A. Mader. Biosensorik für biochemische Erkennungsprozesse. Master's thesis, LMU München, 2011.

[98] David J Whitehouse. *Surfaces and their Measurement*. Elsevier, 2004.

[99] S. Kesel, S. Grumbein, I. Gümperlein, M. Tallawi, A.-K. Marel, O. Lieleg, and M. Opitz. Direct Comparison of Physical Properties of *Bacillus subtilis* NCIB 3610 and B-1 Biofilms. *Applied Environmental Microbiology*, 82(8):2424–2432, 2016.

[100] Heinrich Hertz. Ueber die Beruehrung elastischer Koerper. *Gesammelte Werke*, 1:155–73, 1895.

[101] M. A. Meyers and K. K. Chawla. *Mechanical Behavior of Materials*. Cambridge University Press, 2008.

[102] Student. The Probable Error of a Mean. *Biometrika*, 6(1):1–25, 1908.

[103] J. W. Tukey. Comparing Individual Means in the Analysis of Variance. *Biometrics*, 5(2):99–114, 1949.

[104] F. Moormann. Genome, Genealogy and Genome Analysis. Master's thesis, LMU München, 2014.

[105] Y.-H. Hsueh, L. M. Cozy, L.-T. Sham, R. A. Calvo, A. D. Gutu, M. E. Winkler, and D. B. Kearns. DegU-phosphate activates expression of the anti-sigma factor FlgM in *Bacillus subtilis*. *Molecular Microbiology*, 81(4):1092–1108, 2011.

[106] L. K. Nakamura, M. l. S. Roberts, and F. M. Cohan. Note: Relationship of *Bacillus subtilis* clades associated with strains 168 and W23: A proposal for *Bacillus subtilis subsp. subtilis subsp. nov.* and *Bacillus subtilis subsp. spizizenii subsp. nov.*. *International Journal of Systematic and Evolutionary Microbiology*, 49(3):1211–1215, 1999.

[107] A. M. Earl, R. Losick, and R. Kolter. *Bacillus subtilis* genome diversity. *Journal of bacteriology*, 189(3):1163–1170, 2007.

[108] J. Fritz, M. K. Baller, H. P. Lang, H. Rothuizen, P. Vettiger, E. Meyer, H.-J. Güntherodt, C. Gerber, and J. K. Gimzewski. Translating biomolecular recognition into nanomechanics. *Science*, 288(5464):316–318, 2000.

[109] J. Pei, F. Tian, and T. Thundat. Glucose biosensor based on the microcantilever. *Analytical Chemistry*, 76(2):292–297, 2004.

[110] N. Nugaeva, K. Y. Gfeller, N.. Backmann, M. Düggelin, H. P. Lang, H.-J. Güntherodt, and M. Hegner. An antibody-sensitized microfabricated cantilever for the growth detection of *Aspergillus niger* spores. *Microscopy and Microanalysis*, 13(1):13–17, 2007.

[111] K. R. Buchapudi, X. Huang, X. Yang, H.-F. Ji, and T. Thundat. Microcantilever biosensors for chemicals and bioorganisms. *Analyst*, 136(8):1539–1556, 2011.

[112] H. P. Lang, R. Berger, F. Battiston, J.-P. Ramseyer, E. Meyer, C. Andreoli, J. Brugger, P. Vettiger, M. Despont, T. Mezzacasa, L. Scandella, H.-J. Güntherodt, C. Gerber, and J. K. Gimzewski. A chemical sensor based on a micromechanical cantilever array for the identification of gases and vapors. *Applied Physics A*, 66(1):S61–S64, 1998.

[113] R. M. Donlan. Biofilms: microbial life on surfaces. *Emerging Infectious Diseases*, 8(9):881–890, 2002.

[114] R. Van Houdt and C. W. Michiels. Biofilm formation and the food industry, a focus on the bacterial outer surface. *J Appl Microbiol*, 109(4):1117–1131, 2010.

[115] F. El-Taib Heakal, O. S. Shehata, and N. S. Tantawy. Integrity of metallic medical implants in physiological solutions. *International Journal of Electrochemical Science*, 9:1986–2004, 2014.

[116] D. A. Giljohann, D. S. Seferos, W. L. Daniel, M. D. Massich, P. C. Patel, and C. A. Mirkin. Gold nanoparticles for biology and medicine. *Angewandte Chemie International Edition*, 49(19):3280–3294, 2010.

[117] Jost Wingender and Hans-Curt Flemming. Biofilms in drinking water and their role as reservoir for pathogens. *Int J Hyg Environ Health*, 214(6):417–423, 2011.

[118] J. C. Love, L. A. Estroff, J. K. Kriebel, R. G. Nuzzo, and G. M. Whitesides. Self-assembled monolayers of thiolates on metals as a form of nanotechnology. *Chemical Reviews*, 105(4):1103–1169, 2005.

[119] R. G. Nuzzo and D. L. Allara. Adsorption of bifunctional organic disulfides on gold surfaces. *Journal of the American Chemical Society*, 105 (13):4481–4483, 1983.

[120] O. Krispin and R. Allmansberger. The *Bacillus subtilis* AraE protein displays a broad substrate specificity for several different sugars. *Journal of Bacteriology*, 180(12):3250–3252, 1998.

[121] O. Krispin and R. Allmansberger. The *Bacillus subtilis* galE gene is essential in the presence of glucose and galactose. *Journal of Bacteriology*, 180(8):2265–2270, 1998.

[122] T. Sun and J. Altenbuchner. Characterization of a mannose utilization system in *Bacillus subtilis*. *Journal of Bacteriology*, 192(8):2128–2139, 2010.

[123] B. Lorenz, L. Álvarez de Cienfuegos, M. Oelkers, E. Kriemen, C. Brand, M. Stephan, E. Sunnick, D. Yüksel, V. Kalsani, K. Kumar, D. B. Werz, and A. Janshoff. Model system for cell adhesion mediated by weak carbohydrate-carbohydrate interactions. *Journal of the American Chemical Society*, 134(7):3326–3329, 2012.

[124] S.-I. Hakomori. Carbohydrate-carbohydrate interaction as an initial step in cell recognition. *Pure & Applied Chemistry*, 63:473–482, 1991.

[125] J. M. de la Fuente and S. Penadés. Understanding carbohydrate-carbohydrate interactions by means of glyconanotechnology. *Glycoconjugate Journal*, 21(3-4):149–163, 2004.

[126] M. A. Novak. *Evolutionary Dynmaics: Exploring the Equations of Life*. Belknap Press of Harvard University Press, Cambridge, MA, USA, 2006.

[127] I. Gümperlein. Elasticity Analysis of Bacterial Biofilms by Atomic Force Microscopy. Master's thesis, LMU München, 2015.

[128] L. Shi, R. Ardehali, K. D. Caldwell, and P. Valint. Mucin coating on polymeric material surfaces to suppress bacterial adhesion. *Colloids and Surfaces B: Biointerfaces*, 17(4):229–239, 2000.

[129] J. Deutscher, A. Galinier, and I. Martin-Verstraete. Carbohydrate Uptake and Metabolism. In *Bacillus subtilis and Its Closest Relatives*, pages 129–150. American Society of Microbiology, 2002.

[130] M. Scalabrini, J. Hamon, I. Linossier, V. Ferrières, and K. Réhel. *Pseudomonas aeruginosa* resistance of monosaccharide-functionalized glass surfaces. *Colloids and Surfaces B: Biointerfaces*, page 110383, 2019.

[131] Claire Valotteau, Christophe Calers, Sandra Casale, Jan Berton, Christian V Stevens, Florence Babonneau, Claire-Marie Pradier, Vincent Humblot, and Niki Baccile. Biocidal properties of a glycosylated surface: sophorolipids on Au (111). *ACS applied materials & interfaces*, 7(32):18086–18095, 2015.

[132] Claire Valotteau, Niki Baccile, Vincent Humblot, Sophie Roelants, Wim Soetaert, Christian V Stevens, and Yves F Dufrêne. Nanoscale antiadhesion properties of sophorolipid-coated surfaces against pathogenic bacteria. *Nanoscale Horizons*, 2019.

[133] U. U. Nwodo, E. Green, and A. I. Okoh. Bacterial exopolysaccharides: functionality and prospects. *International Journal of Molecular Sciences*, 13(11):14002–14015, 2012.

[134] S. Arnaouteli, C. E. MacPhee, and N. R. Stanley-Wall. Just in case it rains: building a hydrophobic biofilm the *Bacillus subtilis* way. *Current Opinion in Microbiology*, 34:7 – 12, 2016. Growth and development: Eukaryotes * Growth and development: Prokaryotes.

[135] C. Falcón García, F. Stangl, A. Götz, W. Zhao, S. A. Sieber, M. Opitz, and O. Lieleg. Topographical alterations render bacterial biofilms susceptible to chemical and mechanical stress. *Biomaterials science*, 7(1):220–232, 2019.

[136] M. Klotz, M. Kretschmer, A. Goetz, S. Ezendam, O. Lieleg, and M. Opitz. Importance of the biofilm matrix for the erosion stability of *Bacillus subtilis* NCIB 3610 biofilms. *Royal Society of Chemistry*, 9:11521–11529, 2019.

[137] J. Huang, S. Liu, C. Zhang, X. Wang, J. Pu, F. Ba, S. Xue, H. Ye, T. Zhao, K. Li, Y. Wang, J. Zhang, L. Wang, C. Fan, T. K. Lu, and C. Zhong. Programmable and printable *Bacillus subtilis* biofilms as engineered living materials. *Nature Chemical Biology*, 15(1):34–41, 2019.

[138] Chen Zhang, Jiaofang Huang, Jicong Zhang, Suying Liu, Mengkui Cui, Bolin An, Xinyu Wang, Jiahua Pu, Tianxin Zhao, Chunhai Fan, Timothy K. Lu, and Chao Zhong. Engineered *Bacillus subtilis* biofilms as living glues. *Materials Today*, 2019.

[139] A. Ostrowski, A. Mehert, A. Prescott, T. B. Kiley, and N. R. Stanley-Wall. YuaB functions synergistically with the exopolysaccharide and TasA amyloid fibers to allow biofilm formation by *Bacillus subtilis*. *Journal of Bacteriology*, 193(18):4821–4831, 2011.

List of Figures

List of Tables

List of Publications

S. Kesel, B. v. Bronk, C. Falcon-Garcia, A. Goetz, O. Lieleg and M. Opitz
Matrix composition determines dimensions of *Bacillus subtilis* NCIB 3610 biofilm colonies grown on LB agar
RSC Advances, doi:10.1039/c7ra05559e (2017)
Figures, Tables and results from this article were reproduced in this thesis with permission from the Royal Society of Chemistry.

S. Kesel*, S. Grumbein*, I. Gümperlein, M. Tallawi, A-K. Marel, O. Lieleg and M. Opitz
Direct comparison of physical properties of *Bacillus subtilis* NCIB 3610 and B-1 biofilms
Applied and Enviromental Microbiology, 82(8):2424-2432, doi:10.1128/AEM.03957-15 (2016)
Figures, Tables and results from this article were reused in this thesis within the rights retained by the author.

S. Kesel, F. Moormann, I. Gümperlein, A. Mader, M. Morikawa, O. Lieleg and M. Opitz
Genome sequence of the biofilm producing *Bacillus subtilis* strain B-1 isolated from an oil field
Genome Announcements, 2(6):e01163-14, doi:10.1128/genomeA.01163-14. (2014)
Figures, Tables and results from this article were reused in this thesis within the rights retained by the author.

S. Kesel, A. Mader, P.H. Seeberger, O. Lieleg and M. Opitz
Carbohydrate-coating reduces adhesion of biofilm forming *Bacillus subtilis* to gold surfaces
Applied and Environmental Microbiology, Published ahead of print 18 July 2014, doi:10.1128/AEM.01600-14 (2014)
Figures, Tables and results from this article were reused in this thesis within the rights retained by the author.

Mader A., von Bronk B., Ewald B., **Kesel S.**, Schnetz K., Frey E., Opitz M.
Amount of colicin release in *Escherichia coli* is regulated by lysis gene expression of the

Colicin E2 operon
PLoS ONE 10(3): e0119124, doi:10.1371/journal.pone.0119124 (2015)

Kesel S., Mader A., Höfler C., Mascher T., Leisner M.
Immediate and Heterogeneous Response of the LiaFSR Two-Component System of Bacillus subtilis to the Peptide Antibiotic Bacitracin.
PLoS ONE 8(1): e53457, doi:10.1371/journal.pone.0053457 (2013)

Danksagung

An dieser Stelle möchte ich all denjenigen danken, die mich im Laufe meiner Doktorarbeit unterstützt, motiviert und begleitet haben. Mein Dank gilt:

Madeleine Opitz, für die hervorragende Betreuung, ihr immer offenes Ohr, ihre Unterstützung mit Rat und Tat und die Fülle an Dingen die ich von ihr lernen konnte.

Joachim Rädler, für die tolle Arbeitsatmosphäre an seinem Lehrstuhl.

den **Kooperationspartnern**, allen voran der AG Lieleg, für die produktive Zusammenarbeit und die vielen verschiedenen Methoden, die ich dadurch zusätzlich lernen konnte.

der gesammten **AG Optiz**, insbesondere Andreas (Danke auch für die Diskussionsrunden im Hof), Alex und Bene, es war mir eine Freude mit euch im Labor zu arbeiten.

Gerlinde, Charlott und Susi, die mit ihrem Wissen und ihrer Hilfe so manches Experiment vereinfacht haben.

dem ganzen **LS Rädler**, insbesondere Sonja und so viele andere, die hier alle namentlich aufzuzählen die Seite sprengen würde.

meiner **Familie und Freunden**, auf Euch kann ich mich immer verlassen und ich liebe die Traditionen unserer stetig wachsenden Großfamilie.